National Library of Canada

Acquisitions and Bibliographic Services Branch

395 Wellington Street
Ottawa, Ontario
K1A 0N4

Bibliothèque nationale du Canada

Direction des acquisitions et des services bibliographiques

395, rue Wellington
Ottawa (Ontario)
K1A 0N4

Your file Votre référence

Our file Notre référence

NOTICE

The quality of this microform is heavily dependent upon the quality of the original thesis submitted for microfilming. Every effort has been made to ensure the highest quality of reproduction possible.

If pages are missing, contact the university which granted the degree.

Some pages may have indistinct print especially if the original pages were typed with a poor typewriter ribbon or if the university sent us an inferior photocopy.

Reproduction in full or in part of this microform is governed by the Canadian Copyright Act, R.S.C. 1970, c. C-30, and subsequent amendments.

AVIS

La qualité de cette microforme dépend grandement de la qualité de la thèse soumise au microfilmage. Nous avons tout fait pour assurer une qualité supérieure de reproduction.

S'il manque des pages, veuillez communiquer avec l'université qui a conféré le grade.

La qualité d'impression de certaines pages peut laisser à désirer, surtout si les pages originales ont été dactylographiées à l'aide d'un ruban usé ou si l'université nous a fait parvenir une photocopie de qualité inférieure.

La reproduction, même partielle, de cette microforme est soumise à la Loi canadienne sur le droit d'auteur, SRC 1970, c. C-30, et ses amendements subséquents.

Canada

Combined Boundary Element And Finite Element Analysis of Composite Bridges

By

Ezeedin M. Galuta

A Ph.D. Thesis

submitted to the School of Graduate Studies and Research
in partial fulfillment of the requirements for the
Doctor of Philosophy
in Civil Engineering Degree*

University of Ottawa
Ottawa, Ontario, Canada
July 1993

*The Doctor of Philosophy of Civil Engineering Program
is a joint program with Carleton University
administered by the Ottawa-Carleton
Institute in Civil Engineering

ISBN 0-315-95949-5

UNIVERSITÉ D'OTTAWA
UNIVERSITY OF OTTAWA

Acknowledgments

I wish to express sincere gratitude to my supervisor Dr. M. S. Cheung for his guidance throughout the course of this study.

Thanks are also due to my advisory committee, Dr. S. F. NG, Dr. M. Saatcioglu, Dr. G. Hartley and Dr. Tanaka for their suggestions regarding the direction and the content of this thesis.

I would like to thank Dr. W. Li for his time in discussing various aspects of this thesis. Thanks also due to my friends Dr. H. Abida and Mr. H. Ibrahim for their help and support.

I shall be always grateful to my wife and my parents for their support and patience throughout the time of this study.

Abstract

In this thesis, the coupling of boundary element and finite element methods and its application to analyze bridges are studied for the first time. The coupling technique is implemented to analyze slab on girders and box girder bridges. The boundary element method is employed to model the bridge deck while the finite element method is used to model the girders.

The finite elements and boundary elements are connected at a number of interface nodes in the longitudinal direction. For the finite element region, a static condensation technique is applied to condense the non-interface degrees of freedom. Then the finite element equations are transformed into boundary element equations and the compatibility interface mechanism required to combine the two methods is developed.

A computer program which combines boundary element and finite element methods in one solution is developed in this thesis. Different types of bridges with different load cases are considered in the study in order to test the performance of the combined method. It has been shown that the results obtained by the combined method (BEM-FEM) are in good agreement with the finite strip solution. The numerical examples, considered in this thesis, demonstrated the accuracy of the results and the simplicity and reduction of the input data.

Contents

Acknowledgements i

Abstract ii

1 Introduction **1**

1.1 General 1

1.2 Study Needs 4

1.3 Objectives and Scope 6

1.4 Thesis Description 7

2 Review of Past Work **9**

2.1 General 9

2.2 Direct Boundary Element Method 10

2.3 Coupling of BEM and FEM 13

3 Boundary Element Equations 18

3.1 Introduction 18

3.2 B.I.E For Plate Bending 19

3.2.1 Fundamental Solutions 21

3.3 B.I.E For Plane Stress 23

3.3.1 Fundamental Solutions 23

3.4 Discretization 24

3.5 Evaluation of the B.I.E 26

3.6 Interior Point Solution 28

3.7 Boundary conditions 31

3.8 Location of the Source Point 32

4 Coupling of BEM and FEM 38

4.1 Introduction 38

4.2 Finite Element Equations 39

4.3 Boundary Element Equations 43

4.4 Description of Coupling Theory 45

4.4.1 Case I 45

4.4.2 Case II 50

4.5 Modeling of Bridge Structures 54

5 Convergence of the Results 66

5.1 General 66

5.2 Case Studies 67

5.2.1 Concrete skew slab on two girders bridge 67

5.2.2 Concrete single-cell box girder bridge 68

5.2.3 Concrete slab on two girders bridge 70

5.2.4 Simply supported slab bridge 71

5.2.5 Concrete slab bridge 72

5.3 Choice of mesh sizes and type of elements 73

5.4 Concluding Remarks 74

6 Applications And Results 98

6.1 General 98

6.2 Slab on girder bridges 99

6.2.1 Twin girder bridges 99

6.2.2 Multi girder bridge (Example 4) 102

6.3 Box girder bridges 103

6.3.1 Single-cell box girder bridge 103

6.3.2 Multi-cell box girder bridge 107

7 Conclusions And Recommendations 150

7.1 Summary and Conclusions 150

7.2 Recommendations for Future Research 152

APPENDIX A 160

APPENDIX B 168

List of Figures

3.1 Direction of displacements and forces along the boundaries. . 33

3.2 The source point p and the integration point q. 33

3.3 Directions of the unit moment. 34

3.4 Fundamental solution for plane stress problems (Kelvin solution). 35

3.5 Boundary Discretization. 35

3.6 A quadratic element. 36

3.7 An element divided into two sub-elements. 36

3.8 Degrees of freedom along the interface. 37

3.9 The location of the source point outside the domain. 37

4.1 Local degrees of freedom for a flat shell element. 58

4.2 Rectangular finite elements used in the program. 59

4.3 Local and global coordinate systems. 59

4.4 B.E. and F.E. regions for case I 60

4.5 B.E. and F.E. regions for case II 61

4.6 Typical cross sections. 62

4.7 Modeling of a two-cell box girder bridge. 62

4.8 The compatibility requirements at the interfaces. 63

4.9 Modeling of a slab on girder bridge. 64

4.10 A flow chart describing the major steps of the BACBAF. . . 65

5.1 The dimensions and material properties for Example 5.2.1. . 81

5.2 BE and FE idealizations for Example 5.2.1. 83

5.3 The dimensions and material properties for Example 5.2.2. . 84

5.4 BE and FE idealizations using quadratic elements for Example 5.2.2. 85

5.5 Loading and material properties of the bridge for Example 5.2.3. 86

5.6 BE idealization using linear element for Example 5.2.3. 87

5.7 BE idealization for the top slab. 88

5.8 BE and FE idealizations using linear elements. 89

5.9 BE and FE idealizations using linear elements. 90

5.10 BE and FE idealizations using quadratic elements for Example 5.2.3. 91

5.11 BE and FE idealizations using quadratic elements. 92

5.12 Details of the bridge in Example 5.2.5. 93

5.13 Vertical deflection along the center of span. 94

5.14 Variation of the longitudinal moment along the span. 95

5.15 Vertical deflection along the center of span. 96

5.16 Variation of the longitudinal moment along the span. 97

6.1 Geometrical and material properties of the bridge for Example 1 115

6.2 BE and FE idealizations using quadratic elements. 116

6.3 The bridge dimensions, material properties and loading for example 2. 117

6.4 Details and loading of the bridge for Example 3. 118

6.5 BE idealizations for the top slab. 119

6.6 A slab on steel girders bridge. 120

6.7 Details and loading of the bridge for Example 5. 121

6.8 BE and FE idealizations for a single-cell bridge using linear elements. 122

6.9 BE and FE idealizations for a single-cell bridge using quadratic elements. 123

6.10 Details and loading of the bridge for Example 6. 124

6.11 Geometrical and material properties of the bridge for Example 7125

6.12 Dimensions and loading of the bridge for Example 8. 126

6.13 A two-cell box girder bridge. 127

6.14 A two-cell box girder bridge under four trucks. 128

6.15 Vertical deflection along center of the span. 129

6.16 Variation of longitudinal moment along the span. 130

6.17 Vertical deflection along the girder. 131

6.18 Variation of transverse moment at the mid span. 132

6.19 Vertical deflection along the center of span. 133

6.20 Variation of transverse moment at the mid span. 134

6.21 Variation of transverse moment at x = 7.0 m. 135

6.22 Vertical deflection along the center of span. 136

6.23 Vertical deflection along the interior girder. 137

6.24 Variation of the longitudinal moment along the span. 138

6.25 Vertical deflection along the center of span. 139

6.26 Variation of the longitudinal moment along the span. 140

6.27 Variation of transverse moment at the mid span. 141

6.28 Vertical deflection along the center of span. 142

6.29 Vertical deflection along the girder. 143

6.30 Variation of the longitudinal moment along the span. 144

6.31 Variation of transverse moment at the mid span. 145

6.32 Vertical deflection along the girder. 146

6.33 Variation of the normal moment along the girder. 147

6.34 Vertical deflection along the center of span. 148

6.35 Variation of the longitudinal moment along the span. 149

List of Tables

5.1 Deflection along the span for Example 5.2.1. 75

5.2 Longitudinal moment along the span for Example 5.2.1. 75

5.3 Vertical deflection along the span for Example 5.2.2 76

5.4 Longitudinal moment along the span for Example 5.2.2 76

5.5 Rotation along the girder for Example 5.2.2 77

5.6 Vertical deflection along the girder for Example 5.2.2 77

5.7 Transverse moment along the mid span for Example 5.2.2 78

5.8 Transverse moment along the mid span for Example 5.2.2 78

5.9 Vertical deflection along the girder for Example 5.2.2 79

5.10 Comparison of the equivalent shear for Example 5.2.4. 79

5.11 Vertical deflection and longitudinal moment for Example 5.2.5. . 80

6.1 Longitudinal moment along the span for Example 2 110

6.2 Deflection along the span for Example 3 111

6.3 Deflection along the girder for Example 3 111

6.4 Longitudinal moment along the span for Example 3 112

6.5 Vertical girder displacements for Example 6 112

6.6 Deflection along the center of the span for Example 10 113

6.7 Longitudinal moment along the center of wheel loads for Example 10 114

Chapter 1

Introduction

1.1 General

In the past twenty years, various numerical techniques for the solution of the differential or integral equations encountered in many engineering problems have been developed. These numerical methods can be categorized as domain or boundary methods, depending on whether the numerical analysis involves a disctretization of the domain or the boundary.

In bridge analysis, the domain-type methods most commonly used are finite element and finite strip methods. These methods are known to be the most powerful and versatile tools, which can be applied to analyze different types of bridges. A brief description of the these methods follows.

The basic concept of the **finite element method** is the discretization of the continuum into elements of finite size and the assumption of a displacement or stress distribution within each element expressed in terms of a set of unknown nodal values. The minimization of the global potential energy yields a set of linear algebraic equations whose solution determines these unknown values. In regions where field gradients are expected to change rapidly, either smaller elements or higher order elements are used. The method can be applied to deal with any specific configuration of bridge structure and supports. It is suitable for analysis involving all types of static and dynamic loads and all kinds of elastic and inelastic deformation. However, the efficiency of the method needs to be improved because the finite element solution usually requires significant storage capacity and tedious and lengthy input data files. Also, in the bridges subjected to moving concentrated loads, the accuracy of numerical results tends to decrease because of element discretization and the mesh needs to be refined in order to simulate the local effects of the wheel loads. An immediate consequence of this is a change of input data, which becomes a serious drawback for practical applications.

Finite strip method can be considered as a special form of the finite element procedure using the displacement approach or the so-called semi-analytical finite element method. If a structure has constant cross-section and its boundary conditions at both ends do not change transversely, then the structure can be divided into a number of finite strips instead of finite elements for its stress analysis. In each strip, the displacement components at any point are expressed in terms of the displacement parameters of nodal lines by means of

simple polynomials in the transverse direction and continuously differentiable smooth series in the longitudinal direction. Thus the number of dimensions of the analysis is reduced by one. However, if the bridge is subjected to concentrated loads, in order to simulate corresponding local stresses, many terms and a large number of longitudinal sections are required and the finite strip method becomes less economical.

These difficulties associated with domain-type methods (i.e. FEM and FSM) can be overcome in some situations by using the "Boundary Element Method". **Boundary Element Method (BEM)** recently has become a popular and powerful numerical method. The boundary element method involves the transformation of the governing differential equations within the domain under consideration, to an integral equation defined on the surface of the domain, thus enabling the reduction of the dimensionality of the problem by one. The boundary may then be discretized into a number of elements over which a polynomial form of the solution is assumed. This enables the evaluation of the relevant integrals, usually by some numerical process, resulting in a final system of linear algebraic equations. The advantages of the method are readily apparent and have been extensively discussed and demonstrated in the literature [12-14]. As only the boundary of the domain needs to be discretized, the resulting system of equations are considerably smaller than those involving domain solutions (e.g. finite element and finite strip methods), and considerable saving in the time required for data preparation can be achieved. A very important implication of the method is that there is no interpolation of the solution within the domain, and for a given solution on the surface, the re-

sults at interior points involve no approximation. There are two approaches to formulate the boundary element equations. The first approach called 'Direct boundary element (DBEM)', which is based on the Betti-Maxwell's reciprocal theorem. The second is an indirect approach, which is based on the principle of superposition (IBEM).

The coupling of the two methods is indeed a welcome proposition for many researchers in the field of mathematical modeling, and it is shown to preserve the advantages of each method, and eliminate their individual disadvantages [15,26]. The domain is represented by boundary elements or finite elements, depending upon the geometry and boundary conditions of a given problem.

1.2 Study Needs

As mentioned earlier, there are some difficulties encountered when the domain type methods (e.g. FEM and FSM) are used to analyze local stresses in bridges subjected to moving loads. However, these difficulties can be overcome if the BEM and FEM are combined in one solution. In the combined method, the BEM can be used to model the bridge deck and the other bridge components, such as girders and diaphragms can be modeled by FEM. In this case, for instance, analyzing the bridge deck by BEM would be more efficient than by FEM or FSM, where only the boundaries along the bridge deck have to be discretized into one-dimensional elements. Therefore, the dimensions of the analysis are reduced, consequently the input data and computer storage

capacity are significantly reduced. The combined method is useful especially when the bridge is subjected to moving loads, where in FEM it is necessary to subdivide the slab into a number of finer meshes, thus it often leads to huge number of simultaneous equations and large band width, while in BEM the moving loads do not affect the size of the mesh and the mesh does not require any change. A simple combination of boundary element and finite element methods was carried out in the past (e.g. [11], [15] and [46]). In these studies, the technique was implemented to analyze one and two-dimensional problems using low order degrees of freedom. In some cases, the compatibility requirements were not fully achieved. This shows a need to extend the coupling technique to 3-dimensional problems such as bridges and to improve the compatibility requirements.

The boundary element and finite element methods cannot be directly linked as they are normally formulated, because they do not relate the same sets of variables. The finite element method relates nodal displacements and forces, whereas the boundary element method relates nodal displacements and tractions. Hence for coupling to be achieved one of the methods must be transformed to make it compatible with the other method. In this study the finite element equations are transformed into boundary element equations. One of the main problems in boundary element equations is that of singularities, however, these difficulties can be overcome if the integral equations are evaluated analytically. For composite bridges, in order to include the composite action between the bridge deck and the girders, the degrees of freedom of an element must include both bending and in-plane actions (e.g . flat shell element can

be used).

If these problems can be successfully solved, different types of bridge superstructures, such as slab on girders and box girder bridges can be easily and economically analyzed by using the combined method (BEM-FEM).

1.3 Objectives and Scope

The main objective of this thesis is to extend the coupling technique, that combines the advantages of both, boundary element and finite element methods, to spatial structures. A new hybrid model, in which the compatibility requirements are satisfied, is developed and validated. The hybrid method should be able to model and analyze different types of bridges with a reduced number of operations and without compromise in accuracy. The objectives of this research can be summarized as follows :

1. Review of the boundary element equations for in-plane and bending actions to form the flat shell element equations.

2. Enhancement of the performance of the combined method using some techniques such as, double nodes at the corners and the determination of suitable location of source points.

3. Development of the compatibility requirements at the interfaces between boundary element and finite element regions.

4. Development of a computer program to combine BEM and FEM where any order of elements can be used.

5. Application of the combined method to the slab on girders and box girder bridges and comparison with other numerical techniques, in terms of :

   - Validity of the method and accuracy of the results.
   - Computation requirements, such as simplicity and reduction of input data.

1.4 Thesis Description

The thesis is divided into seven chapters as follows :

Chapter 1 introduces the boundary element method as a numerical technique and presents its advantages over the domain-type methods such as finite element and finite strip methods. The advantages of combining the two methods (BEM and FEM) are also discussed, this is followed by a presentation of the objectives and scope of the thesis and a brief thesis description.

Chapter 2 presents a literature review of the recent approaches in boundary element method. Also, a brief review of a coupling technique between BEM and FEM and its application for different areas is presented.

Chapter 3 introduces a review of the boundary element equations for both

bending and plane stress actions, which are then combined to form the boundary element equations for a flat shell element. The numerical evaluation of the integral equations is presented. Many techniques are used to improve the accuracy of the solution such as determining the suitable location of the source point and using double nodes at the corners, etc..

In chapter 4, the mathematical formulation of the coupling between BEM and FEM is developed. The compatibility and equilibrium conditions at the interface between slab and girders are satisfied. Two cases were considered here. In the first case the compatibility requirements will be satisfied between two interfaces while the second case is dealing with three interfaces.

Chapter 5 investigates the convergence of the results using the combined method. The convergence is investigated by using different meshes and by increasing the order of the elements. The simplicity and the reduction of the input data are considered in the chapter.

Chapter 6 includes the application of the combined method (BEM-FEM) to two types of bridges. A few numerical examples are presented to validate the combined method (BEM-FEM). Comparisons were made between the results obtained from the (BEM-FEM) and the finite strip method.

Chapter 7 contains the summary, conclusion of the study and recommendations for future research.

Chapter 2

Review of Past Work

2.1 General

One of the most interesting features of the boundary element method is that it is easy to combine the technique with other numerical methods (e.g. finite element method). In order to profit from the advantages of the two numerical techniques (e.g BEM and FEM), a combination of the two seems ideal. Such a combination should allow for the use of the most appropriate techniques over each domain of a problem with a reduced number of operations and without compromise in accuracy. In many problems, the boundary element method may provide the appropriate conditions to represent a large or infinite domain while the finite element method can solve complex material properties in a finite domain.

The coupling technique of the boundary element and finite element methods has been studied by many researchers. Mainly two different approaches were used for the coupling technique. The first approach consists of transforming the boundary element equations into a stiffness system where a large number of operations is required to achieve the stiffness matrix. In the second approach the finite element equations are directly combined with the boundary element equations, forming a square system of equations which includes the interface tractions as unknowns plus the unknowns associated with the boundary element region.

This chapter includes an overview of the past research for boundary element formulations and coupling of boundary element and finite element solutions.

2.2 Direct Boundary Element Method

The early implementations of the boundary element formulation for potential problems can be traced to Jaswon and Ponter [24]. They presented a numerical technique for solving the boundary integral equations by discretizing the boundary into a series number of elements and assumed a constant source density within each element.

Rizzo [33] and Cruse [20] applied the boundary element method to elasticity problems. The authors presented a formulation for two and three dimensional elastostatics problems using the Kelvin fundamental solution. Also they

demonstrated that, for a given problem, the boundary element method could become more efficient than the finite element or finite difference methods where the dimension of the problem could be reduced by one.

Brady and Bray [10] applied the boundary element method to determine the displacements introduced by excavation in the stressed medium as well as the stress distribution in a rock medium after the excavation.

A complete formulation of boundary element method to two and three dimensional plasticity problems was developed by Tells and Brebbia [41]. They gave a correct expression for the internal stresses which included the derivatives of the singular integrals.

The last decade has seen a great amount of research in the use of boundary element method for solution of elastostatics and elastodynamics problems and it is impossible to refer to all works directly. Therefore, the reader is referred to the bibliography at the end of this thesis.

For bending of elastic plates, several investigations have been carried out in an attempt to solve plate bending problems. Different approaches were developed to formulate the boundary integral equations.

The first application of boundary integral equations for plate bending can be attributed to Jaswon and Maiti [25]. Their formulations were limited to analyze clamped and simply supported plates. In the case of simple loadings, they transformed the plate problem into a biharmonic boundary value case.

This implied solving it as a function of two potentials.

Altiero and Sikarskie [4] have presented a technique based on an indirect approach. The approach consists of embedding a real plate inside a fictitious plate for which the Green's function is known. Then the force and the moment distributions associated with the real plate were determined. Their applications were restricted to clamped plates because of the difficulties associated with the other boundary conditions.

Wu and Altiero [44] extended the boundary integral formulation to include arbitrary boundary conditions. They assumed that the density of the force and moment distribution were acting at a certain distance along the boundary. The approach, although appropriate for solving different types of plate problems, needs to define the appropriate distance where the fictitious boundary should be located.

The direct formulation of boundary integral equations for plate bending was introduced by Bezine [8], Bezine and Gamby [9] and Stern [36,37]. In references [8] and [9] Bezine introduced the formulation of boundary integral equations for constant elements and presented some numerical results. All the examples were restricted to the analysis plates subjected to concentrated loads because the formulation did not include a transformation of domain integrals into boundary integrals.

Stern [36,37] has presented a general boundary integral formulation to solve plate bending problems. Although the procedure can be applied to any plate

problems, it has disadvantages. Firstly, because the formulation of the boundary element equations includes the evaluation of domain integrals, the numerical scheme becomes a drawback in some cases. Secondly, the formulation includes discontinuities on the boundary, which makes the procedure unstable for different boundary conditions.

Totenham [43] presented another approach to avoid the singularity associated with formulation of the boundary element equations.

Additional work to increase the accuracy and the computational efficiency of the method was done by Abdel-Akher and Hartley [2,3] . Their publications involved the enhancement of the performance of the boundary element method by introducing new techniques such as a new treatment of curved boundary and evaluating the boundary and domain integrals analytically.

2.3 Coupling of BEM and FEM

The coupling of BEM and FEM was first discussed by Zienkiewicz et al [46]. An energy functional was used in combination with the boundary integral equations which were derived from the collocation method. The coupling technique was applied to potential and fluid-structure problems. Applications of the method to elastostatics problems were relatively few.

Brebbia and Georgio [15] examined the coupling of BEM and FEM for two dimensional elastostatics problems using two different approaches. In both approaches, the boundary element and finite element equations were directly linked by the requirements of compatibility of displacements and equilibrium of forces at the interface. In the first approach the boundary element region was treated as an equivalent finite element, while in the second approach, the finite element region was treated as an equivalent boundary element. A non-symmetric boundary element stiffness matrix was obtained using the idea of virtual work rather than the energy functional. A few numerical examples were considered in order to examine the combined solution for two-dimensional elastostatics problems. A program was developed by the authors which combined constant boundary elements with quadratic finite elements and although the coupling technique was not fully compatible, it still gave good results in practice.

Kelly et al. [26] summarized different procedures for combining the boundary element method with the other numerical techniques. He applied the boundary element method to solve potential problems. A non-symmetric and a symmetric stiffness formulations were compared using quadratic shape functions. In one example the symmetric matrix gave better results than the non-symmetric one.

The method was also applied to fluid-structure interaction problems. Estofff and Autes [21] investigated a coupled fluid-structure system subjected to dynamics loads. Linear finite elements were used to model the linear elastic

structure while the adjacent fluid was represented by boundary elements. Numerical examples were presented to show how the method could be applied to fluid-structure interaction problems.

In geotechnical engineering, Brebbia [13] analyzed a two-dimensional soil-structure interaction problem using the coupling technique. Constant boundary elements were used to model the soil continuum, while the structure was discretized using finite elements. The coupling of boundary element and finite element stiffnessess were achieved in two ways. In the first method, the mid-nodes of the boundary elements were placed in such a way that they coincide with the finite element nodes along the interface. In the second method, the end points of the boundary elements were placed to coincide with the finite element nodes. In the later case the number of the nodes at the interface was greater than the number of equations by one.

A coupling technique based on the direct boundary element formulation was discussed by Ohtsu [32] for two-dimensional elastostatics problems. The technique was investigated by torsion and bending problems in reinforced concrete beams. Isoparametric element of quadratic shape function was utilized in the boundary element and finite element formulations. A reasonable agreement of displacements was observed when the results were compared with FEM results.

Hong and Dawkins [23] analyzed the behavior of a U-frame structure using the coupling technique. Finite elements were used to simulate the U-frame structure while the surrounding soil mass was modeled using boundary elements. Isoparametric quadrilateral finite elements and linear boundary elements were

used. The authors assumed that the horizontal displacements of the soil were negligible at a sufficient distance from the structure centerline while the vertical displacements were negligible at a certain depth below the ground surface.

It can be seen that a fair amount of work concerned with the combination of the boundary element and finite element methods has been carried out. However, there has been lack of work on complex structures (e.g. 3-D problems). In the above studies the application of coupling techniques (BEM-FEM) were limited to certain types of problems such as potential and 2-D elastostatics problems.

Application of the coupling technique to problems in plate bending appeared more recently by Ng, Cheung and Xu [31]. A non-composite slab on girders was analyzed. A plate bending boundary element was used to model the slab while beam elements were used to model the girders. They assumed that only vertical internal forces interact between the slab and the beam elements. These interaction forces were concentrated at particular nodes defined along the beams. Full compatibility was not achieved in this approach (only vertical deflection was compatible). Moreover, the method could not be used in composite bridges.

Komatsu and Nagai [27] analyzed thin walled box girders by combining the boundary element method with the Thin walled Segment Method (TSM).

The boundary element method was applied to regions with large stress gradient while the TSM was used in regions with small stress variations. A small portion of the girder was modeled by BEM while the remainder was analyzed by TSM. The authors assumed that the displacement field consisted only of two in-plane displacements (i.e. the rotations are not included as degrees of freedom). The compatibility conditions were satisfied only along the transverse sections (i.e. compatibility was not satisfied in the longitudinal direction), therefore, the method cannot be used as a general method to analyze different types of bridges.

Chapter 3

Boundary Element Equations

3.1 Introduction

The mathematical formulation of the boundary element method for flat shell elements which includes the composite action between slab and girders is presented. The development presented herein includes a review of the boundary element equations and the fundamental solutions for both plate bending and plane stress problems. The boundary integral equations are solved by dividing the boundary into a discrete number of elements and assuming interpolation functions for the unknowns. The integral equations for both bending and membrane actions are combined to form the flat shell element equations. Some numerical aspects involved in the boundary element formulation are presented in this chapter.

3.2 B.I.E For Plate Bending

The Boundary Integral Equations (BIE) of the plates can be established by applying the Betti-Maxwell reciprocal theorem.

Applying unit force and unit moment at the source point of each node and implementing the Betti-Maxwell theorem, two boundary integral equations can be written [1] and [38] as :

$$C_b w_p + \oint_s (WS^{fz} + \Theta M^{fz})ds = \iint_A q w^{fz} dA + \oint_s (SW^{fz} + M\Theta^{fz})ds \quad (3.1)$$

$$C_b \theta^{\xi}{}_p + \oint_s (WS^{m\xi} + \Theta M^{m\xi})ds = \iint_A q w^{m\xi} dA + \oint_s (SW^{m\xi} + M\Theta^{m\xi})ds \quad (3.2)$$

where

M and S are the moment and the shear force along the boundary respectively,

W and θ are the deflection and slope along the boundary respectively,

w_p and θ_p^{ξ} are the deflection and slope inside the plate respectively,

fz and m are superscripts referring to force and moment fundamental solutions,

q and A are the applied load and loaded area,

C_b is a parameter defining the location of the point p and

ξ is a parameter that gives the direction of the unit moment.

The positive directions of the boundary displacements and forces are shown in Figure 3.1.

If the boundaries have corners, then it is necessary to add the terms $\sum_{i=1}^{N_c} \Delta T_i W_i$ and $\sum_{i=1}^{N_c} \Delta T_i W_i$ to equations (3.1) and (3.2) as follows :

$$C_b w_p + \oint_s (WS^{fz} + \Theta M^{fz})ds + \sum_{i=1}^{N_c} W_i \Delta T_i^{fz} = \iint_a q w^{fz} dA + \oint_s (SW^{fz} + M\Theta^{fz})ds + \sum_{i=1}^{N_c} \Delta T_i w_i^{fz} \qquad (3.3)$$

$$C_b \theta^{\xi}_p + \oint_s (WS^{m\xi} + \Theta M^{m\xi})ds + \sum_{i=1}^{N_c} W_i \Delta T_i^{m\xi} = \iint_a q w^{m\xi} dA + \oint_s (SW^{m\xi} + M\Theta^{m\xi})ds + \sum_{i=1}^{N_c} \Delta T_i W_i^{m\xi} \qquad (3.4)$$

where N_c represents the number of the corners and ΔT denotes the effective corner force and it is given as :

$$\Delta T = T^+ - T^- \qquad (3.5)$$

T^+ and T^- are the twisting moments at the corner as shown in Figure (3.1).

3.2.1 Fundamental Solutions

The displacement at any point q in a plate caused by a unit concentrated force at the source point p is defined as a force fundamental solution and it is given by [38]:

$$w^{fz}(p,q) = \frac{r^2}{8\pi D}\ln(r) \tag{3.6}$$

where r is the distance between points q and p, as shown in Figure 3.2 and fz is a superscript referring to the force fundamental solution. Differentiating the force fundamental solution and substituting the results into plate bending equations, the expressions for slope, moment, shear and twisting moment can be obtained as :

$$\Theta^{fz}(p,q) = \frac{r\cos(\phi)}{8\pi D}(1+2\ln r) \tag{3.7}$$

$$M^{fz}(p,q) = -\frac{(1+\nu)(1+\ln)}{4\pi} - \frac{(1-\nu)\cos 2\phi}{8\pi} \tag{3.8}$$

$$S^{fz}(p,q) = -\frac{1}{4\pi r}[2\cos\phi + (1-\nu)(\cos\phi - \kappa r)\cos(2\phi)] \tag{3.9}$$

$$T^{fz}(p,q) = \frac{(1-\nu)}{4\pi}\sin\phi\cos\phi \tag{3.10}$$

where ϕ is the angle between r and the outward normal to the boundary at point q and κ is the curvature of the boundary at point q.

The second fundamental solution corresponds to a unit moment which can be obtained by differentiating equation (3.6) with respect to the coordinates of point p in the ξ-direction [38] ;

$$w^{m\xi}(p,q) = \frac{r}{4\pi D}\ln(r)\cos(\beta) \tag{3.11}$$

where β is the angle between ξ and r, see Figure 3.3. The expressions for slope, moment, shear and torsional moment are :

$$\Theta^{m\xi}(p,q) = \frac{1}{2\pi D}[\ln r\cos(\beta+\phi) + \cos\phi\cos\beta] \tag{3.12}$$

$$M^{m\xi}(p,q) = -\frac{1}{2\pi r}[(1+\nu)\cos\phi - (1-\nu)\sin(\beta)\sin(2\phi)] \tag{3.13}$$

$$\begin{aligned} S^{m\xi}(p,q) &= \frac{1}{2\pi r^2}[\{3-\nu-2(1-\nu)\sin^2\phi\}\cos(\phi+\beta) \\ &- 2(1-\nu)(\cos\phi-\kappa r)(\sin\beta\sin(2\beta)] \end{aligned} \tag{3.14}$$

$$T^{m\xi}(p,q) = \frac{(1-\nu)}{2\pi r}\cos(2\phi)\sin(\beta) \tag{3.15}$$

3.3 B.I.E For Plane Stress

The development of the Boundary Integral Equations (BIE) for plane stress problems follows the same procedure of the plate bending formulation and the body forces are neglected here for simplicity. Applying unit forces in x and y directions at the source points of each node, and implementing the Betti-Maxwell theorem, we obtain two integral equations for every node :

$$C_i u_p + \oint_s (u N_x{}^{fx} + v N_y{}^{fx}) ds = \oint_s (u^{fx} N_x + v^{fx} N_y) ds \qquad (3.16)$$

$$C_i v_p + \oint_s (u N_x{}^{fy} + v N_y{}^{fy}) ds = \oint_s (u^{fy} N_x + v^{fy} N_y) ds \qquad (3.17)$$

where C_i is the coefficient which may be determined by conditions of rigid body motion [14], u and v are the boundary displacements in x and y directions respectively, N_x and N_y are the boundary in-plane forces and f_x *and* f_y are superscripts identifying the fundamental solutions of the unit forces in the x and y directions respectively.

3.3.1 Fundamental Solutions

The fundamental solutions for a two-dimensional plane stress problem are known as the Kelvin fundamental solutions (see Fig. 3.4). The fundamental solutions for displacements are given as :

$$u^{fx}(p,q) = \frac{1}{8\pi G(1-\nu)}[(3-4\nu)\ln\frac{1}{r} + r_{,1}{}^2] \qquad (3.18)$$

$$v^{fy}(p,q) = \frac{1}{8\pi G(1-\nu)}[(3-4\nu)\ln\frac{1}{r} + r_{,2}{}^2] \qquad (3.19)$$

Cruse [20] gives the expression of the fundamental solutions for tractions using an indicial notation, i.e.

$$N^f{}_{ij}(p,q) = -\frac{(1-2\nu)}{4\pi r(1-\nu)}[\frac{\partial r}{\partial n}\{\delta_{ij} + \frac{2}{1-2\nu}r_{,i}r_{,j}\} - n_j r_{,i} + n_i r_{,j}] \qquad (3.20)$$

where $N_{ij}(p,q)$ corresponds to the traction in the x_i direction at q(x) due to the application of a unit force in the x_j direction at p(x) (e.g. when $i = j = 1$, $N_{11}{}^f(p,q) = N_x{}^{fx}(p,q)$), n is the normal to the boundary of the plate and δ_{ij} is the kroneckor delta (δ_{ij} =1 when $i = j$ and = 0 when $i \neq j$)

3.4 Discretization

In order to evaluate the integral equations (3.3), (3.4), (3.16) and (3.17) the boundary is divided into a discrete number of elements as shown in Figure 3.5. The boundary functions are expressed in terms of their nodal values using interpolation functions. The integrals in equation (3.16) are evaluated by summing up the contributions of all elements, thus equation (3.16) becomes:

$$C_i u_p + \sum_{i=1}^{N_E} \int_{si} (u(si)N_x{}^{fx} + v(si)N_y{}^{fx})dsi = \sum_{i=1}^{N_E} \int_{si} (N_x(si)u^{fx} + N_y(si)v^{fx})dsi \qquad (3.21)$$

where N_E is the number of elements and u(si), v(si), $N_x(si)$ and $N_y(si)$ are polynomial approximations of the boundary functions u, v, N_x and N_y.

The boundary functions are expressed in terms of their nodal values and inte-

gral equation (3.21) can be written as :

$$C_i u_p + \sum_{i=1}^{N_E} \int_{si} (N_x{}^{fx}[\sum_{j=1}^{N_N} L_j u_j] + N_y{}^{fx}[\sum_{j=1}^{N_N} L_j v_j])dsi = \sum_{i=1}^{N_E} \int_{si} (u^{fx}[\sum_{j=1}^{N_N} L_j N_{xj}] + v^{fx}[\sum_{j=1}^{N_N} L_j N_{yj}])dsi \quad (3.22)$$

N_N is the number of nodes per element and L_j is the shape function for node j (Lagrangian).

In a similar way, the integral equations (3.3), (3.4) and (3.17) can be written as :

$$C_i v_p + \sum_{i=1}^{N_E} \int_{si} (N_x{}^{fy}[\sum_{j=1}^{N_N} L_j v_j] + N_y{}^{fy}[\sum_{j=1}^{N_N} L_j v_j])dsi = \sum_{i=1}^{N_E} \int_{si} (u^{fy}[\sum_{j=1}^{N_N} L_j N_{xj}] + v^{fy}[\sum_{j=1}^{N_N} L_j N_{yj}])dsi \quad (3.23)$$

$$C_b w_p + \sum_{i=1}^{N_E} \int_{si} (S^{fz}[\sum_{j=1}^{N_N} L_j W_j] + M^{fz}[\sum_{j=1}^{N_N} L_j \theta_j])dsi + \sum_{i=1}^{N_c} W_i \Delta T_i{}^{fz} = \int\int_A q w^{fz} dA + \sum_{i=1}^{N_E} \int_{si} (W^{fz}[\sum_{j=1}^{N_N} L_j S_j] + \theta^{fz}[\sum_{j=1}^{N_N} L_j M_j])dsi + \sum_{i=1}^{N_c} W_i{}^{fz} \Delta T_i \quad (3.24)$$

$$C_b \theta^m{}_p + \sum_{i=1}^{N_E} \int_{si} (S^m[\sum_{j=1}^{N_N} L_j W_j] + M^m[\sum_{j=1}^{N_N} L_j \theta_j])dsi + \sum_{i=1}^{N_c} W_i \Delta T_i{}^m = \int\int_A q w^m dA + \sum_{i=1}^{N_E} \int_{si} (W^m[\sum_{j=1}^{N_N} L_j S_j] + \theta^m[\sum_{j=1}^{N_N} L_j M_j])dsi + \sum_{i=1}^{N_c} W_i{}^m \Delta T_i \quad (3.25)$$

3.5 Evaluation of the B.I.E

The accuracy of the BEM results depends directly on the accuracy of the integration technique. To deal with the singular integrals, which appear when evaluating the boundary integral equations, special techniques are applied either to evaluate them analytically or to transform them so that they can be integrated numerically. The integrations of the plate bending equations are performed analytically. In this thesis the same analytical expressions developed by [1] for the evaluation of the boundary integral equations are used. Details of these equations can be found in the same reference. The analytical integrations are used to reduce the difficulties associated with the numerical integrations. In addition to that, the integral equations which include singular terms are evaluated by placing the source points at small distance outside the domain of the plate. The suitable location of the source points is provided later in this chapter.

In plane stress equations, the integrations are performed numerically. When the source point $(x_p,\ y_p)$ is not considered as a node of the element $(x_q,\ y_q)$, the distance r is not equal to zero, therefore, the integration can be performed simply by using Gaussian quadrature.

If the source point (x_p, y_p) is too close to, or coincides with, the field point (x_q, y_q), which is a Gauss point, then a singularity may occur in the fundamental solution equations which include the terms $\ln \frac{1}{r}$ and $\frac{1}{r}$. A mathematical approach can be employed in order to evaluate the integrals which contain sin-

gular terms. The basic concept of this approach is to divide the integral into two parts. The first part contains the singular terms which can be evaluated by special numerical techniques, while the second part contains the regular terms which can be evaluated by means of Gauss quadrature formula.

These integrals with u^j and v^j which include the singular terms can be written in a simple form as follow :

$$\int_{si} f(\ln \frac{1}{r}) L(\xi) J(\xi) d\xi \tag{3.26}$$

Equation(3.26) can be integrated using a special Gauss quadrature formula with logarithmic weighting function, i.e.

$$\int_0^1 f(\xi) \ln \frac{1}{\xi} d\xi \simeq \sum_{i=1}^{n} W_i f(\xi_i) \tag{3.27}$$

where the integration point coordinates ξ_i and the weighting factors W_i are given in reference [39].

In equation (3.26), the integral is a function of $\ln \frac{1}{r}$ not $\ln \frac{1}{\xi}$ and in order to use the logarithmic Gauss formula, a new system of coordinates is established as described next.

Consider a quadratic element with intrinsic coordinates $\xi = -1$, $\xi = 0$ and $\xi = 1$ as shown in Figure 4.1. When the source point is the first or the third node of the element, the interval $-1 \leq \xi \leq +1$ can be transformed into $0 \leq \eta \leq 1$, where $\eta = \frac{1+\xi}{2}$ for the first node and $\eta = \frac{1-\xi}{2}$ for the third node.

Substituting $R = \frac{r}{l}$, where l is the length of the boundary element si. Equation

(3.26) can be written as:

$$\int_{si} \ln \frac{1}{Rl} L(\xi) J(\xi) d\xi = \int_0^1 \ln \frac{1}{R} L(\xi(R)) \frac{\partial \xi}{\partial R} J(\xi) dR + \int_{-1}^{+1} \ln \frac{1}{l} L(\xi) J(\xi) d\xi \tag{3.28}$$

The first part of equation (3.28) can be integrated using equation (3.27) while the second part is simply integrated by Gauss-Legendre's method.

When the source point is the second node, the element is divided into two sub-elements, (Fig. 3.7). For the first sub-element, the interval $-1 \leq \xi \leq 0$ can be transformed into $0 \leq \eta_1 \leq 1$, where $\eta_1 = 1 + \xi$, while for the second sub-element the integration can be carried out by transforming the interval $0 \leq \xi \leq +1$ into $0 \leq \eta_2 \leq 1$ and setting $\eta_2 = \xi$.

All the integrals involving $N_x{}^f$ or $N_y{}^f$ are function of the term $\frac{1}{r}$. These integrals existed in the same sense of the Cauchy principle value for which there is no suitable quadrature formula to evaluate them. These integrals are evaluated by using the idea of rigid body motions [14].

3.6 Interior Point Solution

The displacements and stresses at any internal point of the domain can be calculated using equations (3.22) to (3.25) with $C_i = C_b = 1$.

For in-plane action, the discretized forms of the boundary integral equations

for displacements can be written as:

$$u_p = \sum_{i=1}^{N_E} \int_{si} (u^{fx}[\sum_{j=1}^{N_N} L_j N_{xj}] - N_x{}^{fx}[\sum_{j=1}^{N_N} L_j u_j])dsi + \sum_{i=1}^{N_E} \int_{si} (v^{fx}[\sum_{j=1}^{N_N} L_j N_{yj}] - N_y{}^{fx}[\sum_{j=1}^{N_N} L_j v_j])dsi \quad (3.29)$$

$$v_p = \sum_{i=1}^{N_E} \int_{si} (u^{fy}[\sum_{j=1}^{N_N} L_j N_{xj}] - N_x{}^{fy}[\sum_{j=1}^{N_N} L_j v_j])dsi + \sum_{i=1}^{N_E} \int_{si} (v^{fy}[\sum_{j=1}^{N_N} L_j N_{yj}] - N_y{}^{fy}[\sum_{j=1}^{N_N} L_j v_j])dsi \quad (3.30)$$

The internal stresses can be computed by differentiating the displacements at the internal points with respect to the coordinates at $p(x)$ and subsequentley applying Hook's Law. The stress at internal points can be written in a compact form as [12] :

$$\sigma_{ij}(p) = \int_{si} [D_{kij}(p,q)P_k(q) - S_{kij}(p,q)U_k(q)]dsi + \int_R D_{kij}q_k dR \quad (3.31)$$

where

$$D_{kij}(p,q) = \frac{1}{4\pi r(1-\nu)}[(1-2\nu)\{\delta_{ki}r_{,j} + \delta_{kj}r_{,i} - \delta_{ij}r_{,k}\} + 2r_{,i}r_{,j}r_{,k}] \quad (3.32)$$

and

$$S_{kij}(p,q) = \frac{G}{2\pi r^2(1-\nu)}[2\frac{\partial r}{\partial n}\{(1-2\nu)\delta_{ij}r_{,k} + \nu(\delta_{ik}r_{,j} + \delta_{jk}r_{,i}) - 4r_{,i}r_{,j}r_{,k}\} + 2\nu(n_i r_{,j}r_{,k} + n_j r_{,i}r_{,k}) + (1-2\nu)(2n_k r_{,i}r,j + n_j\delta_{ik} + n_i\delta_{jk}) - (1-4\nu)n_k\delta_{ij}] \quad (3.33)$$

Equation (3.31) is known as the Somigliana's identity for the stress and it gives the value of the stress at any interior point of the domain. The integrals in

equations (3.29) to (3.31) are not singular because the distance r is never equal to zero. The integrals can be evaluated directly using Gauss quadrature.

For the bending action, the moments are obtained from the second derivative of the deflection [1] ;

$$\{M\}_p = D\{\sum_{i=1}^{N_E}\int_{si}[T^2](W_{,2}S(si)+\Theta_{,2}M(si)-M_{,2}\Theta(si)-S_{,2}W(si))ds + \iint_A qw_{,2}dA+\sum_{i=1}^{N_c}(\{W_{,2}\}_i\Delta T_i-\{\Delta T_{,2}\}_iW_i)\} \quad (3.34)$$

where T is a transformation matrix which includes the direction cosines of ξ with respect to the tangential and normal axes and ,2 is referring to the second derivative of the boundary variables with respect to the coordinates of the source point (x_p, y_p).

The shear force can be obtained from the third derivatives of the deflection, i.e.

$$\{Q\}_p = -D\left\{\sum_{i=1}^{N_e}\int_{si}[T^3](W_{,3}S(si)+\Theta_{,3}M(si)-M_{,3}\Theta(si)-S_{,3}W(si))ds\right\} -D\left\{+\iint_A qw_{,3}dA+\sum_{i=1}^{N_c}(\{W_{,3}\}_i\Delta T_i-\{\Delta T_{,3}\}_iW_i)\right\} \quad (3.35)$$

All the second and third derivatives quantities involved in equations (3.34) and (3.35) are given in reference [1].

3.7 Boundary conditions

When the combined solution is used for analyzing bridges, double nodes are used. Both nodes have the same coordinates, but may have different boundary

conditions. The nodes along the interface (see Fig. 3.8) including the corner node (e.g. C1) have eight boundary variables which are all unknowns (e.g., u, v, W, Θ, N_x, N_y, S and M). The other corner node which belongs to the supported edge (e.g. C2) has only four boundary variables.

At the corner where the traction is discontinuous, the displacements and tractions at the two nodes (C1 and C2) are treated as independent quantities. In order to make the number of unknowns at nodes C1 and C2 equal to the number of boundary integral equations, the corner forces at the two nodes are expressed in terms of their normal rotations on their respective elements, i.e.

$$\Delta T_{C1} = D(1-\nu)(\frac{\partial^2 w}{\partial s \partial n})^{(1)} = D(1-\nu)\sum_{j=1}^{N_{n1}} \frac{\partial L_j^{(1)}}{\partial s}\theta_j \qquad (3.36)$$

$$\Delta T_{C2} = D(1-\nu)(\frac{\partial^2 w}{\partial s \partial n})^{(2)} = -D(1-\nu)\sum_{j=1}^{N_{n2}} \frac{\partial L_j^{(2)}}{\partial s}\theta_j \qquad (3.37)$$

where L_j is the Lagrenge shape function of node j, (1) and (2) are superscripts referring to the elements ending at node $C1$ and starting at node $C2$ respectively and N_{n1} and N_{n2} are number of nodes at elements 1 and 2 respectively.

At the plate edge, four external boundary conditions, either for boundary displacements, or forces are specified as follows :

1. u = v = W = Θ = 0 on a clamped edge.

2. u or v = W = 0 and N_x or N_y = M = 0 on a simply supported edge.

3. $N_x = N_y$ = V = M = 0 on a free edge.

3.8 Location of the Source Point

As mentioned in section 3.5, when the integrals were evaluated analytically, the source points were located outside the domain of the plate to avoid the singular terms such as $\ln(r)$ and $\frac{1}{r}$. This idea was first presented by Totenham [43] and recently by Abdel-Akher [1]. The source points are located at a small distance "d" from the boundary of the plate at a specific boundary node (see Fig. 3.9). The determination of the distance "d" can be related to the geometry of the plate. In addition, the value of "d" should be chosen as large as possible. The location of source points was suggested by Abdel-Akher [1] at a distance equal to $\frac{a}{10,000}$, where , a , is the average distance between the nodes. The author found this value is very small and it had considerable effect on the result of the shear, therefore, the value of "d" should be greater to give a uniform distribution of the shear along the boundary. For the program developed in this study, the value of "d" was specified as 0.2 L, where L is the distance between two consecutive nodes in the element. One example will be provided in Chapter 5 to show the effect of "d" on the results.

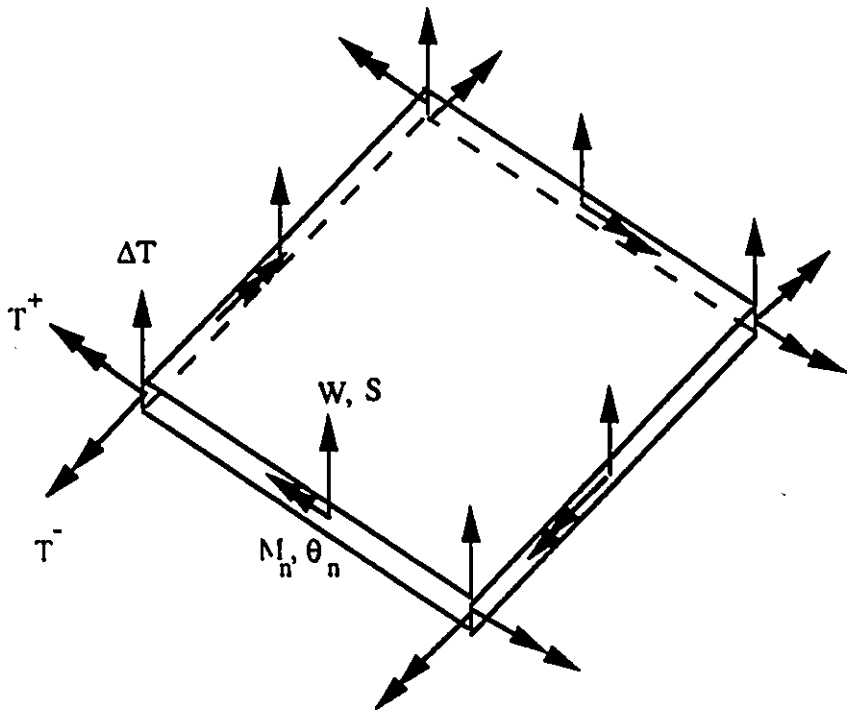

Figure 3.1 Direction of displacements and forces along the boundaries.

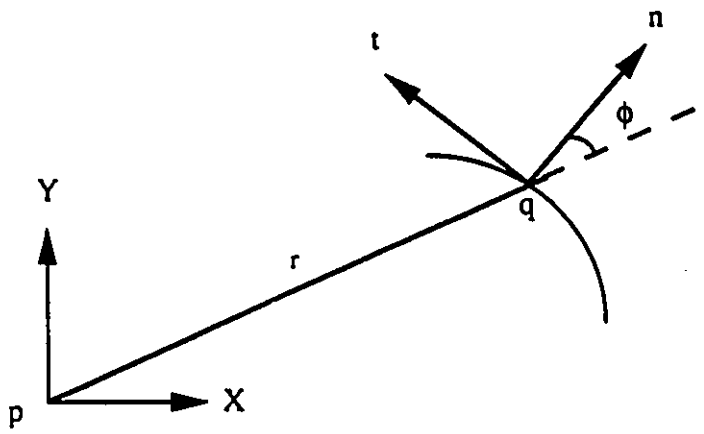

Figure 3.2 The source point p and the integration point q .

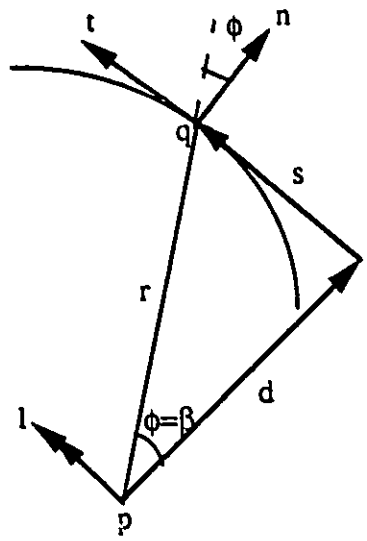

a) A unit moment in n direction

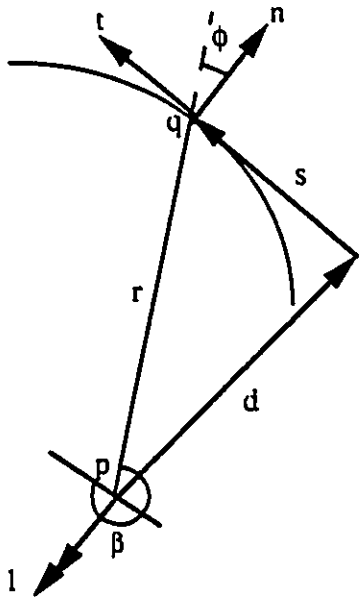

b) A unit moment in t direction

Figure 3.3 Directions of the unit moment .

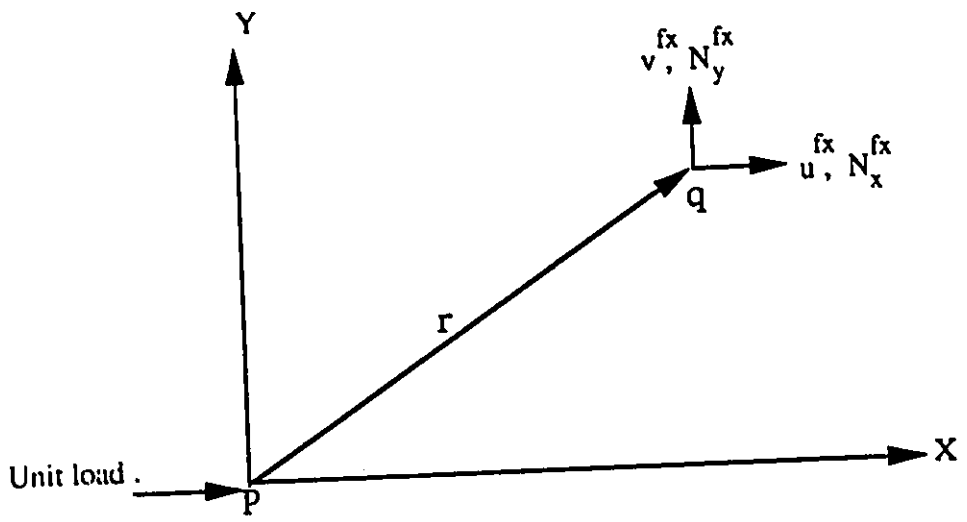

Figure 3.4 Fundamental solution for plane stress problems (Kelvin Solution)

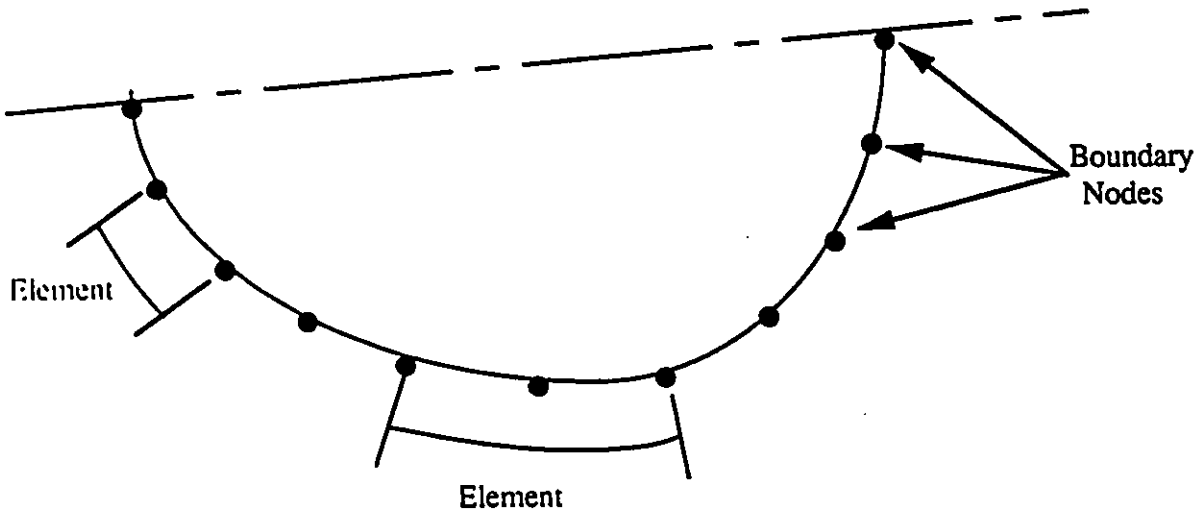

Figure 3.5 Boundary discretization.

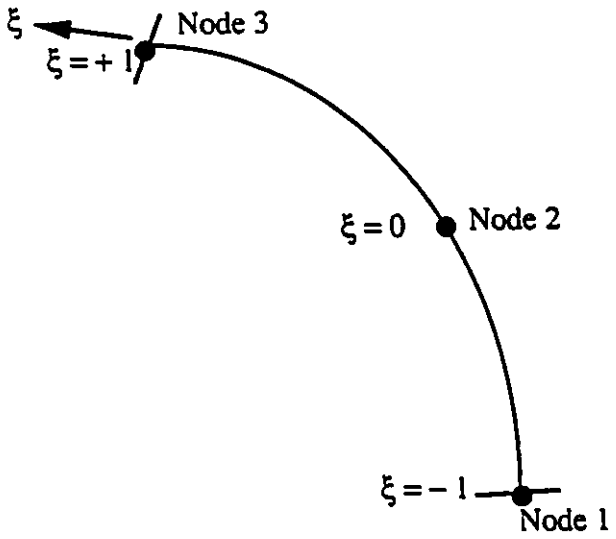

Figure 3.6 A quadratic element.

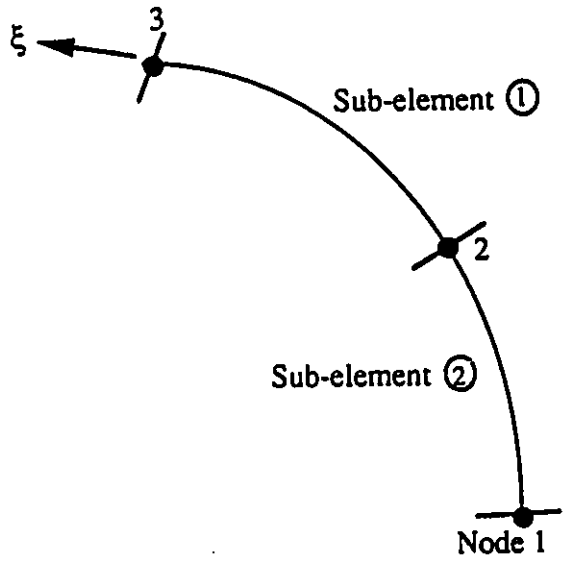

Figure 3.7 An element divided into two sub-elements.

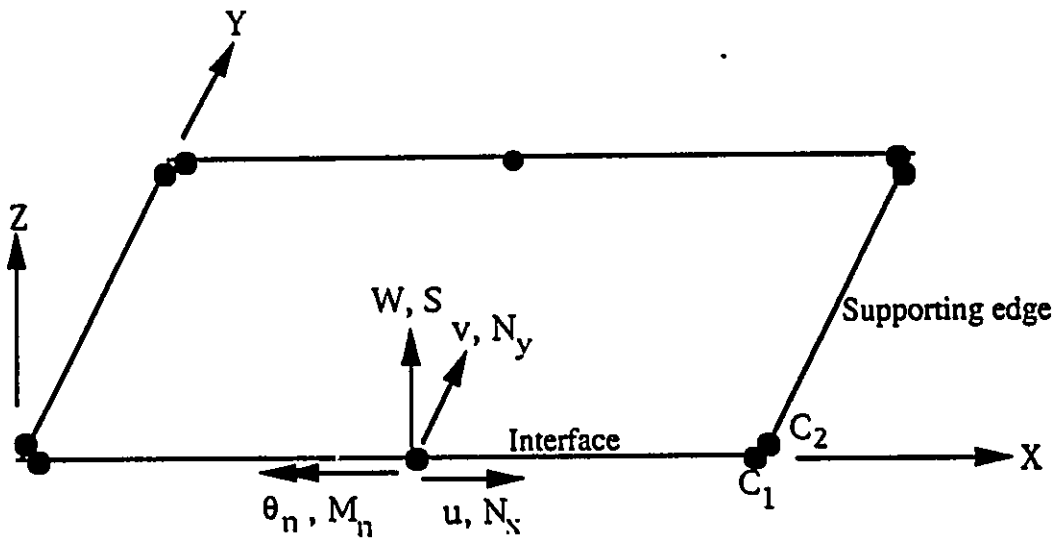

Figure 3.8 Degrees of freedom along the interface.

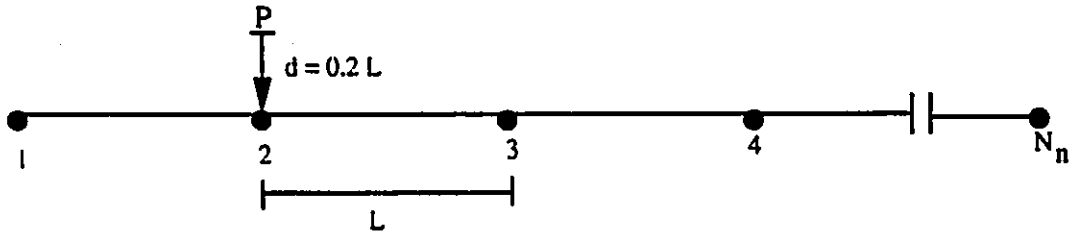

Figure 3.9 The location of the source point outside the domain

Chapter 4

Coupling of BEM and FEM

4.1 Introduction

The mathematical formulation of the coupling technique between boundary and finite elements is developed in this chapter. The approach that is used in this thesis, is to treat a finite element region (i.e. girders) as an equivalent boundary element and combining it with the other boundary element region (i.e. slab). The two regions are connected at a number of nodes (interface). For the finite element region, a static condensation technique is implemented so that the degrees of freedom at the interface are condensed to the same degrees of freedom of the corresponding boundary element region. Then both stiffness matrices of boundary element and finite element methods are assembled in a global matrix and by satisfying the equilibrium and compatibility condi-

tions, one can write the system of equations which can be solved by imposing prescribed boundary conditions.

The combined solution (BEM-FEM) can be applied to different types of bridges. Two different cases will be considered in this thesis. In the first case, the compatibility and equilibrium conditions will be satisfied between two interfaces (i.e. slab and girders), and between three interfaces (i.e. slab, girders and overhangs) in the second case. In both cases the top slab will be modeled using BEM while the FEM is used to model the girders and the bottom slab. The combined solution will be presented in the following sections.

4.2 Finite Element Equations

The FEM is used to model the girders because their geometry is less regular compared to the slab. Linear flat shell elements with four nodes and quadratic flat shell elements with eight or nine nodes are employed in the finite element program (see Fig. 4.2). The use of higher order elements is attractive from an accuracy point of view; however, their use increases the number of degrees of freedom and makes the connectivity of the coupling much more complex.

The formulation of flat shell element is available in references [18] and [45], therefore, only a brief review is presented here.

The flat shell element is the combination of a plate bending element and a membrane element. Consider a flat shell element subjected simultaneously to

in-plane and bending actions as shown in Figure (4.1). For in-plane action, the stiffness matrix can be written as

$$\{f^i\} = [k^i]\{d^i\}$$

where i refers to the in-plane action,

$$\{d^i\} = \begin{Bmatrix} u \\ v \end{Bmatrix} \tag{4.1}$$

and

$$\{f^i\} = \begin{Bmatrix} f_x \\ f_y \end{Bmatrix} \tag{4.2}$$

similarly, for the bending action, the stiffness matrix can be written as:

$$\{f^b\} = [k^b]\{d^b\}$$

Where b refers to the bending action,

$$\{d^b\} = \begin{Bmatrix} w \\ \theta_x \\ \theta_y \end{Bmatrix} \tag{4.3}$$

and

$$\{f^b\} = \begin{Bmatrix} f_z \\ M_x \\ M_y \end{Bmatrix} \tag{4.4}$$

By combining the nodal displacements and forces for both actions, the stiffness matrix for the flat shell element can be written as:

$$\begin{Bmatrix} f_x \\ f_y \\ f_z \\ M_x \\ M_y \end{Bmatrix} = \begin{bmatrix} k^i & 0 \\ 0 & k^b \end{bmatrix} \begin{Bmatrix} u \\ v \\ w \\ \theta_x \\ \theta_y \end{Bmatrix} \tag{4.5}$$

Transformation of displacement and force components from local coordinates $\bar{x}$ $\bar{y}$ $\bar{z}$ to the global coordinates x y z (Fig. 5.3) is carried out as follow :

$$\{d\}_G = [T]\{d\}_L$$

$$\{f\}_G = [T]\{f\}_L$$

in which [T] is the transformation matrix and G and L refer to the global and local systems respectively.

$$[T] = \begin{bmatrix} r & 0 \\ 0 & r \end{bmatrix} \tag{4.6}$$

and

$$r = \begin{bmatrix} \cos\theta x\bar{x} & \cos\theta x\bar{y} & \cos\theta x\bar{z} \\ \cos\theta y\bar{x} & \cos\theta y\bar{y} & \cos\theta y\bar{z} \\ \cos\theta z\bar{x} & \cos\theta z\bar{y} & \cos\theta z\bar{z} \end{bmatrix} \tag{4.7}$$

where $\theta x\bar{x}$ is the angle between x and $\bar{x}$ axes. The final result of the transformation is:

$$[K]_G = [T^T]\,[K]_L\,[T] \tag{4.8}$$

Once the stiffness matrices of all elements have been transformed into the global coordinates system, it is ready to be assembled into overall stiffness matrix in the conventional manner. The finite element matrix can be rearranged according to the interface degrees of freedom as follow :

$$\begin{bmatrix} K_{11} & K_{12} \\ K_{21} & K_{22} \end{bmatrix} \begin{Bmatrix} d_I \\ d \end{Bmatrix} = \begin{Bmatrix} f_I \\ f \end{Bmatrix} \tag{4.9}$$

where d_I and f_I contain only the displacements (u, v, w and θ_n) and forces (f_x, f_y, f_z and M_n) along the interface I.

A static condensation procedure using Gauss elimination is applied to condense the non-interface degrees of freedom. This process is used to reduce the size

of the global stiffness matrix, therefore, equation (4.9) becomes ;

$$[K_I]\{d_I\} = \{f_I\} \tag{4.10}$$

The size of the stiffness matrix now is equal to 4 $N_{in} \times 4$ N_{in} where N_{in} is the number of connecting nodes (interface nodes).

4.3 Boundary Element Equations

The boundary integral equations presented in Chapter 3 are evaluated by adding the contribution of all elements, then the expressions of the fundamental solutions are substituted into the boundary integral equations for all boundary nodes.

If the integral equations are arranged according to displacement terms and force terms then these equations can be written in matrix form as :

$$[H]\begin{Bmatrix} u \\ v \\ w \\ \theta_n \end{Bmatrix} = [G]\begin{Bmatrix} N_x \\ N_y \\ S \\ M \end{Bmatrix} + \{B\} \tag{4.11}$$

where [H] and [G] are coefficient matrices corresponding to the displacements and forces respectively,

$\{B\}$ is the domain integral.

In order to obtain the solution for the unknown boundary variables, the boundary conditions are substituted into equation (4.11). Multiplying the known boundary variables (displacements or forces) with the corresponding coefficients, the right hand side vector may be formed by adding the contribution of the domain integral. The unknown boundary variables are multiplied by their coefficients and placed in the left hand side to form the matrix A, i.e.

$$[A]\{X\} = \{F\} \tag{4.12}$$

Where

$[A]$ is a matrix contains the results of the integrations corresponding to the unknown boundary variables,

$\{X\}$ is a vector containing the unknown boundary variables and

$\{F\}$ is the contribution of the coefficients corresponding to known boundary variables and the domain integral.

Once equation (4.12) is solved all the boundary variables are found.

4.4 Description of Coupling Theory

4.4.1 Case I

In the case I, the solution will be developed for slab-on-girder and box girder bridges without overhangs (i.e. two interfaces). Consider a problem of slab on two girders consisting of two domains, R_1 and R_2, joined by interfaces I_1, and I_2, and which makes use of a boundary element formulation in R_1 and a finite element formulation in R_2 as shown in Figure 4.4.

For region 1, the final expression for boundary element equation is given by equation 4.11 as :

$$[H]\{U\} = [G]\{P\} + \{B\} \tag{4.13}$$

The boundary displacement vector $\{U\}$, and the traction vector $\{P\}$ can be divided into U_b and P_b (non-interface degrees of freedom) and U_{b1}, U_{b2}, P_{b1}, and P_{b2} (interface degrees of freedom). Therefore, the boundary element equation can be written as :

$$[H_{b1}]\{U_{b1}\}+[H_b]\{U_b\}+[H_{b2}]\{U_{b2}\} = [G_{b1}]\{P_{b1}\}+[G_b]\{P_b\}+[G_{b2}]\{P_{b2}\}+\{B\} \tag{4.14}$$

where b_1 and b_2 represent the boundary interfaces 1 and 2 respectively.

For region 2, the FE equations for the girders are given by equation (4.10) as :

$$[K_{g1}]\{d_{g1}\} = \{f_{g1}\} \tag{4.15}$$

$$[K_{g2}]\{d_{g2}\} = \{f_{g2}\} \tag{4.16}$$

where g_1 and g_2 represent the first and the second girder interfaces, $[K_g]$ and $\{d_g\}$ are the stiffness matrix and the displacement vector corresponding to the interface degrees of freedom, which are obtained using the condensation technique described in section 4.2.

As we can see from the above equations, the BEM works with the tractions while the FEM works with the equivalent forces concentrated at the nodes. Therefore, in order to combine the finite element equations with the boundary element equations, one must substitute the nodal forces "f" in terms of the traction "P" i.e.

$$\{f\} = \left[\ M\ \right]\{P\} \tag{4.17}$$

where [M] is a distribution matrix which transforms the traction P into equivalent consistent nodal forces, and it is expressed by the following formula :

$$[M] = \int_{si} \{L_1\}^T \{L_2\} dsi = \int_{-1}^{+1} \{L_1\}^T \{L_2\} |J|\ d\xi \tag{4.18}$$

where $\{L_1\}$ and $\{L_2\}$ are vectors including the interpolation functions for displacements and forces respectively and $|J|$ is the Jacobian.

For example, for the linear element, the shape function either for the displacement or the force is given as:

$$\{L\} = [\ \tfrac{1}{2}(1-\xi)\quad \tfrac{1}{2}(1+\xi)]$$

and

$$|J| = \frac{1}{2}\sqrt{(x_2-x_1)^2+(y_2-y_1)^2}$$

A Subroutine, called MMAT, is written to calculate the M matrix which can be used to handle high order elements using Lagrange interpolation function (up to 10 nodes in each element).

The compatibility of displacements and forces equilibrium conditions at the interfaces I_1 and I_2 require that the displacements at the interface between the slab and girders must be equal. Also the sum of the forces at each interface must be equal to zero, i.e.

$$\begin{Bmatrix} u_{b1} \\ v_{b1} \\ W_{b1} \\ \theta_{b1} \end{Bmatrix} = \begin{Bmatrix} u_{g1} \\ v_{g1} \\ w_{g1} \\ \theta_{g1} \end{Bmatrix},$$

$$\left\{ \begin{array}{c} u_{b2} \\ v_{b2} \\ W_{b2} \\ \theta_{b2} \end{array} \right\} = \left\{ \begin{array}{c} u_{g2} \\ v_{g2} \\ w_{g2} \\ \theta_{g2} \end{array} \right\},$$

$$\left\{ \begin{array}{c} (N_x)_{b1} \\ (N_y)_{b1} \\ S_{b1} \\ M_{b1} \end{array} \right\} + \left\{ \begin{array}{c} (N_x)_{g1} \\ (N_y)_{g1} \\ S_{g1} \\ M_{g1} \end{array} \right\} = 0.$$

and

$$\left\{ \begin{array}{c} (N_x)_{b2} \\ (N_y)_{b2} \\ S_{b2} \\ M_{b2} \end{array} \right\} + \left\{ \begin{array}{c} (N_x)_{g2} \\ (N_y)_{g2} \\ S_{g2} \\ M_{g2} \end{array} \right\} = 0.$$

By satisfying the compatibility and equilibrium conditions at both interfaces, displacements and forces at each interface can be written as :

$$U_b = U_g = U_I = \left\{ \begin{array}{c} u_I \\ v_I \\ W_I \\ \theta_I \end{array} \right\}$$

and

$$P_b = -P_g = P_I = \begin{Bmatrix} (N_x)_I \\ (N_y)_I \\ S_I \\ M_I \end{Bmatrix}$$

Substitute the above conditions into equations 5.14 to 5.16 ;

$$[H_{I1}]\{U_{I1}\}+[H_b]\{U_b\}+[H_{I2}]\{U_{I2}\} = [G_{I1}]\{P_{I1}\}+[G_b]\{P_b\}+[G_{I2}]\{P_{I2}\}+\{B\} \tag{4.19}$$

$$K_{I1}U_{I1} = -M_{I1}P_{I1} \tag{4.20}$$

$$K_{I2}U_{I2} = -M_{I2}P_{I2} \tag{4.21}$$

Equations (4.19) to (4.21) can be coupled in a single matrix equation as :

$$\begin{bmatrix} H_{I1} & H_b & H_{I2} & -G_{I1} & -G_{I2} \\ K_{I1} & 0 & 0 & M_{I1} & 0 \\ 0 & 0 & K_{I2} & 0 & M_{I2} \end{bmatrix} \begin{Bmatrix} U_{I1} \\ U_b \\ U_{I2} \\ P_{I1} \\ P_{I2} \end{Bmatrix} = [G_b]\{P_b\} + \{B\} \tag{4.22}$$

The size of the equation system is $(4\ N_n + 8N_{in}) \times (4N_n + 8N_{in})$

where N_n is the total number of nodes in the slab and N_{in} is the number of the nodes along the interface. After imposing the boundary conditions, the

above equation is rearranged and written as follows :

$$\begin{bmatrix} A_{I1} & A & A_{I2} & -G_{I1} & -G_{I2} \\ K_{I1} & 0 & 0 & M_{I1} & 0 \\ 0 & C & K_{I2} & 0 & M_{I2} \end{bmatrix} \begin{Bmatrix} X_{I1} \\ X \\ X_{I2} \\ P_{I1} \\ P_{I2} \end{Bmatrix} = \{Y\} \qquad (4.23)$$

where X_{I1} and X_{I2} include the unknown displacements along the interfaces (e.g. u, v, w and θ_n),

P_{I1}, P_{I2} represent the unknown forces along the interfaces 1 and 2 (e.g. N_x, N_y, V *and* M) and

X represents the unknowns at the supported edges of the bridge.

Equation (4.23) now can be solved for all boundary unknowns, including the interface unknowns. Then these nodal displacements and forces can be employed in the boundary element equations to calculate the displacements and stresses at any internal points.

4.4.2 Case II

In this case, the coupling technique of BEM and FEM is proposed to model slab-on-girder and box girder bridges with overhangs. (i.e. three interfaces). To illustrate the coupling technique, consider a single box girder bridge with overhangs as shown in Figure (4.5). The boundary element method is used

to model the top slab and the overhangs, while the webs and bottom slab are modeled using the finite element method.

The boundary element equations can be written as :

For plate 1

$$H_{s1}U_{s1} + H_sU_s + H_{s2}U_{s2} = G_{s1}P_{s1} + G_sP_s + G_{s2}P_{s2} + B_1 \tag{4.24}$$

For plate 2

$$H_{s3}U_{s3} + H_sU_s = G_{s3}P_{s3} + G_sP_s + B_2 \tag{4.25}$$

For plate 3

$$H_{s4}U_{s4} + H_sU_s = G_{s4}P_{s4} + G_sP_s + B_3 \tag{4.26}$$

Equations (4.25) and (4.26) can be condensed after imposing the boundary conditions to include only the unknowns corresponding to the interface. Thus equations (5.25) and (5.26) can be written as :

$$H^*_{s3}U^*_{s3} = G^*_{s3}P^*_{s3} \tag{4.27}$$

$$H^*_{s4}U^*_{s4} = G^*_{s4}P^*_{s4} \tag{4.28}$$

where the star denotes matrices derived from the static condensation in equations 4.25 and 4.26.

The finite element equation can be obtained from the assembly of the finite element matrices of both webs and bottom slab after transferring their stiffness matrices to the global system. The overall stiffness matrix then can be reduced to include only the degrees of freedom of both interfaces (i.e. I_1 and I_2) using a static condensation technique, which gives :

$$[K_{g1}K_{g2}]\left\{\begin{array}{c} U_{g1} \\ U_{g2} \end{array}\right\} = [M_{g1}M_{g2}]\left\{\begin{array}{c} P_{g1} \\ P_{g2} \end{array}\right\} \tag{4.29}$$

where g_1 and g_2 are subscripts which represent the interfaces 1 and 2 respectively.

The compatibility and equilibrium conditions at the interfaces can be written as :

$$\left\{\begin{array}{c} u_{s1} \\ v_{s1} \\ W_{s1} \\ \theta_{s1} \end{array}\right\} = \left\{\begin{array}{c} u_{s3} \\ v_{s3} \\ W_{s3} \\ \theta_{s3} \end{array}\right\} = \left\{\begin{array}{c} u_{g1} \\ v_{g1} \\ W_{g1} \\ \theta_{g1} \end{array}\right\} = \left\{\begin{array}{c} u_{I1} \\ v_{I1} \\ W_{I1} \\ \theta_{I1} \end{array}\right\},$$

$$\left\{\begin{array}{c} u_{s2} \\ v_{s2} \\ W_{s2} \\ \theta_{s2} \end{array}\right\} = \left\{\begin{array}{c} u_{s4} \\ v_{s4} \\ W_{s4} \\ \theta_{s4} \end{array}\right\} = \left\{\begin{array}{c} u_{g2} \\ v_{g2} \\ W_{g2} \\ \theta_{g2} \end{array}\right\} = \left\{\begin{array}{c} u_{I2} \\ v_{I2} \\ W_{I2} \\ \theta_{I2} \end{array}\right\},$$

$$\left\{\begin{array}{c} (N_x)_{s1} \\ (N_y)_{s1} \\ S_{s1} \\ M_{s1} \end{array}\right\} + \left\{\begin{array}{c} (N_x)_{s3} \\ (N_y)_{s3} \\ S_{s3} \\ M_{s3} \end{array}\right\} + \left\{\begin{array}{c} (N_x)_{g1} \\ (N_y)_{g1} \\ S_{g1} \\ M_{g1} \end{array}\right\} = 0.$$

and

$$\left\{\begin{array}{c}(N_x)_{s2}\\(N_y)_{s2}\\S_{s2}\\M_{s2}\end{array}\right\}+\left\{\begin{array}{c}(N_x)_{s4}\\(N_y)_{s4}\\S_{s4}\\M_{s4}\end{array}\right\}+\left\{\begin{array}{c}(N_x)_{g2}\\(N_y)_{g2}\\S_{g2}\\M_{g2}\end{array}\right\}=0.$$

In order to reduce the size of the total global matrix, the unknown forces of the finite element region (e.g. P_{g1} and P_{g2}) can be written as a function of the unknown forces of boundary element region (e.g. P_{s1}, P_{s2}, P_{s3} and P_{s4}). Therefore, the above equilibrium equations can be written as :

$$P_{g1}=-(P_{s1}+P_{s3})$$

$$P_{g2}=-(P_{s2}+P_{s4})$$

Substituting the compatibility and equilibrium equations into equation (4.29), we get

$$[K_{g1}K_{g2}]\left\{\begin{array}{c}U_{I1}\\U_{I2}\end{array}\right\}=[-M_{g1}-M_{g2}-M_{g1}-M_{g2}]\left\{\begin{array}{c}P_{s1}\\P_{s2}\\P_{s3}\\P_{s4}\end{array}\right\} \qquad (4.30)$$

Now equations, (4.24), (4.27), (4.28) and (4.30) can be represented in a single

matrix expression and after imposing the boundary conditions, we get

$$\begin{bmatrix} A_{I1} & A_s & A_{I2} & -G_{s1} & -G_{s2} & 0 & 0 \\ A^*_{s3} & 0 & 0 & 0 & 0 & -G^*_{s3} & 0 \\ 0 & 0 & A^*_{s4} & 0 & 0 & 0 & -G^*_{s4} \\ K_{g1} & 0 & K_{g2} & M_{g1} & M_{g2} & M_{g1} & M_{g2} \end{bmatrix} \begin{Bmatrix} X_{I1} \\ X \\ X_{I2} \\ P_{s1} \\ P_{s2} \\ P_{s3} \\ P_{s4} \end{Bmatrix} = \{Y\} \quad (4.31)$$

Once equation (4.31) is solved, all the boundary unknowns including the interface unknowns are found. By substituting these unknowns into the boundary elements equations, all the displacements and stresses at any internal points can be calculated.

4.5 Modeling of Bridge Structures

Different types of bridges can be modeled using the coupling technique described earlier. The same idea of modeling single box girder and slab on two girders bridges can be used to model multi-cell box girder and multi-girder bridges. In all bridge types the top slabs are modeled using boundary elements and the other bridge components such as webs and bottom slabs can be modeled using finite elements. Two examples will be considered as

a further illustration of the capability of the combined method for modeling different types of bridges.

Consider a two-cell box girder bridge as shown in Figure 4.6-a. The bridge is divided into boundary element and finite element regions. The finite element region consists of the webs and bottom slab while the top slab is considered as a boundary element region. The formulation of the final finite element matrix is developed using the same procedure described in section 4.2. Then the non-interface variables are taken as a function of the other variables (i.e. interface degrees of freedom) to obtain the stiffness matrix which includes the equations corresponding only to the interface degrees of freedom.

The second region, which is the top slab, is divided into two regions as shown in Figure 4.7-a. Each region is consisted of two interfaces, then these regions are assembled to form the whole slab with three interfaces (see Fig. 4.7-b). The BE and FE regions can be combined by satisfying the compatibility requirements along the interfaces based on the two cases described in section 4.3. The compatibility requirements along the interfaces 1 and 3 (e.g. I_1 and I_3) are satisfied by using the procedure described in case I, while for interface 2 (e.g. I_2), case II is used to satisfy the compatibility requirements between boundary element and finite element regions (see Fig. 4.8) , i.e.

$$U_{s1} = U_{g1} = U_{I1},$$

$$U_{s2} = U_{g2} = U_{s3} = U_{I2},$$

$$U_{s4} = U_{g3} = U_{I3},$$

$$P_{s1} = -P_{g1} = P_{I1},$$

$$P_{s2} + P_{s3} + P_{g2} = 0$$

and

$$P_{s4} = -P_{g3} = P_{I3}$$

After substituting the above conditions into the boundary element and finite element equations, all the equations can be coupled in a single matrix form as :

$$\begin{bmatrix} H_{s1} & H_{s2} & 0 & H & -G_{s1} & -G_{s2} & 0 & 0 \\ 0 & H_{s3} & H_{s4} & H & 0 & 0 & -G_{s3} & -G_{s4} \\ K_{I1} & K_{I2} & K_{I3} & 0 & M_{g1} & M_{g2} & M_{g2} & M_{g3} \end{bmatrix} \begin{Bmatrix} U_{I1} \\ U_{I2} \\ U_{I3} \\ U \\ P_{I1} \\ P_{s2} \\ P_{s3} \\ P_{I3} \end{Bmatrix} = \{Y\} \tag{4.32}$$

Substitute the boundary conditions in the above equation and solve for the boundary unknowns.

In the second example, a slab on three girders is considered as shown in Figure 4.9. The combined solution is derived in the same manner. The top is divided into four boundary regions as shown in Figure 4.9-a (i.e. overhangs and entire slabs). The boundary element equations for the overhangs are reduced to the size of $4N_{in}$, where N_{in} is the number of the nodes at the interface. The re-

interface. The reduction is achieved by imposing the boundary conditions and eliminating all the variables not connecting with the interface using static condensation. The boundary element and finite element equations are linked with the requirements of displacement continuity and force equilibrium along the interfaces using the same procedure described in case II. The M matrix is established for the interface nodes and BE and FE regions are linked to form the final system of equations.

The coupling technique is implemented in a computer program called **BACBAF** (**B**ridge **A**nalysis using **C**ombined **B**oundary element **A**nd **F**inite element methods). The model consists of three parts, in the first part the boundary element equations required to model the slab are established while the second part is concerned with the finite element equations required to model the girders. The third part deals with the coupling technique between BEM and FEM, where the compatibility and equilibrium conditions have to be achieved. A flow chart describing the major steps of the program BACBAF is shown in Figure 4.10.

The program can be used either to model slab bridges using BEM or to model slab on girder and box girder bridges using the combined method. Different types of boundary elements and boundary conditions can be handled by the program. Details of the input data required to run the program and the function of the major Subroutines are described in Appendix A.

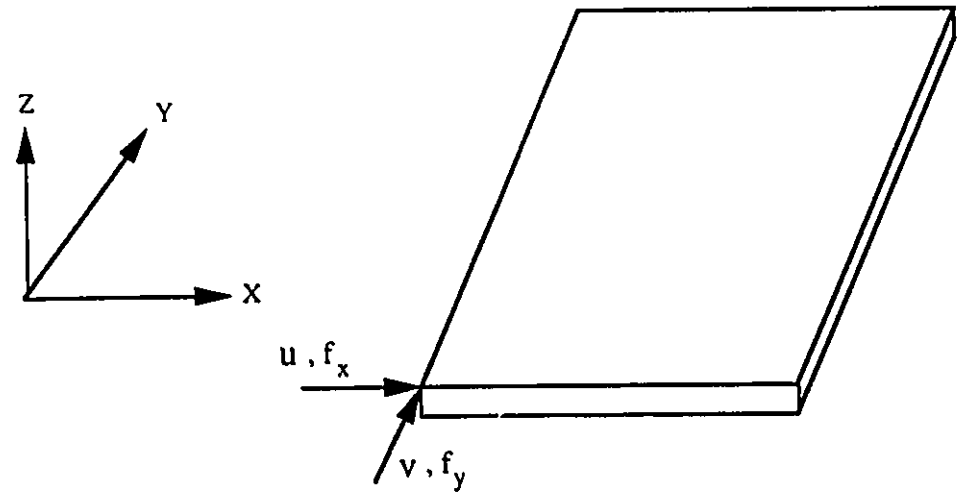

a) Displacements and forces for the in-plane action.

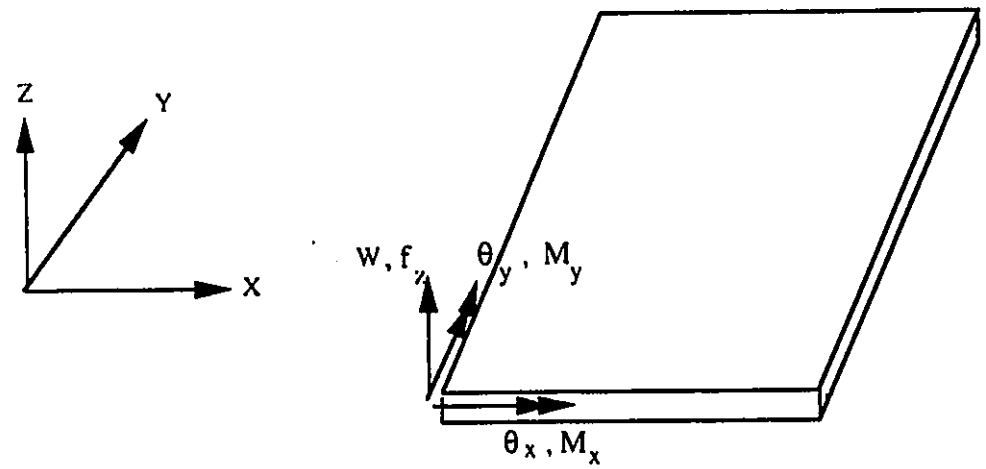

b) Displacement and forces for the bending action.

Figure 4.1 Local degrees of freedom for a flat shell element .

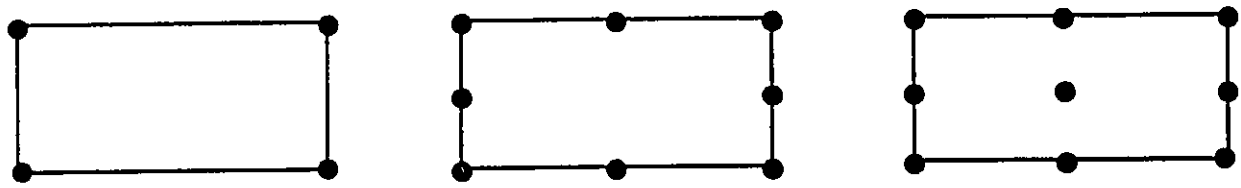

Figure 4.2 Rectangular finite elemenets used in the program

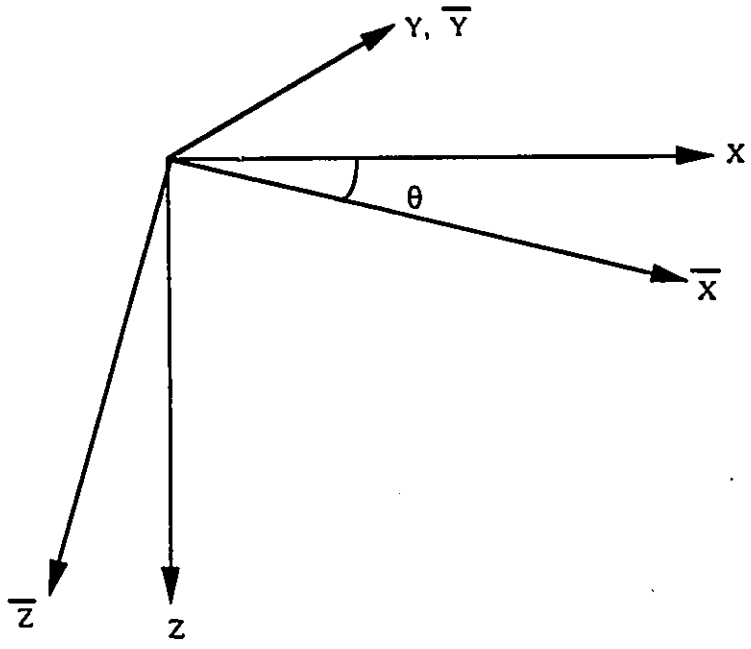

Figure 4.3 Local and global coordinate systems.

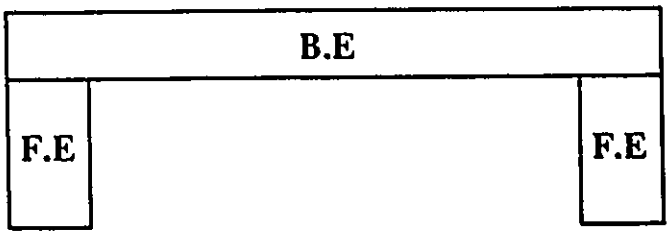

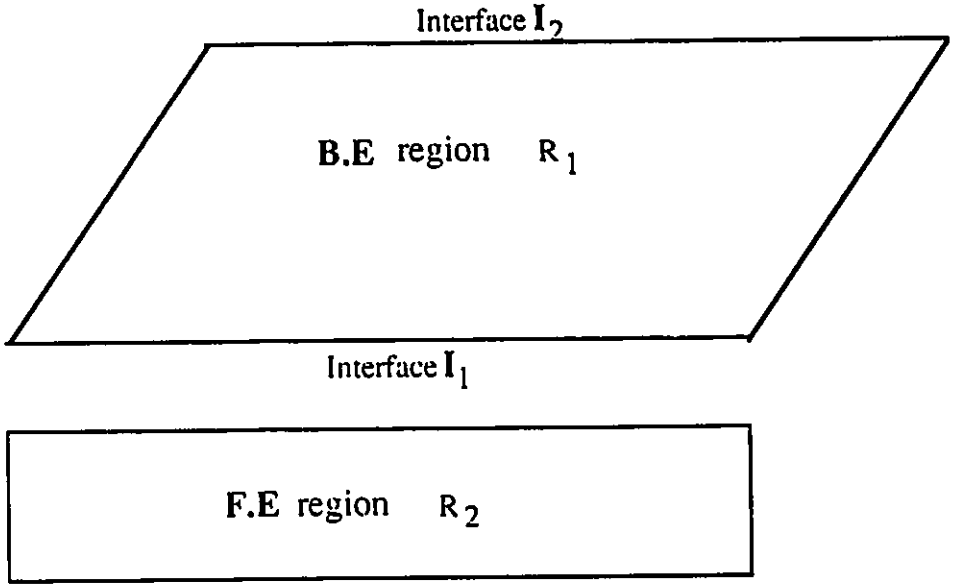

Figure 4.4 B.E and F.E. regions for case I.

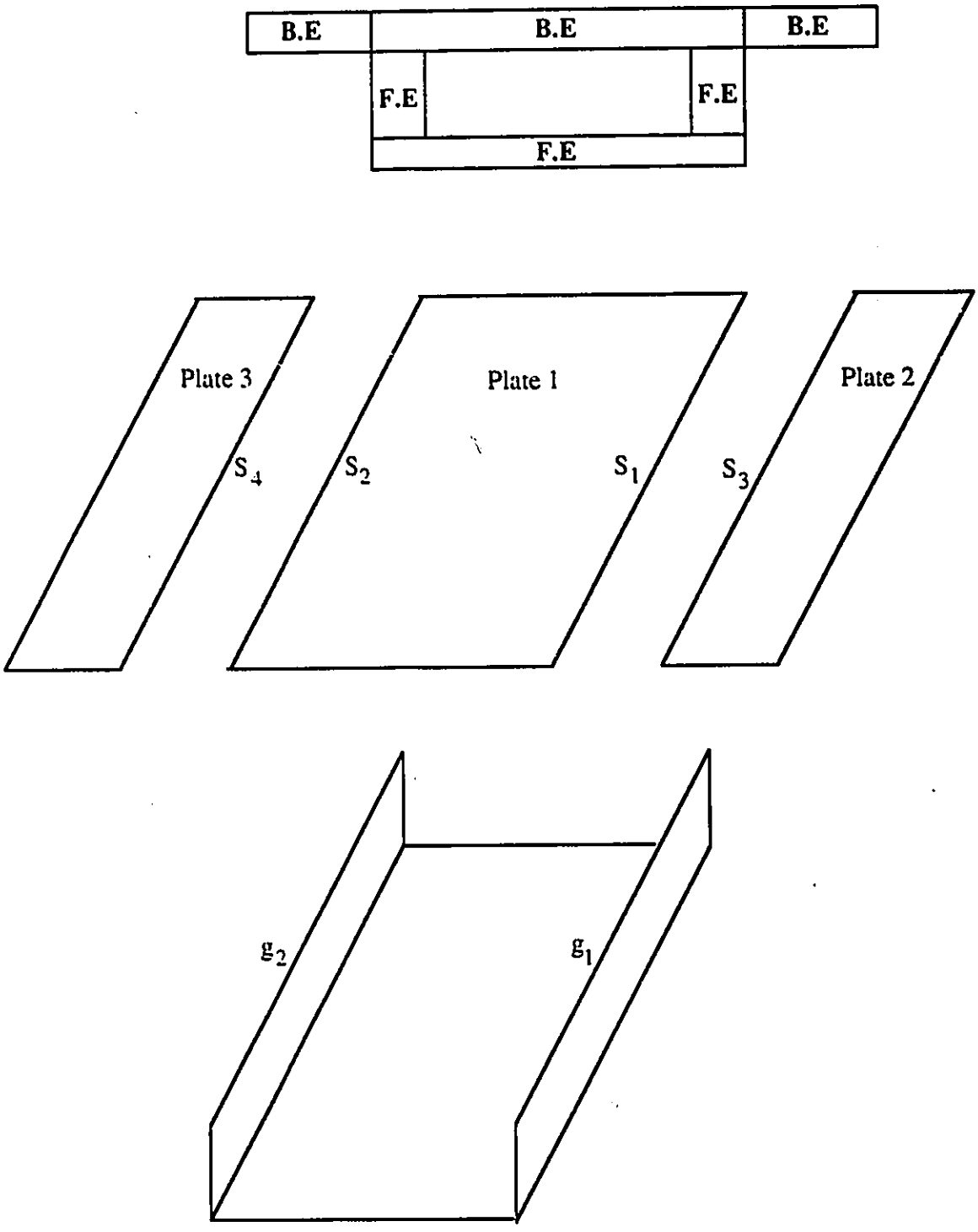

Figure 4.5 B.E and F.E. regions for case II

a) A two-cell box girder bridge.

b) A slab on girder bridge.

Figure 4.6 Typical cross sections.

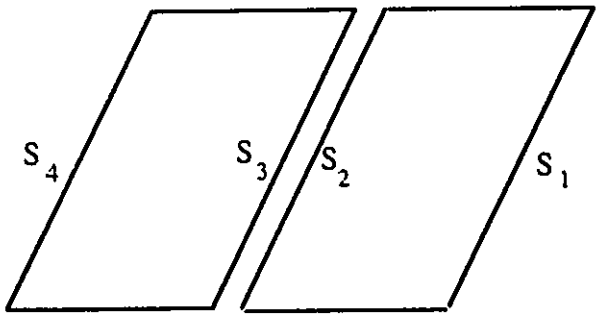

a) The top slab is divided into two regions

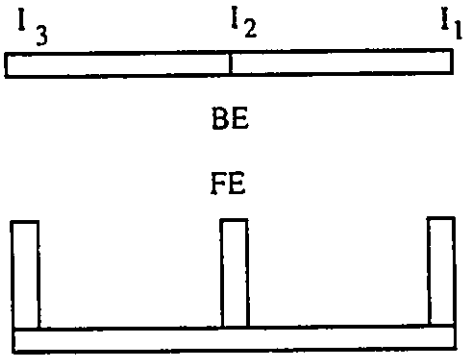

b) A bridge divided into BE and FE regions

Figure 4.7 Modeling of a two-cell box girder bridge

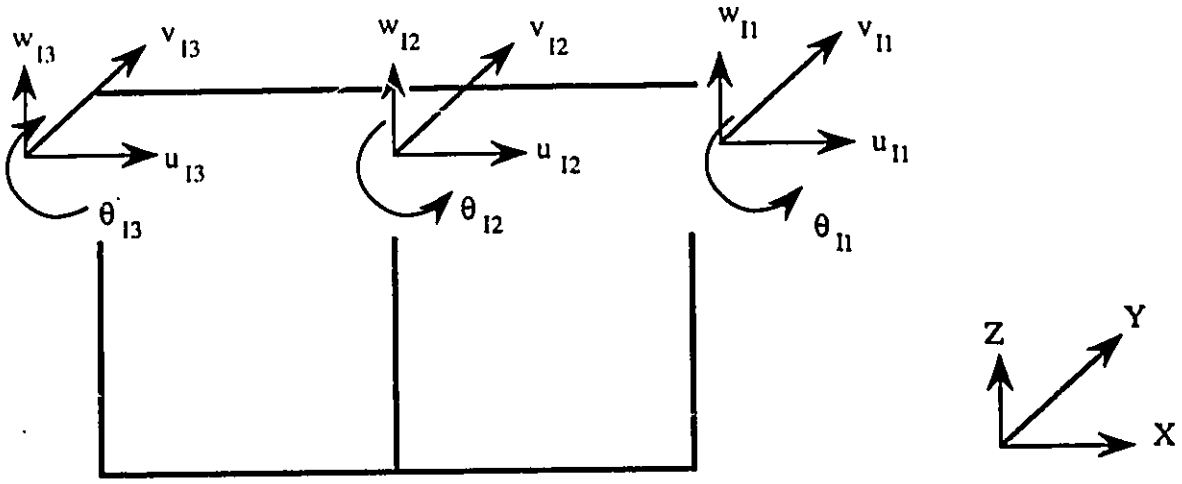

a) The compatibility of displacements at the interfaces

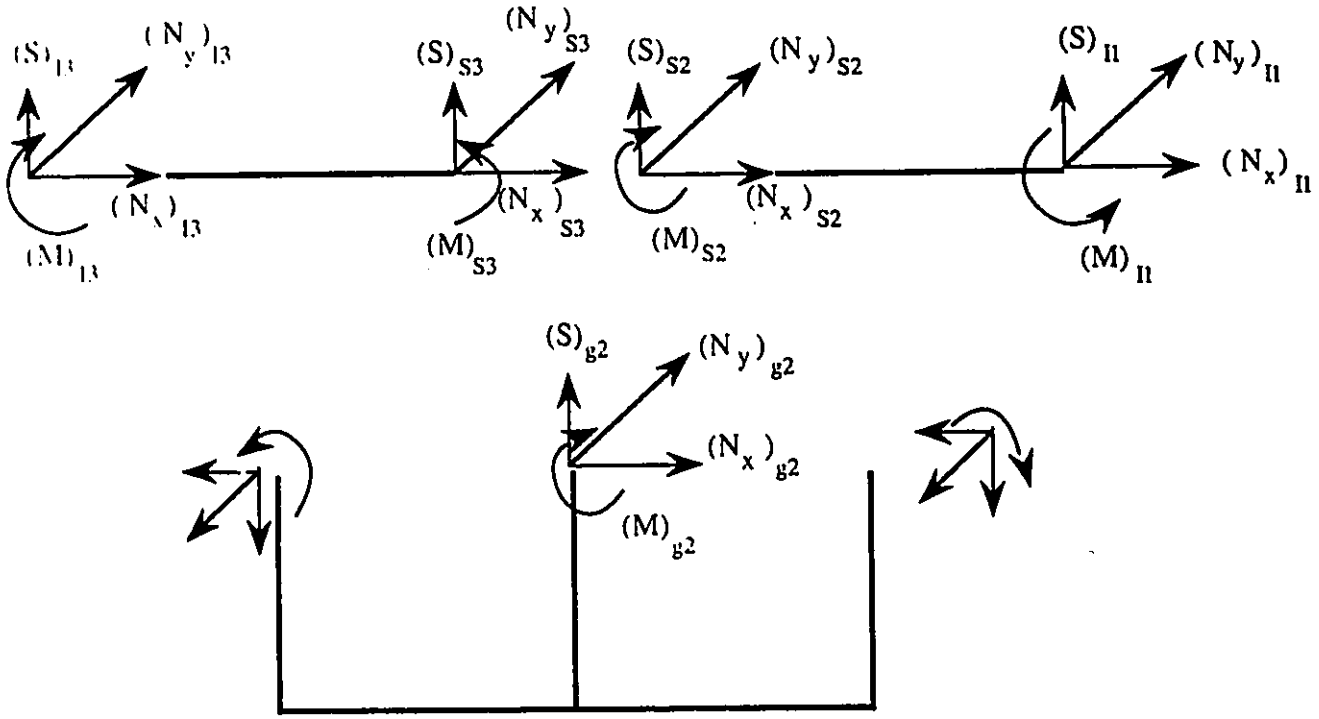

b) The equilibrium of forces at interfaces

Figure 4.8 The compatibility requirements at the interfaces

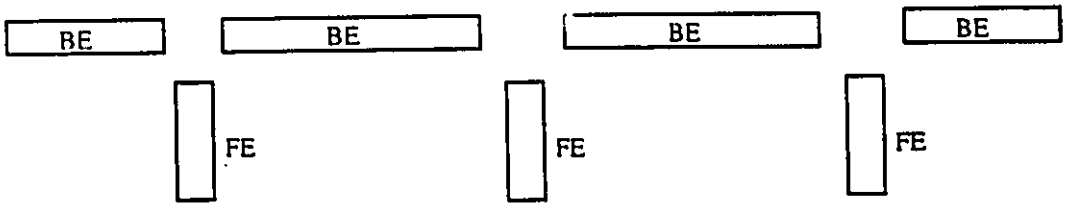

a) The bridge is divided into BE and FE regions.

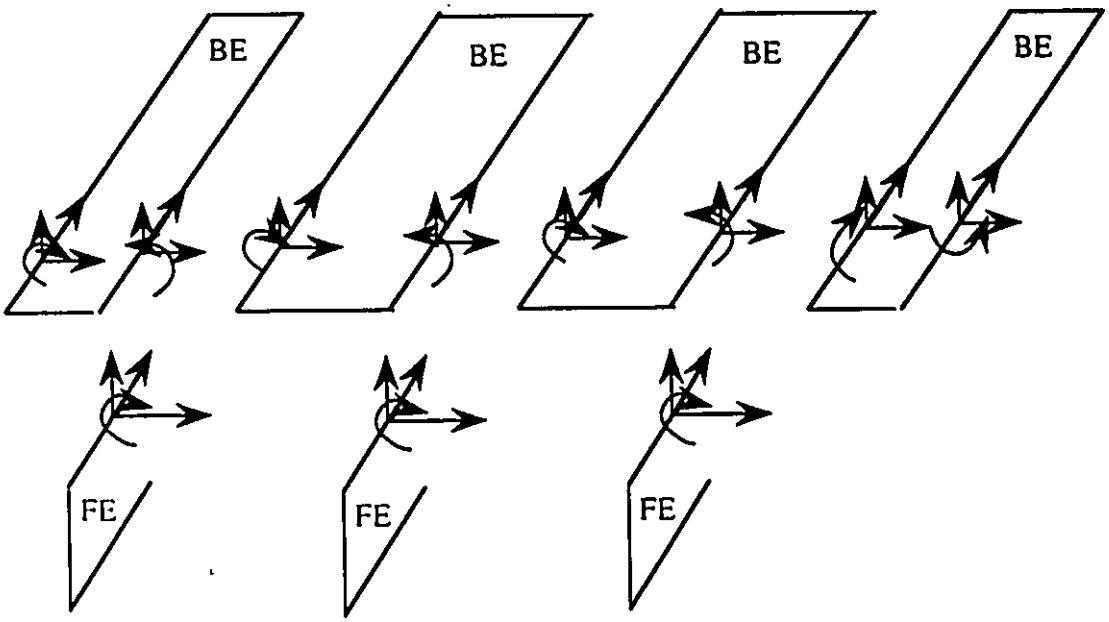

b) The degrees of freedom along the interfaces.

Figure 4.9 Modeling of a slab-on-girder bridge.

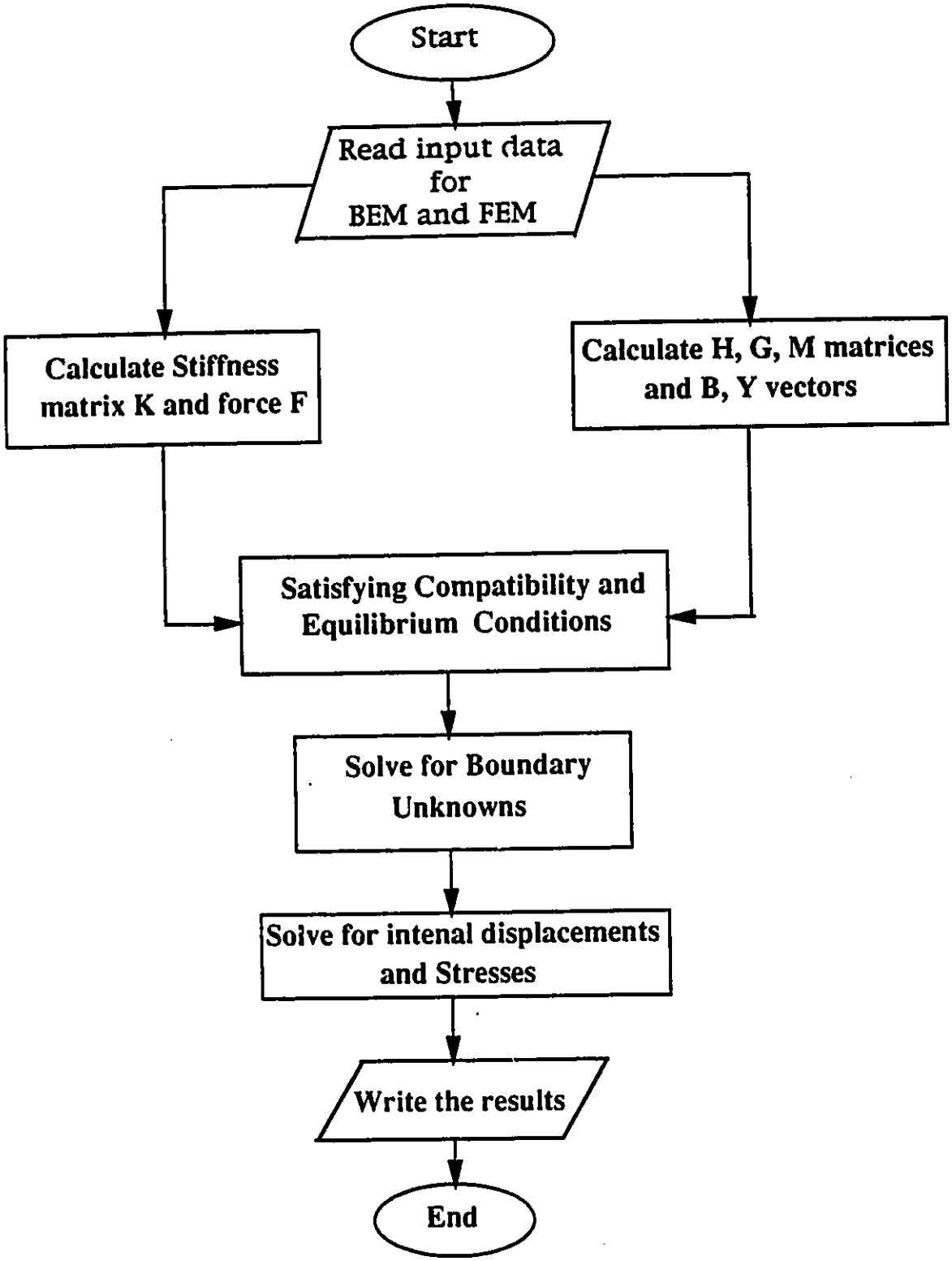

Figure 4.10 A flow chart describing the major steps of the BACBAF

Chapter 5

Convergence of the Results

5.1 General

The objective of this chapter is to study the convergence and accuracy of the results using different mesh sizes and different type of elements and to show the simplicity and reduction of the input data. Convergence is investigated by changing the number of the elements and keeping the order of the elements the same and vice versa. Linear, quadratic and higher order elements were employed in the boundary element idealization, and 4-node and 8-node rectangular flat shell elements were used in the finite element idealization. Four cases consisted of slab, slab-on-girder and box girder bridges are investigated. Results obtained from the combined method were then compared with the finite strip solution.

5.2 Case Studies

5.2.1 Concrete skew slab on two girders bridge

A concrete skew slab on two girders with an angle of 10 degrees was analyzed to study the accuracy and convergence of the combined method. The loading consists of a point load of 110 kN distributed uniformly on a small patch [34]. The dimensions and material properties of the bridge are given in Figure 5.1. Convergence was investigated by increasing the order of the elements and using the same number of the nodes for all three meshes. In the first mesh, the bridge deck was discretized longitudinally into 6 quadratic elements with 13 nodes (2^{nd} order element) and transversely into one quadratic element with 3 nodes resulting in a total number of 14 elements. In the second mesh, the total number of elements was reduced to 8 elements using 4^{th} order element and the same number of the nodes was used. The third mesh consisted of two boundary elements (6^{th} order element) along the longitudinal direction and one element along the transverse direction, therefore, the total number of elements used to model the slab was 6 elements. In all three meshes the girder was modeled by a 6×1 mesh using 8-node rectangular element, where 6 and 1 denote the number of mesh division over the length and the width respectively. The boundary element and the finite element idealizations are shown in Figures 5.2-a to 5.2-d.

The results of the deflections and the moments for the three meshes are

summarized in Tables 5.1 and 5.2. The maximum difference in the deflection and the moment results for the three meshes is about 3%. It is evident from the Tables that the use of higher order elements produced no significant change in the results.

A fourth mesh which consisted of only 4 boundary elements was used to model the whole slab and a 4×1 mesh was used to model each girder (see Figures 5.2-e and 5.2-f). This gives a significant reduction in input data files. The deflection and the moment results in Tables 5.1 and 5.2 can be considered as converged solutions.

5.2.2 Concrete single-cell box girder bridge

A concrete single-cell box girder bridge subjected to two different cases of loading. In the first case, the bridge was subjected to uniformly distributed load of 40 kN/m^2. The bridge dimensions and material properties are shown in Figure 5.3. Only one type of elements , i.e. quadratic elements, was used to model the bridge while the number of the elements is variable. The objective of this example is to study the effect of mesh sizes for different loading.

The 8-node flat shell element, shown in Figure 4.2, was used to model the bottom slab and the webs while quadratic elements were used to model the top slab. Three different meshes were used to simulate the behavior of the bridge. The boundary element and the finite element idealizations are described in Figures 5.2-a, 5.2-d and 5.4. In this example, the number of the

quadratic elements used to model the top slab is increased from 6 to 14. For the webs and the bottom slab, 2×1, 4×1 and 6×1 meshes were used in the finite element idealization.

The results of the deflection and the longitudinal moment along the center of the bridge for the three meshes are compared with FSM in Tables 5.3 and 5.4. The maximum percentage errors for meshes no. 1, 2 and 3 were 6%, 3% and 2% for the deflection, and 4%, 2% and 1% for the longitudinal moment respectively. As such, the deflection and the longitudinal moment for the three meshes can be considered as converged solutions.

Similar observation can be made when comparing the results of transverse moments at the mid-span with those obtained from FSM. In Table 5.7, the values of the transverse moment for mesh 1 are overestimated near the boundary due to singularity. At the boundary, larger moment values are obtained for the three meshes. A much more accurate solution near the boundary would be expected if additional elements are used in the boundary element idealization. It can also be shown from the results that meshes 2 and 3 have sufficient elements for the deflection and the longitudinal moment convergence.

The convergence of the results for the rotation and the deflection along the girders is investigated in Tables 5.5 and 5.6. The maximum difference in the rotation and the deflection computed using mesh 3 is about 9% and 3% near the corner. The percentage error is converged towards the center of the bridge.

In the second case, the bridge was subjected to two concentrated loads acting on the girders at the mid span. The comparison of the transverse moment at the mid span using the three meshes is made with the FSM in Table 5.8. Meshes no. 1 and 2 (i.e. 2×1 and 4×1) have insufficient elements for the moment convergence. The maximum difference in the moment is high for both meshes, i.e. 53% and 33% close to the boundary. Similar observation can be made for 6×1 mesh, where the percentage error in this mesh can be as high as 26% near the boundary. The values of the transverse moment for all meshes are infinity at the boundary as expected. The comparison of the deflection along the girder using mesh no. 3 is given in Table 5.9. The maximum difference in the deflection obtained by BEM-FEM is about 2%.

5.2.3 Concrete slab on two girders bridge

A concrete slab on two girders bridge was considered to investigate the convergence of the results using different mesh sizes. The bridge was simply supported, 6.0 m long, 5.2 m wide and 1.25 m deep. The thickness of the slab was 0.25 m while the girders were 0.30 m thick as shown in Figure 5.5. The bridge was loaded by a uniformly distributed load over the whole slab. The loading and material properties are also shown in Figure 5.5. The bridge was analyzed by both the BEM-FEM and FSM. Linear and quadratic elements were used to model the bridge using eight different mesh divisions :

i) The BEM-FEM solution used 6 × 1, 6 × 2, 8 × 1 and 8 × 2 meshes (4-node element) for girders (see Figures 5.8-b, 5.8-c, 5.9-b and 5.9-c) and 20, 24 linear boundary elements for the entire slab and 16, 20 elements for the overhangs as shown in Figures 5.6, 5.7-c and 5.7-d.

ii) The BEM-FEM solution used 4 × 1, 4 × 2, 6 × 2 and 8 × 1 (8-node element) for girders, 28, 36 and 44 quadratic boundary elements for the entire slab, and 22, 30 and 38 for the overhangs as shown in Figures 5.10 and 5.11.

The results of the deflection along the center of the span are plotted in Figures 5.13 and 5.15 using the eight meshes. In Figure 5.13, a significant difference in the results can be seen when the girder was modeled using 6 × 1 and 8 × 1 meshes. The results converged quickly when two layers were used. In Figure 5.15, there is no significant difference in the results when quadratic elements are used. The bending moment M_x along the center of the bridge is compared with FSM in Figures 5.14 and 5.16. The results obtained using linear and quadratic elements always very close to the FSM solution.

5.2.4 Simply supported slab bridge

A simply supported slab bridge subjected to uniform load of 10 kN/m^2 was chosen to study the effect of the distance "d". The following material properties are used ; E = 10000 MPa, and $\nu = 0.3$. The value of ν was chosen as 0.3 in order to compare the results with Timoshenko's values. The length of the slab on each side is 10.0 m and the thickness was 0.1 m. The effect of 'd' on

the value of the shear force along the boundary of the slab was investigated for both linear and quadratic elements using d = 0.2 L. A total of 20 elements were used to model the slab. In Table 5.10 the results of the shear force are compared with those obtained by reference [1] and Timoshenko's values. It can be seen that in the case of d = 0.2 L the shear forces converge near the corner while the convergence for $\frac{a}{10,000}$ (given by reference [1]) is relatively slow.

5.2.5 Concrete slab bridge

A concrete slab bridge under two truck was analyzed to show the advantages of BEM over the FEM in terms of the reduction of the input data and the computer time. The dimensions, loading and material properties are given in Figure 5.12. The bridge was analyzed by both FEM and BEM. In the FEM, the slab was discretized into 84 elements with 291 nodes (8-node element was used), while the BEM mesh was consisted only of 12 elements with 31 nodes. The CPU times required to run the problem were 9 and 1 seconds for FEM and BEM respectively. The results of the central deflection and longitudinal moment along the slab are given in Table 5.11. As we can see, the FE mesh requires more refinement in the vicinity of the point loads, in addition to that, the loads must be coincided with the nodes otherwise a change of the mesh or a static distribution of loads will take place. On the other hand, in the BEM, the number and position of the loads moving over the slab do not change the BE mesh and only the boundary of the slab needs to be discretized. Therefore, the BEM is more efficient than FEM to analyze bridges under moving live loads.

5.3 Choice of mesh sizes and type of elements

In the first example, the convergence of the results was investigated by changing the order of the elements while the finite element idealization for the girder remained the same. The maximum difference in the results of the deflection and the moment along the span for the three meshes was within 3%. The deflection and the moment results can be considered as converged solutions. For mesh no. 4, it is interesting to note that the BEM-FEM solution for this mesh gave almost the same results as the pervious meshes, although the slab was modeled by 1 boundary elements (8^{th} order) along its longitudinal direction and 1 boundary element (2^{nd}) along the transverse direction. However, using higher order elements decrease the required input data. The input data for this example is given in the Appendix B.

In the second example, the finite element idealization using 2×1 and 4×1 meshes has insufficient elements for the moment convergence for concentrated loads. A refinement of mesh size is required in order to obtain a more accurate solution. Mesh no.3 (i.e. 6×1) indicates a general agreement for the results of the deflection and the moment except in the vicinity of the concentrated load.

In the third example, when 4-node element was used in the FE idealization the 6×1 mesh tends to underestimate the values of the deflection while the results obtained by 8×1 (4-node) indicated that FE idealization for the girder is coarse. The results of deflection using 2 layers (i.e. 6×2 and 8×2) or 1 layer of quadratic elements were converged quickly. It is clear that a minimum

of 2 layers (4-node element) are required to model the girders in order to get a converged solution. Also, it can be shown in this example, there is no need to idealize the bridge deck with more than 28 and 22 quadratic elements , and 4×1 mesh to idealize the girders, as such, the deflection and the moment at the interior points can be considered as converged solutions.

5.4 Concluding Remarks

The following conclusions are made based on the previous case studies :

1. High order elements in the boundary element idealization is not necessary in order to obtain accurate results. However, higher order element decrease the required input data files.

2. The FE idealization for the girders and the bottom slab requires at least 2 layers of 4-node element or 1 layer of 8-node element in order to obtain solutions that are sufficiently accurate.

3. BEM-FEM solution can be used to predict local slab moments and deflections directly under the wheel loads.

4. The convergence of the solution for concentrated loads is generally achieved by increasing the number of the elements.

5. It is recommended that the source points be located at a distance of $0.2\ L$, where L is the distance between two consecutive nodes.

Table 5.1: Deflection along the span for Example 5.2.1.

Span	FSM	BEM-FEM (mm)			
(m)	(mm)	Mesh 1	Mesh 2	Mesh 3	Mesh 4
1.	0.105	0.109	0.108	0.108	0.106
2.	0.237	0.246	0.244	0.243	0.242
2.5	0.322	0.333	0.331	0.330	0.328
3.	0.421	0.433	0.430	0.429	0.428
3.5	0.520	0.534	0.531	0.531	0.529
3.885	0.574	0.568	0.564	0.564	0.563
4.	0.580	0.589	0.585	0.585	0.587

Table 5.2: Longitudinal moment along the span for Example 5.2.1.

Span	FSM	BEM-FEM (kN.m/m)			
(m)	(kN.m/m)	Mesh 1	Mesh 2	Mesh 3	Mesh 4
1.	1.60	1.65	1.66	1.66	1.71
2.	4.47	4.56	4.56	4.57	4.54
2.5	6.97	7.06	7.06	7.08	7.06
3.	10.80	10.83	10.82	10.84	10.82
3.5	17.23	17.03	17.03	17.04	17.01
3.885	25.56	24.78	24.78	24.78	24.74
4.	26.82	25.99	25.99	25.99	25.94

Table 5.3 Vertical deflection along the span for example 5.2.2. (under unifromly distributed load).

Span	FSM	BEM-FEM (mm)		
(m)	(mm)	Mesh 1	Mesh 2	Mesh 3
0.5	0.189	0.202	0.193	0.191
1.0	0.340	0.356	0.349	0.344
1.5	0.445	0.454	0.458	0.451
2.0	0.510	0.509	0.528	0.519
2.5	0.546	0.539	0.566	0.556
3.0	0.557	0.550	0.577	0.569

Table 5.4 Longitudinal moment along the span for example 5.2.2. (under unifromly distributed load).

Span	FSM	BEM-FEM (kN.m/m)		
(m)	(kN.m/m)	Mesh 1	Mesh 2	Mesh 3
0.5	7.381	7.076	7.222	7.296
1.0	12.780	12.505	12.819	12.783
1.5	16.240	16.485	16.307	16.281
2.0	18.210	18.671	18.268	18.295
2.5	19.180	19.455	19.312	19.287
3.0	19.470	19.583	19.648	19.583

Table 5.5 Rotation along the girder for example 5.2.2.
(under unifromly distributed load).

Span	FSM	BEM-FEM (mesh 3)	Error
(m)	$\theta \times 10^{-4}$	$\theta \times 10^{-4}$	%
0.5	0.747	0.773	9
1.0	1.310	1.442	8
1.5	1.677	1.826	7
2.0	1.895	2.038	7
2.5	2.005	2.154	6
3.0	2.039	2.187	6

Table 5.6 Vertical deflection along the girder for example 5.2.2.
(under unifromly distributed load).

Span	FSM	BEM-FEM (mm)	Error
(m)	(mm)	Mesh 3	%
0.5	0.045	0.044	3
1.0	0.084	0.083	2
1.5	0.117	0.116	0.8
2.0	0.141	0.140	0.7
2.5	0.155	0.156	0.6
3.0	0.160	0.161	0.6

Table 5.7 Transverse moment along the mid span for Example 5.2.2 (under uniformly distributed load)

Span Width (m)	FSM (kN.m/m)	BEM-FEM (kN.m/m)		
		Mesh 1	Mesh 2	Mesh 3
1.50	5.779	5.352	5.863	5.884
1.75	5.528	5.148	5.594	5.629
2.00	4.784	4.566	4.794	4.876
2.25	3.575	3.687	3.491	3.649
2.50	1.947	2.650	1.739	1.981
2.75	-.051	1.696	-.354	-.106
3.00	-3.671	-	-	-

Table 5.8 Transverse moment along the mid span for Example 5.2.2 (under point loads)

Span Width (m)	FSM (kN.m/m)	BEM-FEM (kN.m/m)		
		Mesh 1	Mesh 2	Mesh 3
1.50	1.52	0.71	1.19	1.42
1.75	1.58	0.84	1.21	1.46
2.00	1.80	1.28	1.28	1.59
2.25	2.31	2.33	1.54	1.87
2.50	3.54	4.74	2.49	2.61
2.75	6.86	11.21	6.59	5.72
3.00	-4.09	-	-	-

Table 5.9 Vertical deflection along the girder for Example 5.2.2
(under point loads)

Span	FSM	BEM-FEM (mesh 3)	Error
(m)	(mm)×10^{-1}	(mm)×10^{-1}	%
0.5	0.239	0.242	1
1.0	0.473	0.476	0.6
1.5	0.692	0.694	0.2
2.0	0.895	0.889	0.6
2.5	1.102	1.074	2
3.0	1.279	1.312	2

Table 5.10: Comparison of the equivalent shear for Example 5.2.4.

X(m)	d = $\frac{a}{10,000}$		d = 0.2 L		Timoshenko
	Linear	Quadratic	Linear	Quadratic	
0.0	23.2	-8.5	8.8	-0.63	0.
1.0	18.2	23.4	21.1	23.3	22.2
2.0	34.3	30.4	33.1	30.1	31.5
3.0	37.6	38.1	37.9	38.2	38.0
4.0	41.5	40.9	41.3	40.5	40.6
5.0	42.1	42.0	42.1	42.1	42.0

Table 5.11: Vertical deflection and longitudinal moment for Example 5.2.5.

Span (m)	BEM		FEM	
	W (mm)	$M_x(kN.m/m)$	W (mm)	$M_x(kN.m/m)$
1.5	38.3	3.83	38.1	5.62
3.5	85.29	10.19	84.78	13.34
4.5	105.3	12.22	104.7	16.38
6.0	129.5	13.60	128.7	19.77
7.5	145.2	19.76	144.3	23.72
8.5	150.2	20.78	149.2	24.72
9.75	149.8	18.78	148.9	23.92
11.0	142.4	17.07	141.5	22.64
14.0	98.8	16.69	98.0	17.50
15.0	77.2	14.78	76.6	15.76
16.75	33.5	4.87	33.2	5.80

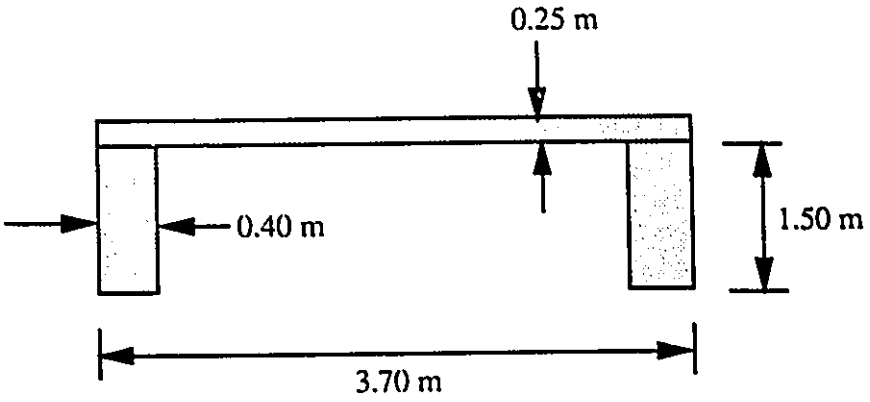

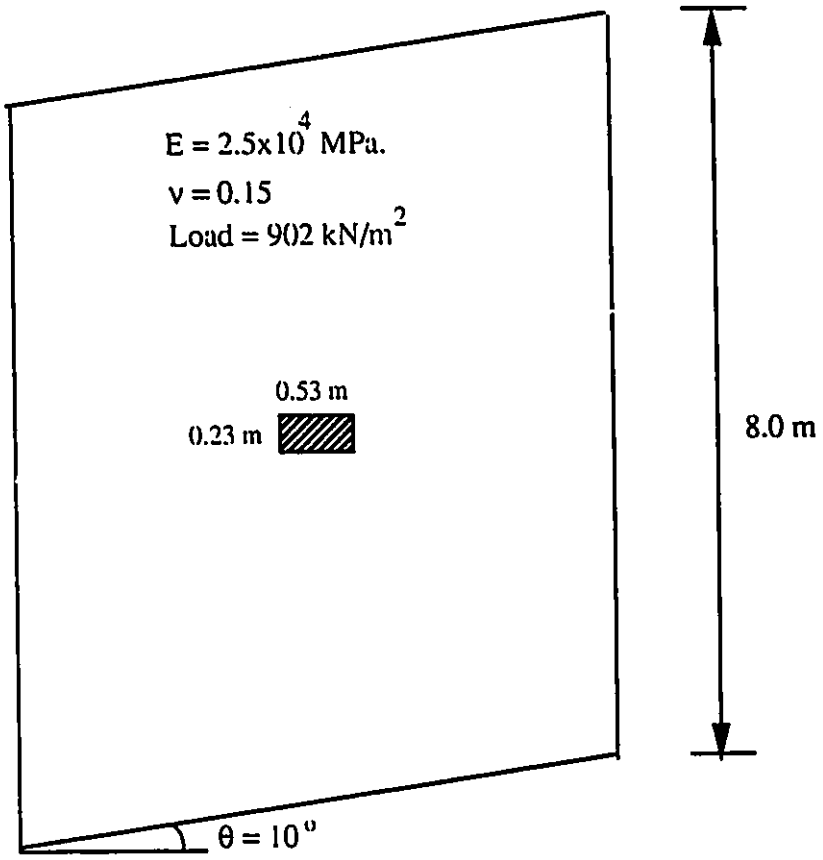

Figure 5.1 The dimensions and material properties for example 5.2.1.

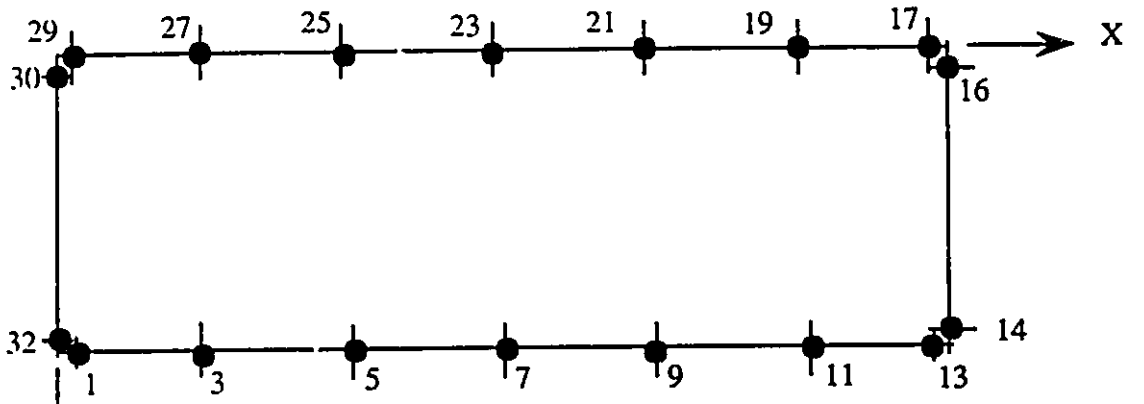

a) Mesh no. 1 for the slab

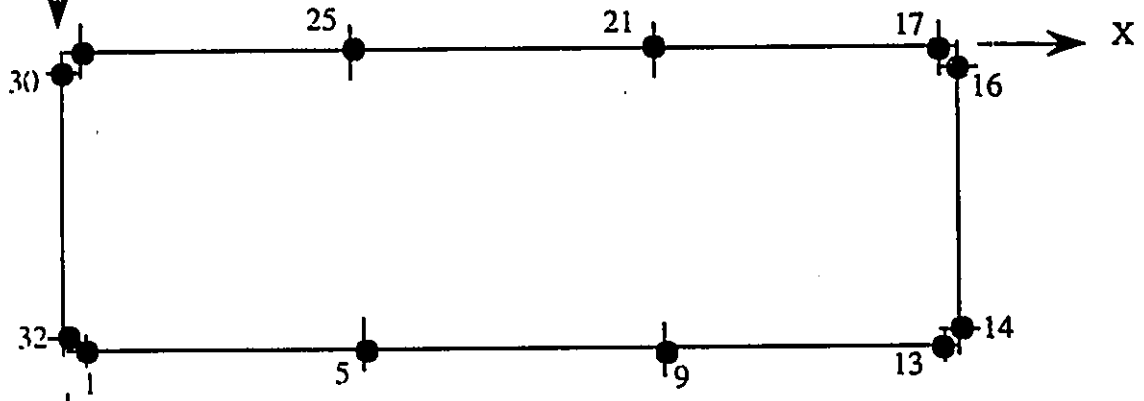

b) Mesh no. 2 for the slab

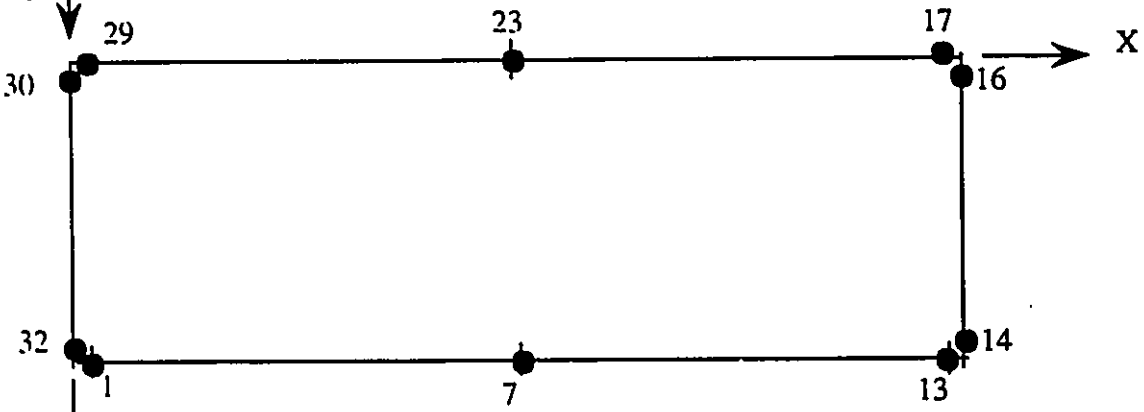

c) Mesh no. 3 for the slab

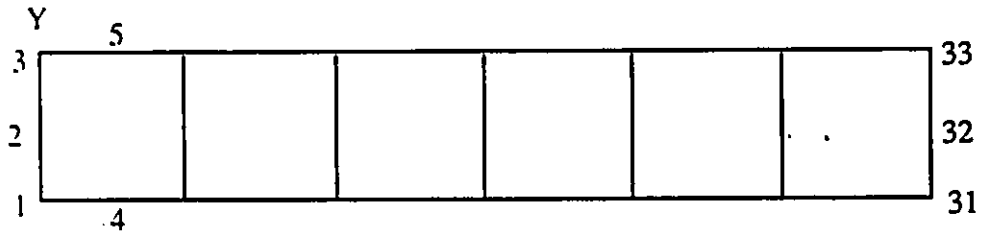

d) 6x1 mesh for the girder

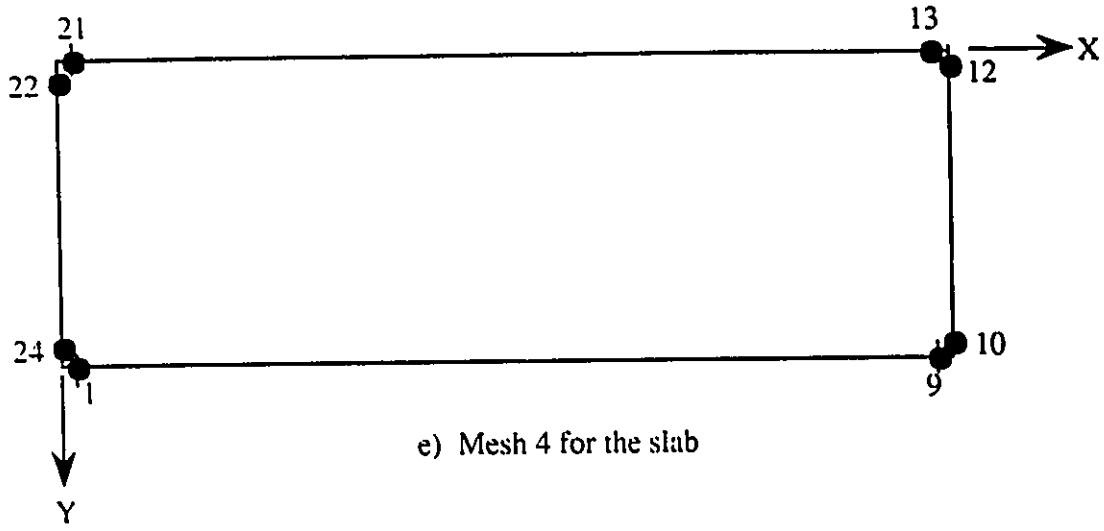

e) Mesh 4 for the slab

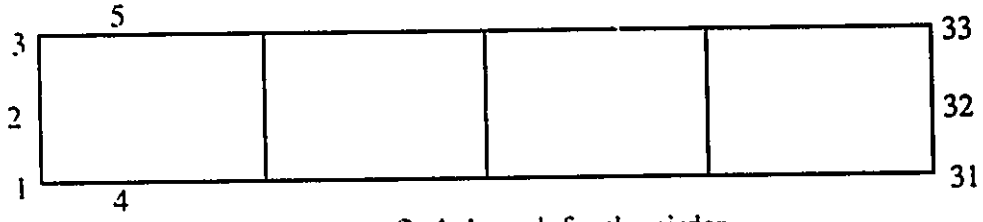

f) 4x1 mesh for the girder

Figure 5.2 BE and FE idealizations for example 5.2.1.

Loading = 40. kN/m ^{2}

E= 2.5 x10 ^{4} MPa

v = 0.15

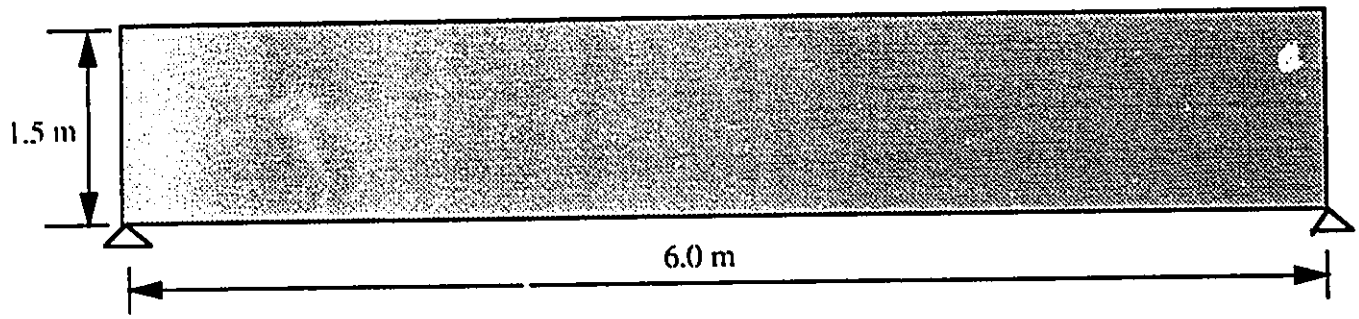

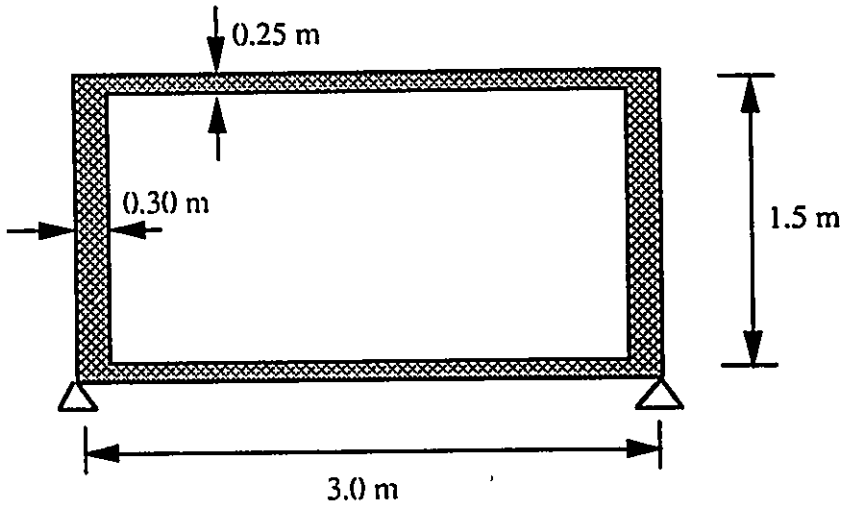

Figure 5.3 The dimensions and material properties for example 5.2.2.

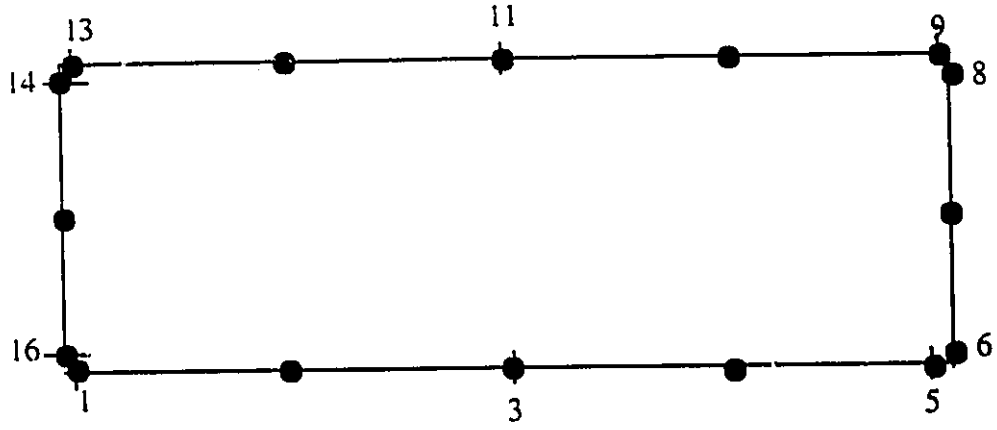

a) BE idealization for the slab

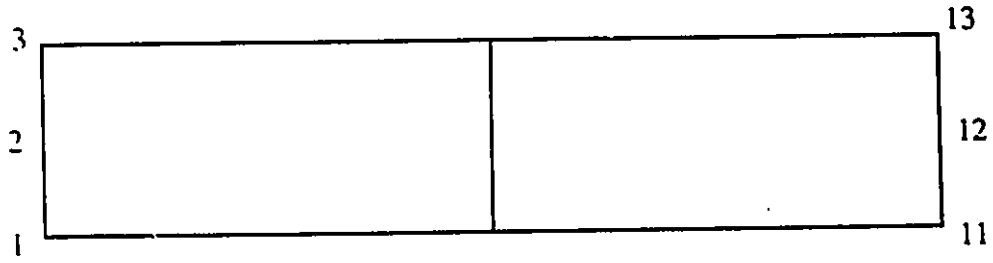

b) FE idealization for the bottom slab and webs (2x1 mesh).

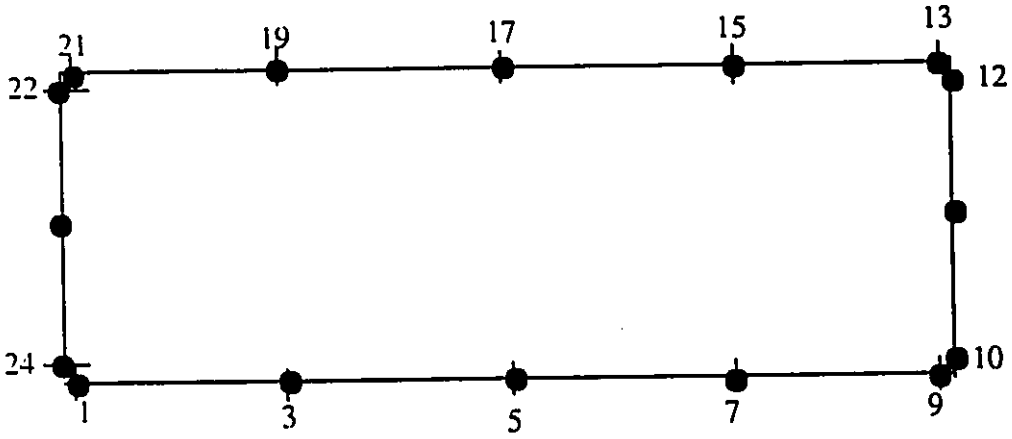

c) BE idealization for the slab

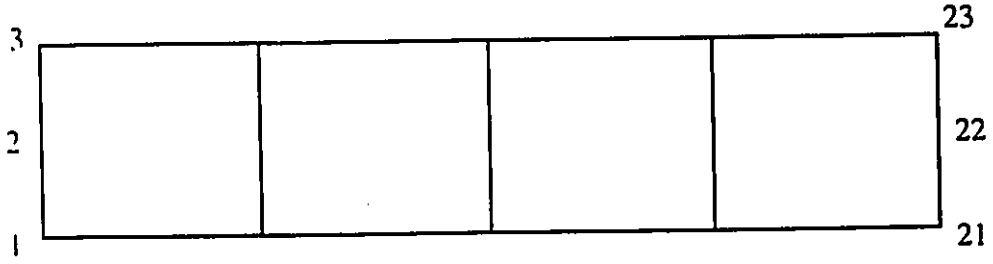

d) FE idealization for the bottom slab and webs (4x1 mesh).

Figure 5.4 BE and FE idealizations for using quadratic elements for example 5.2.2.

$E=3.2x10^3$ MPa
$\nu=0.15$
Load = 10 kN/m^2

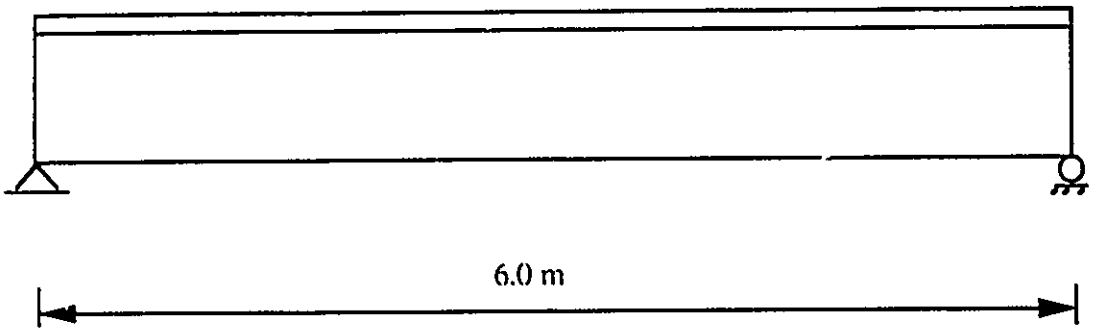

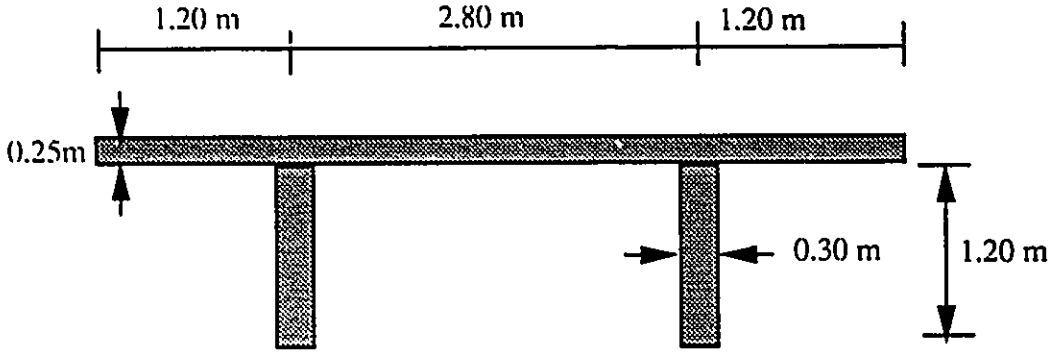

Figure 5.5 Loading and material properties of the bridge for example 5.2.3.

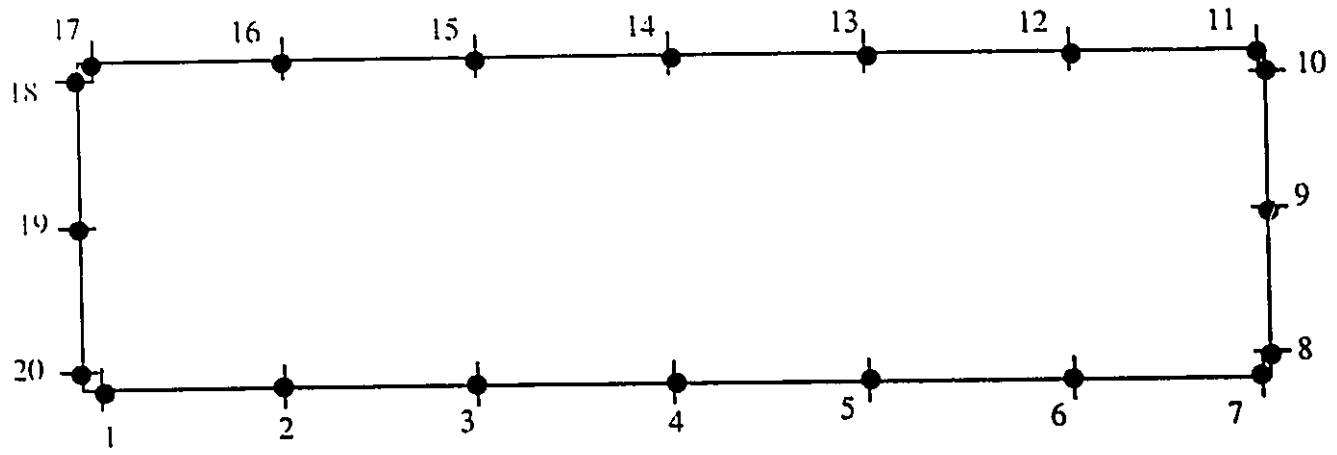

a) BE idealization for entire slab using linear elements.

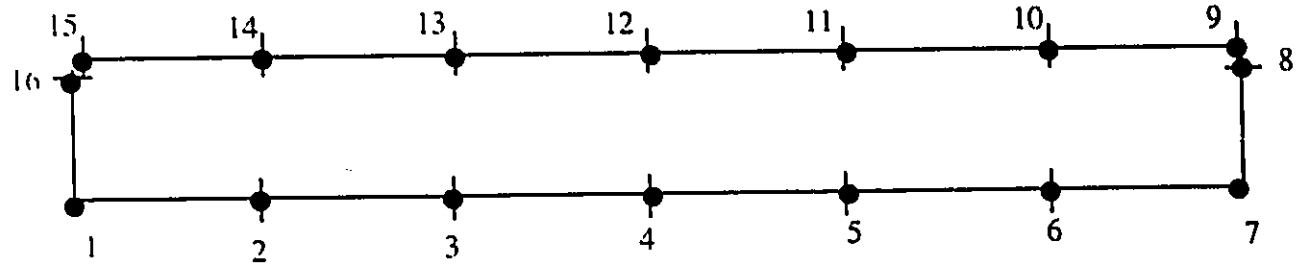

b) BE idealization for overhangs using linear elements.

Figure 5.6 BE idealizations using linear elements for example 5.2.3.

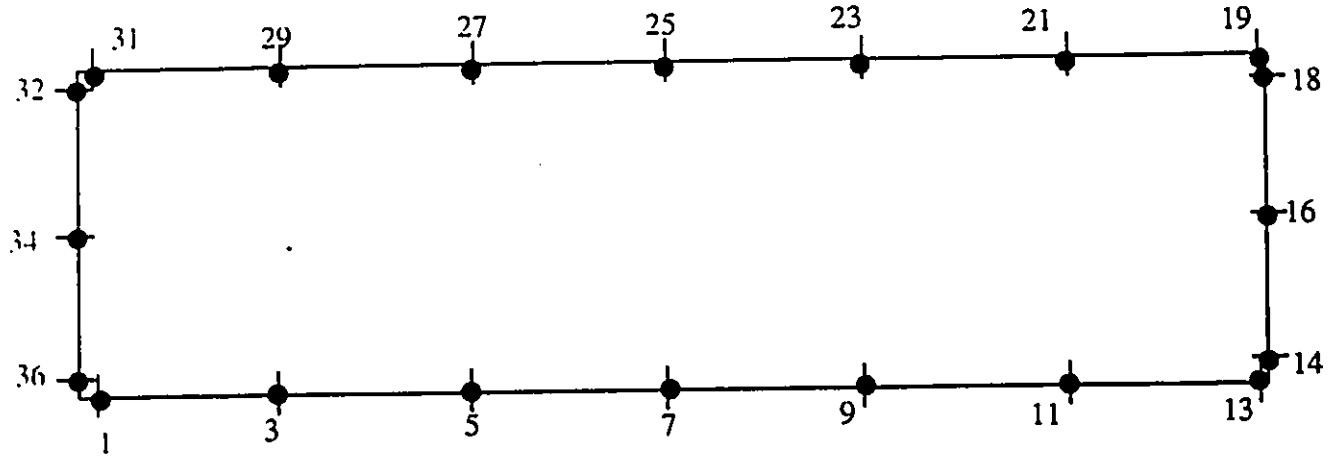

a) BE idealization for entire slab using quadratic elements.

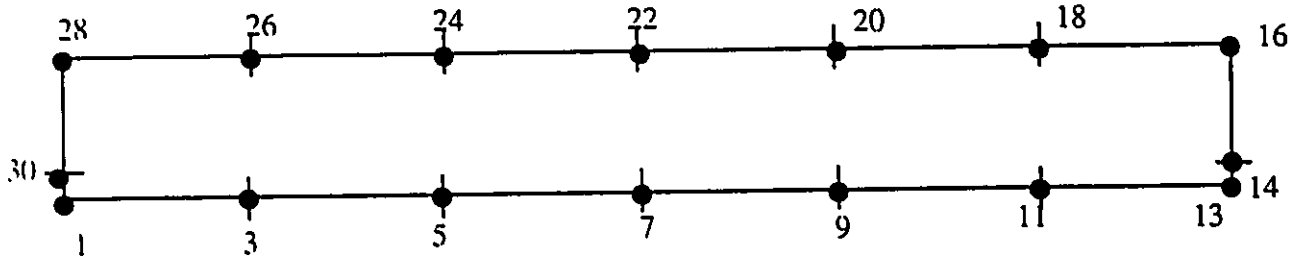

b) BE idealization for overhangs using quadratic elements.

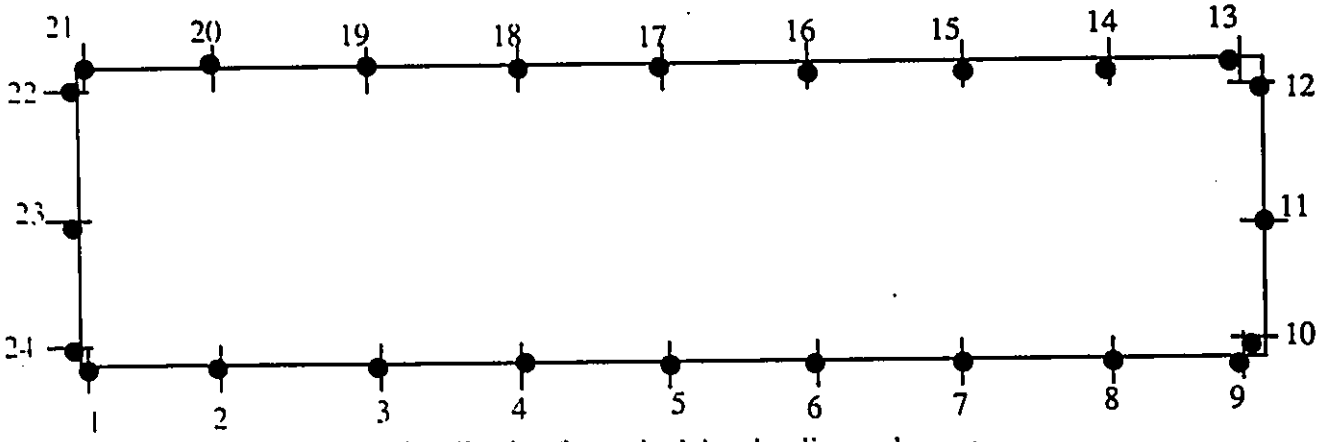

c)BE idealization for entir slab using linear elements

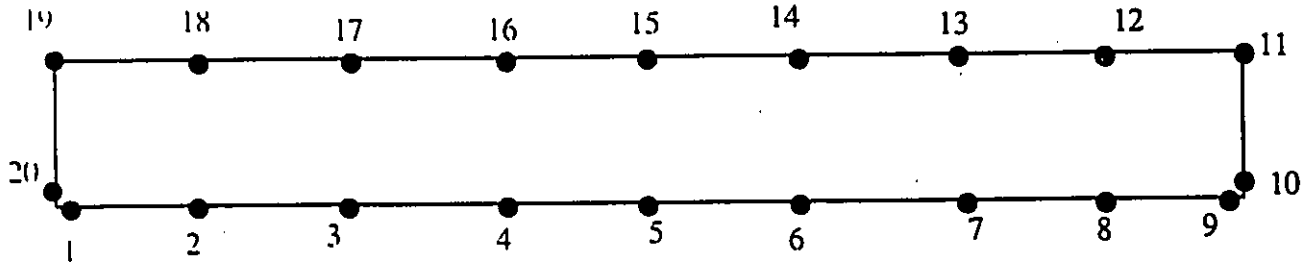

d)BE idealization for overhangs using linear elements.

Figure 5.7 BE ideaalization for the top slab.

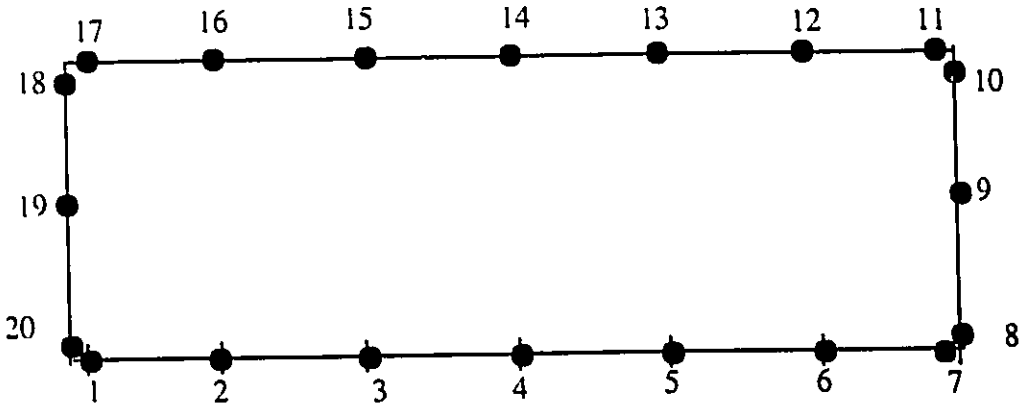

a) BE idealization for the slab

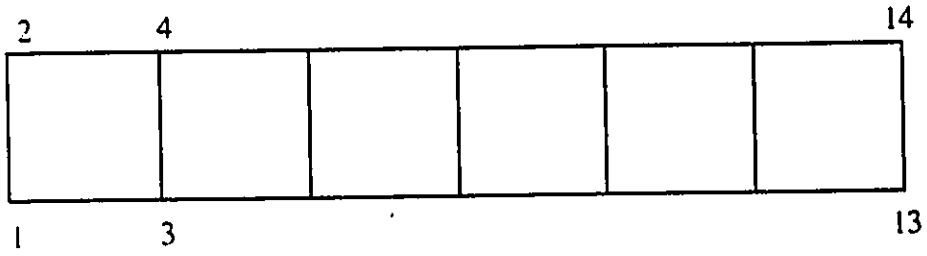

b) FE idealization for the girder (6x1mesh).

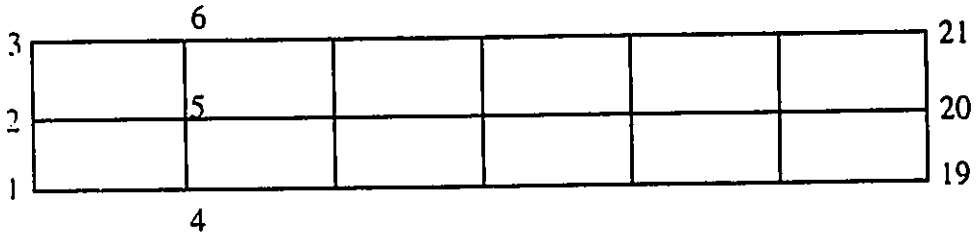

c) FE idealization for the girder (6x2 mesh).

Fig. 5.8 BE and FE idealizations using linear elements.

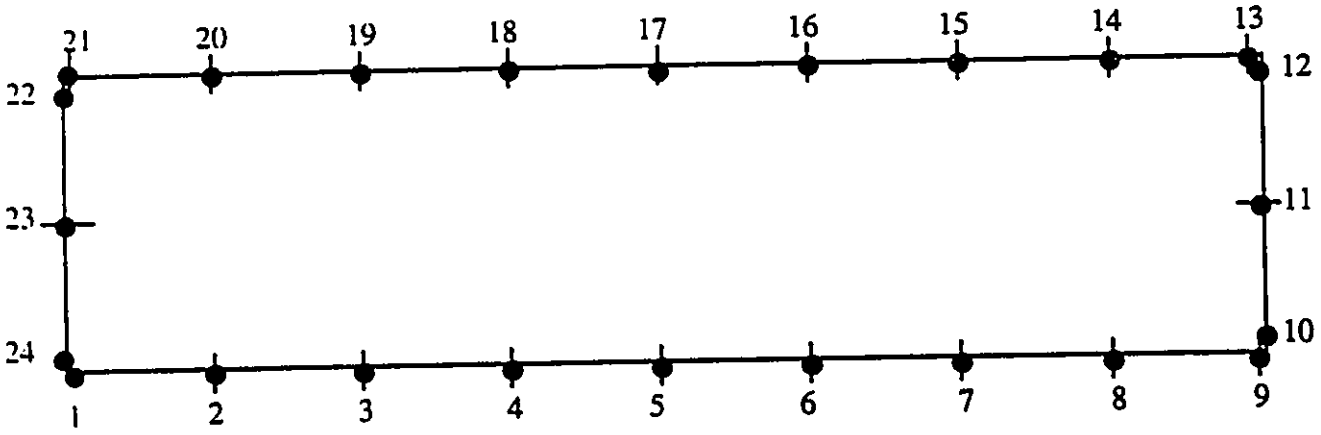

a) BE idealization for the slab using linear elements.

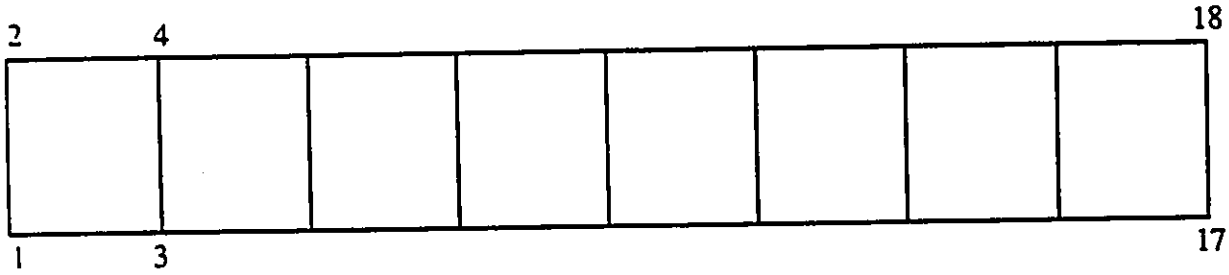

b) FE idealization for the girder using 4-nodes element (8x1 mesh).

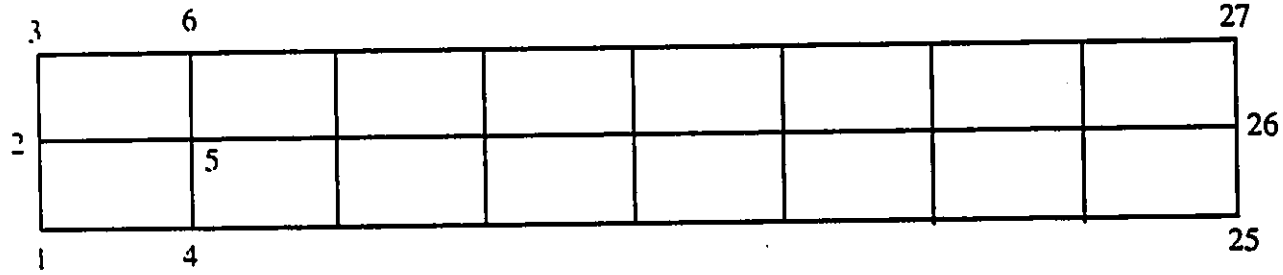

c) FE idealization for the girder using 4-nodes element (8x2 mesh).

Figure 5.9 BE and FE idealizations using linear element.

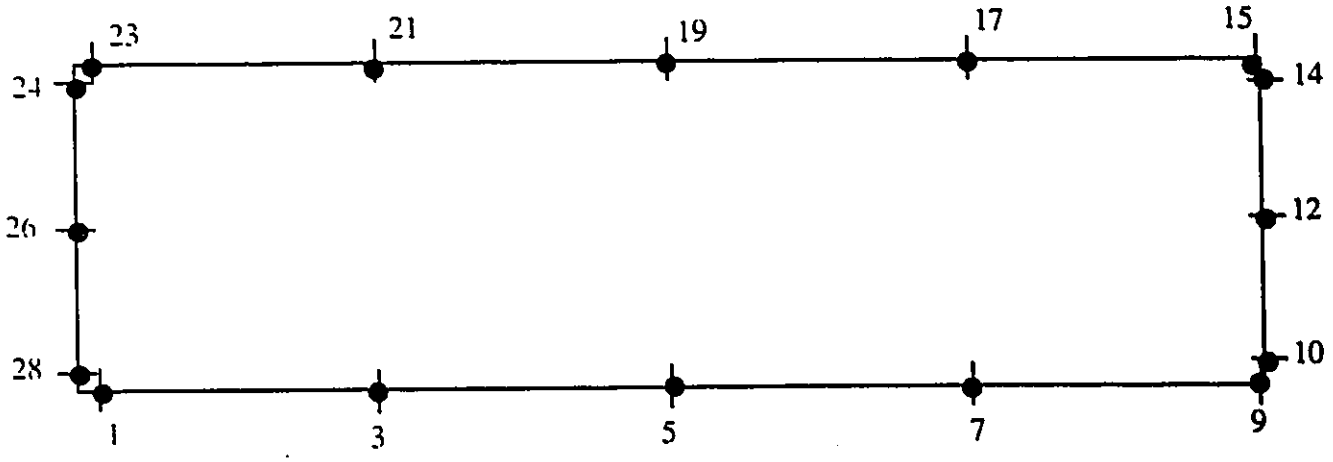

a) BE idealization for entire slab using quadratic elements.

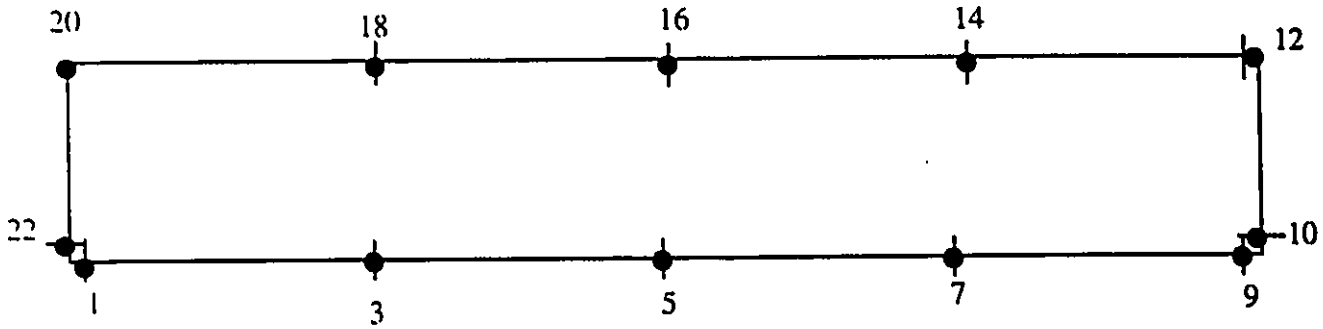

b) BE idealization for overhangs using quadratic elements.

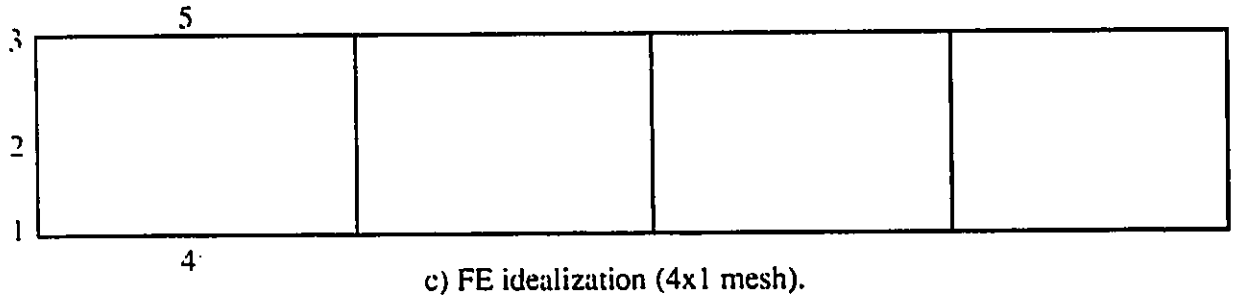

c) FE idealization (4x1 mesh).

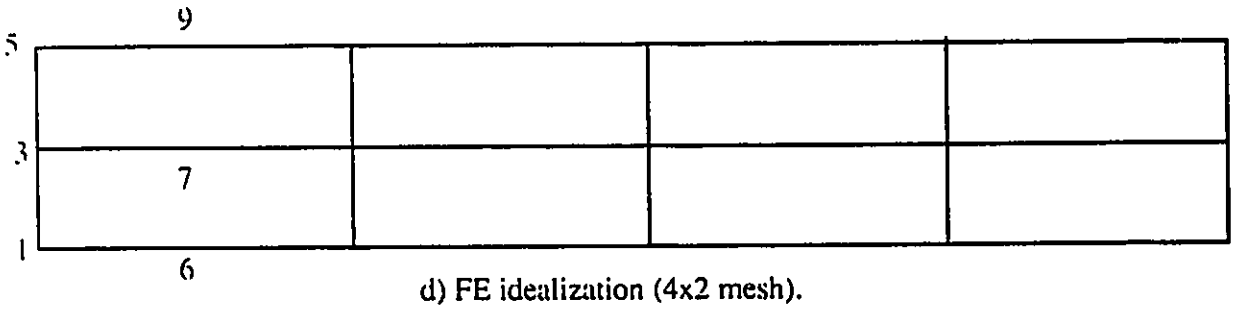

d) FE idealization (4x2 mesh).

Figure 5.10 BE and FE idealizations using quadratic elements for example 5.2.3.

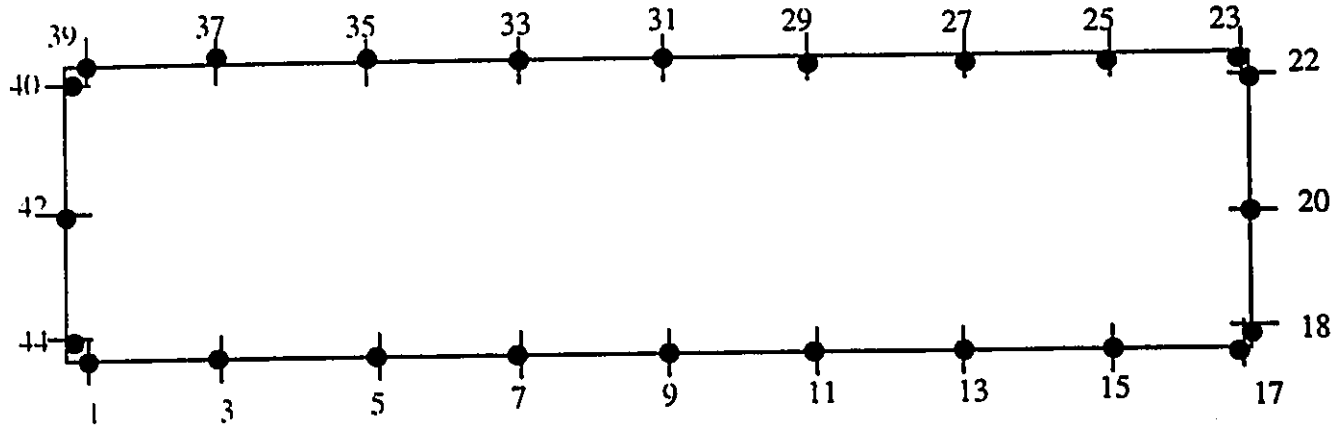

a) BE idealization for entire slab.

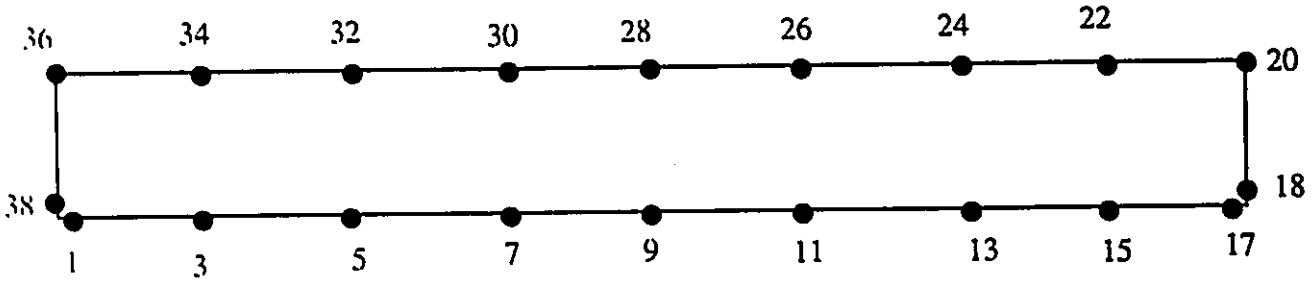

b)BE idealization for overhang.

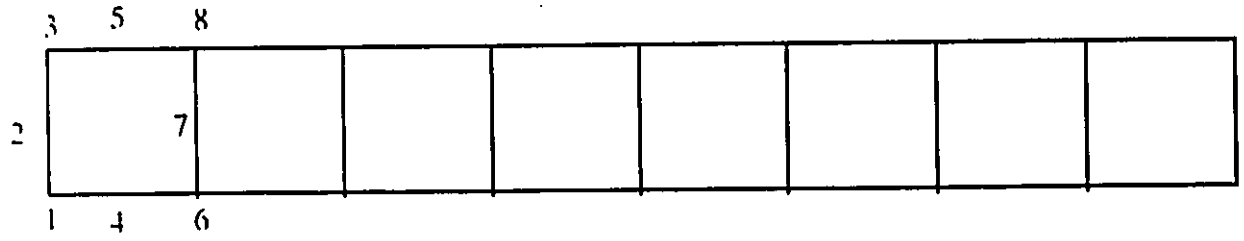

c) FE idealization using 8x1 mesh

Figure 5.11 BE and FE idealizations using quadratic elements for example 5.2.3.

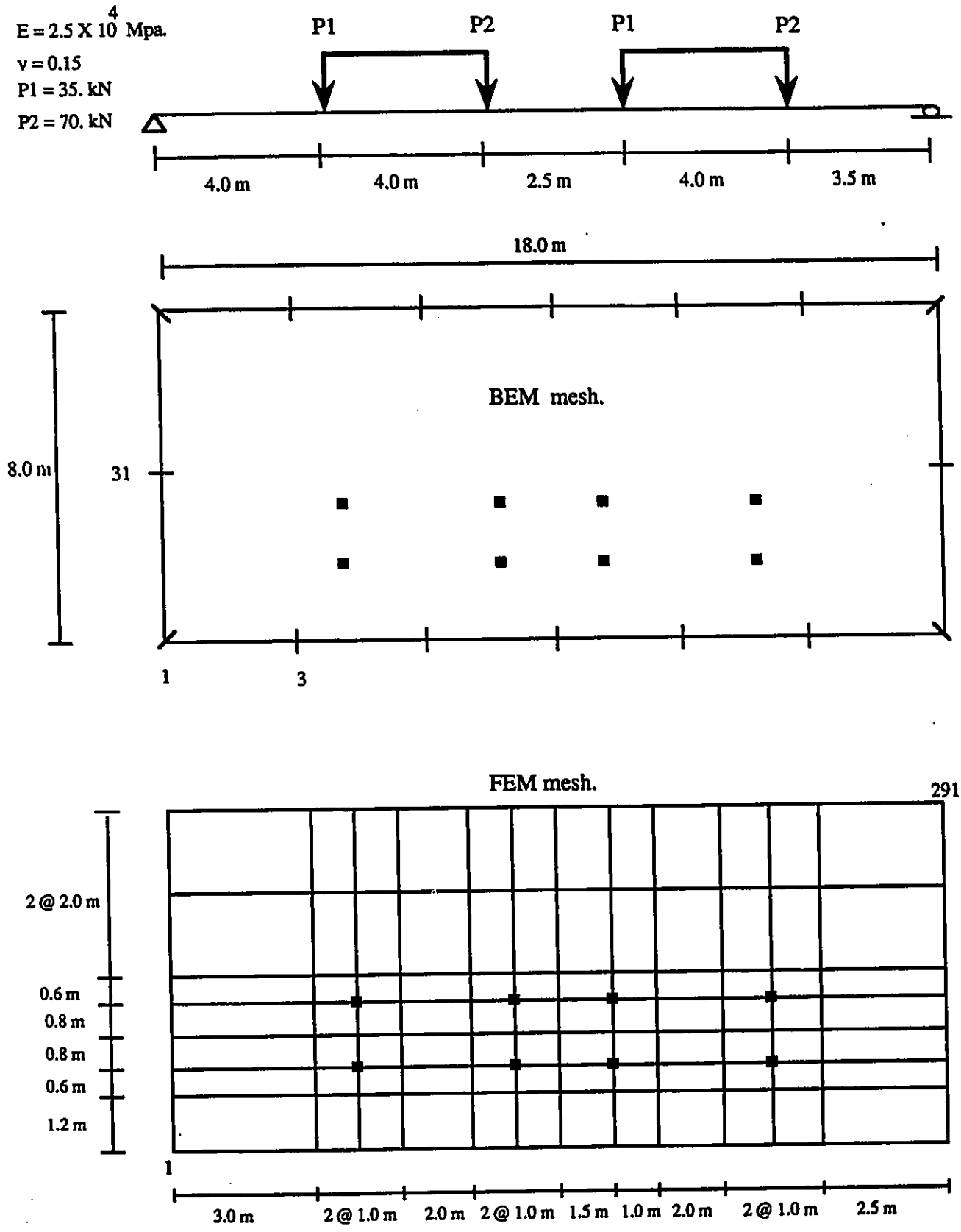

Figure 5.12 Details of the bridge in example 5.2.5.

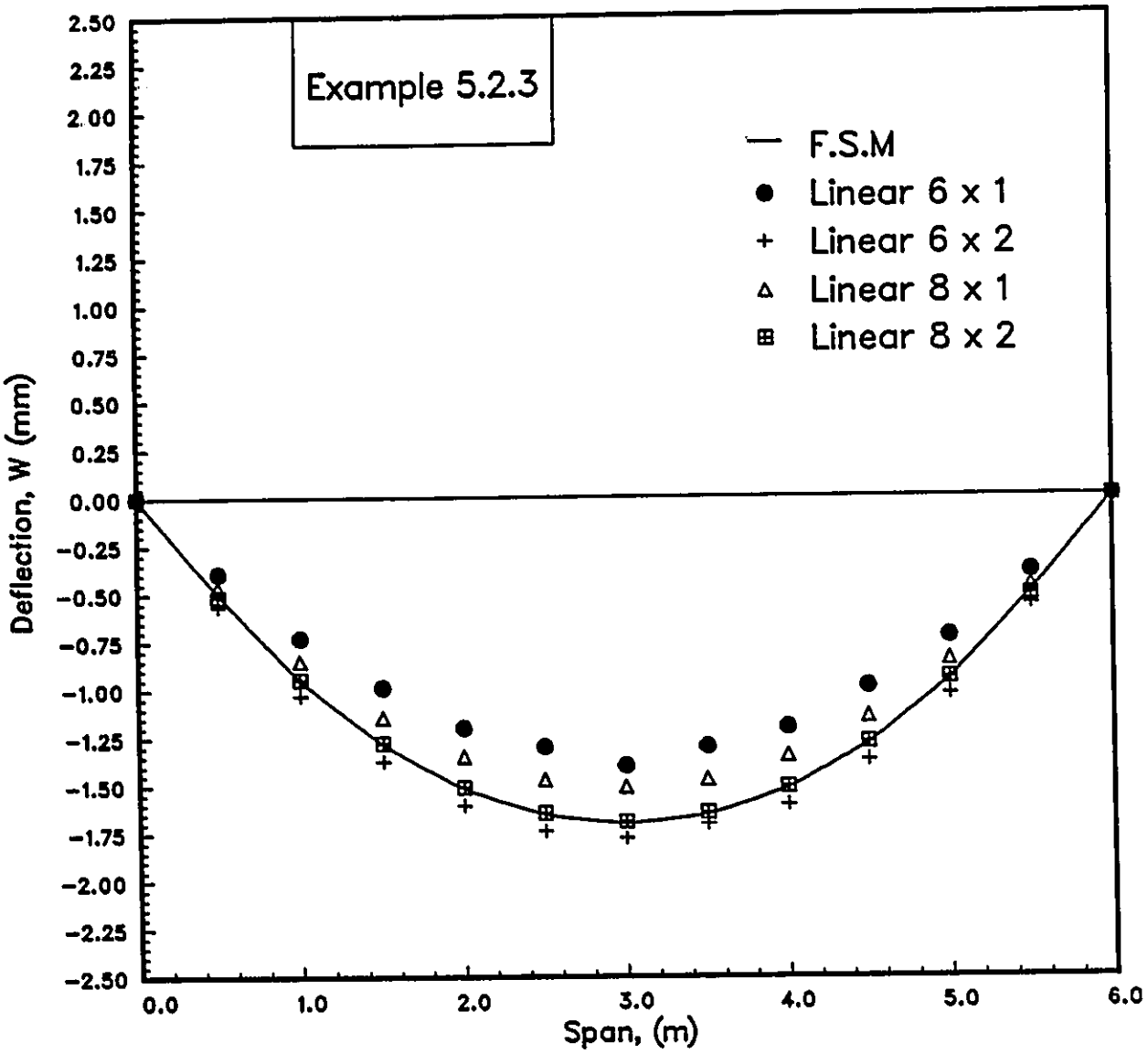

Figure 5.13: Vertical deflection along the center of span.

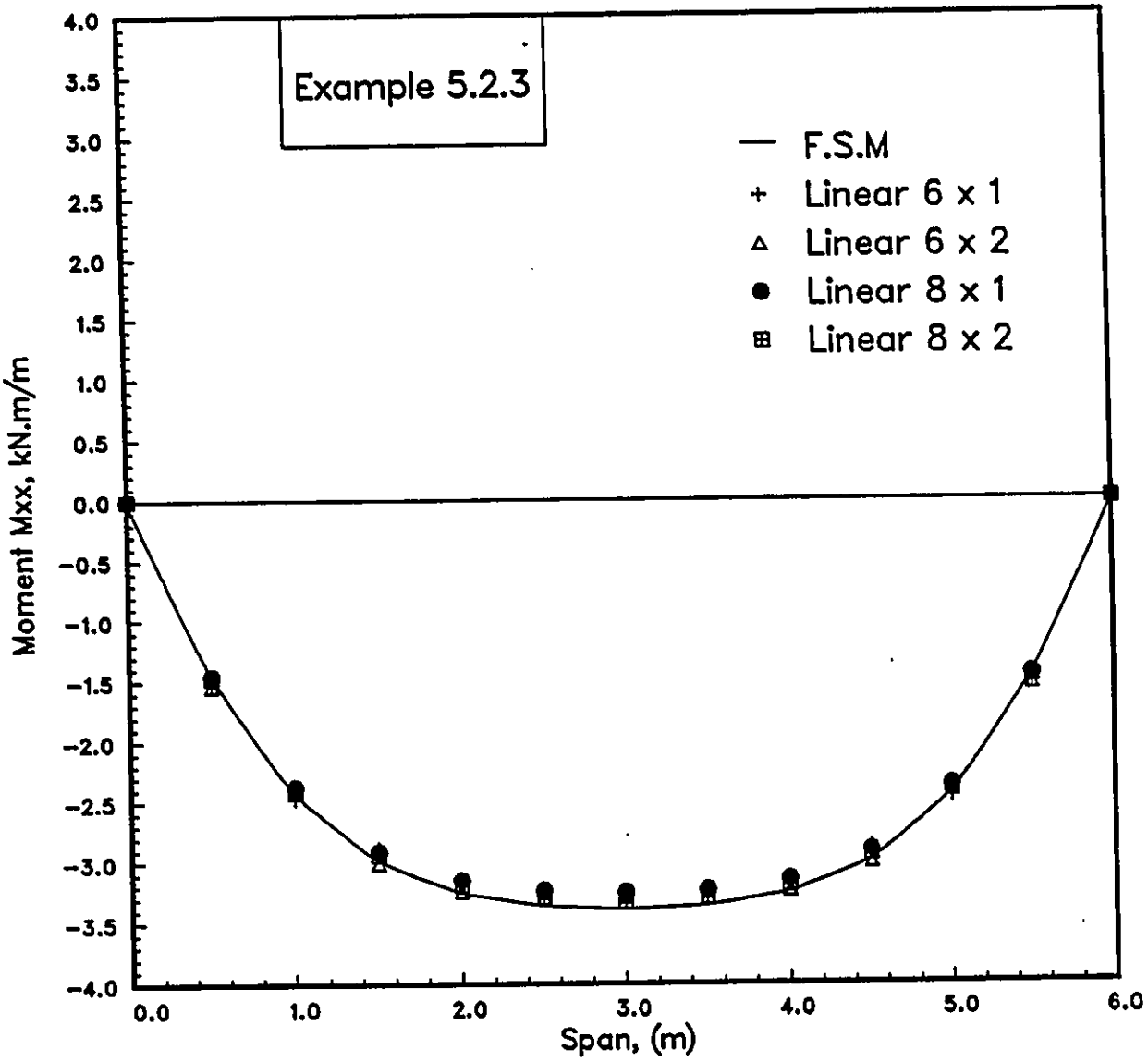

Figure 5.14: Variation of the longitudinal moment along the span.

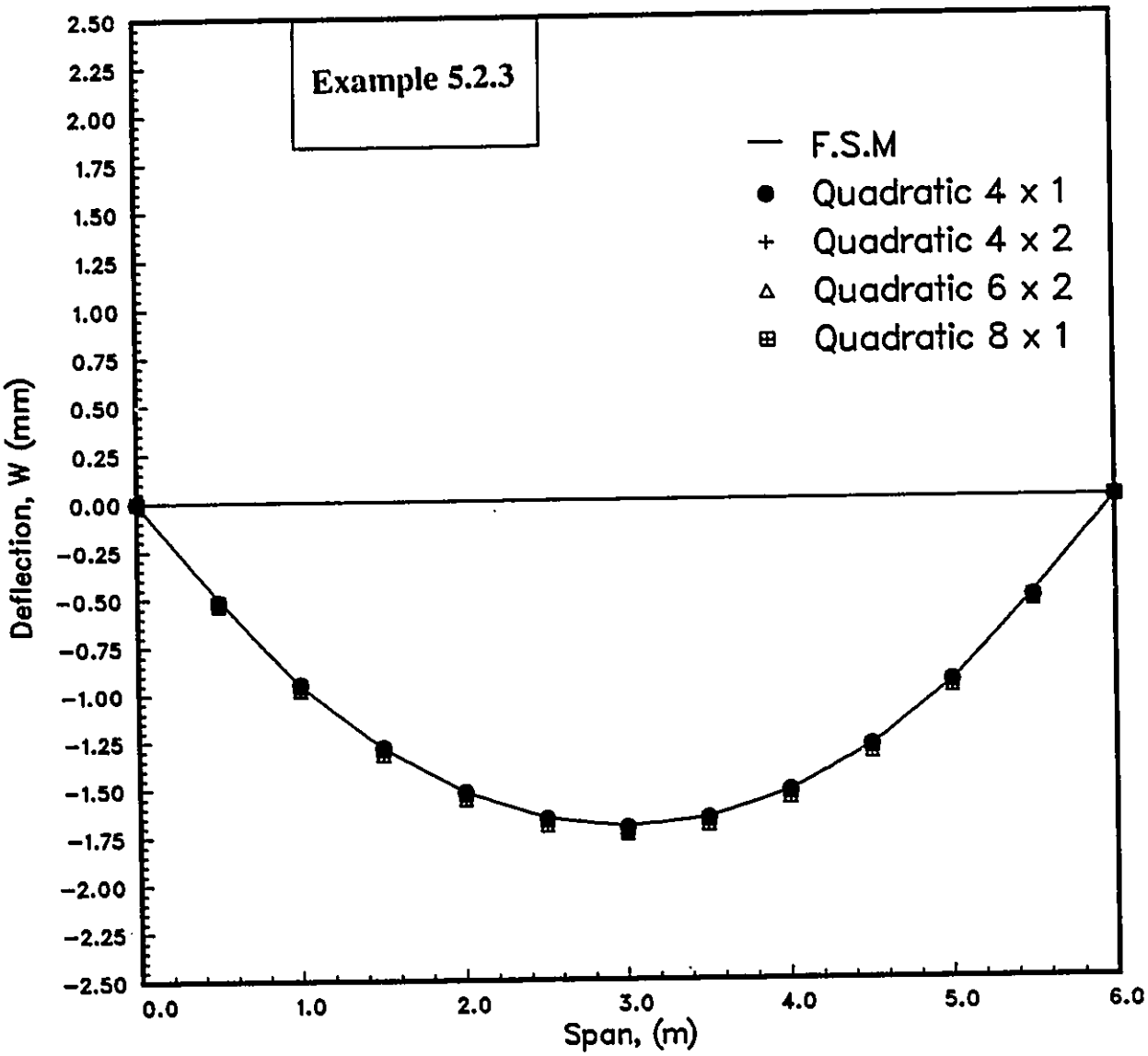

Figure 5.15: Vertical deflection along the center of span.

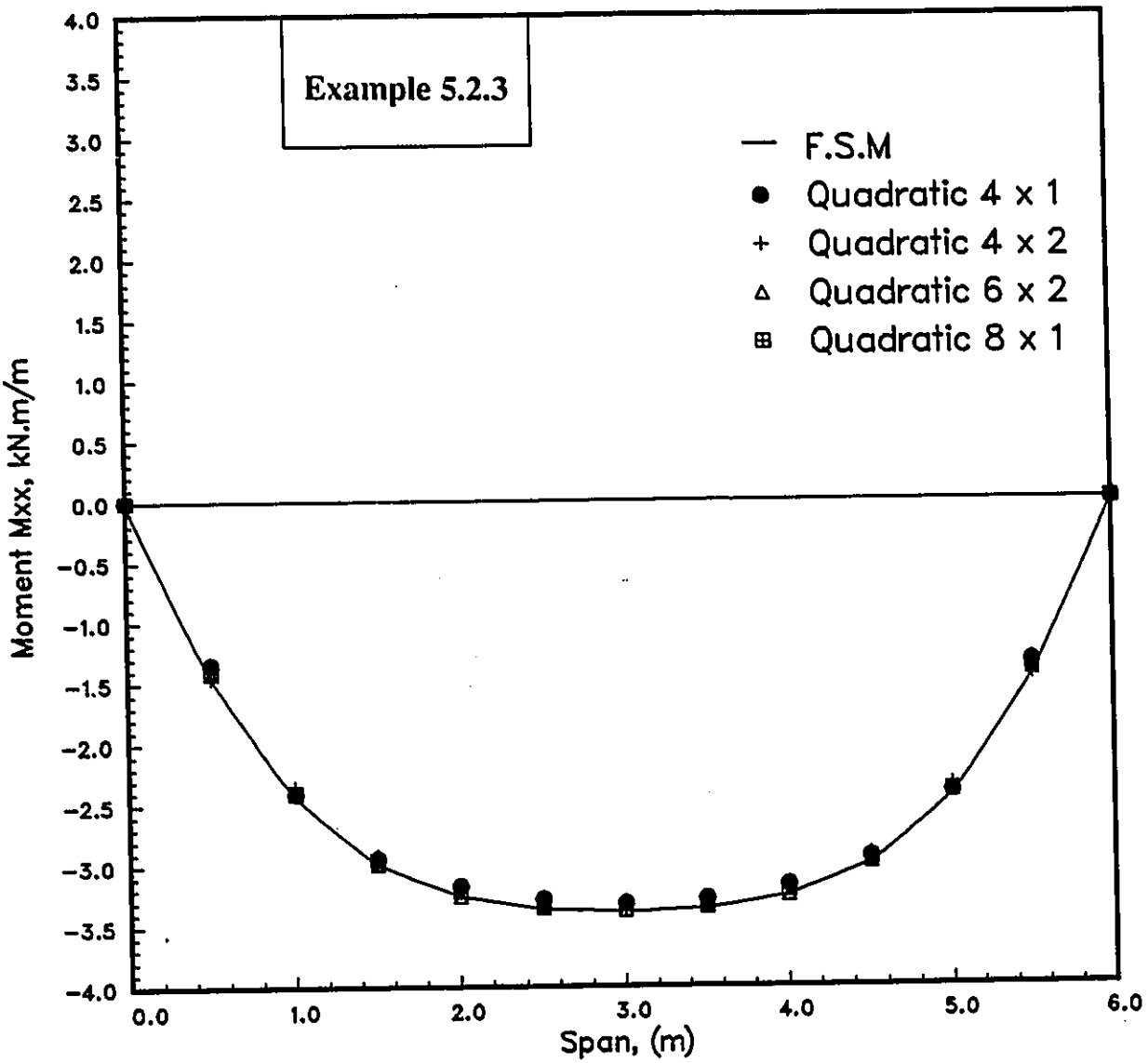

Figure 5.16: Variation of the longitudinal moment along the span.

Chapter 6

Applications And Results

6.1 General

The performance and the convergence of the combined method (BEM-FEM) have been tested through several case studies. The objective of this chapter is to demonstrate the applicability of the combined method to model and analyze various common types of bridges. A series of slab on girder and box girder bridges were analyzed to show the validity of the combined method. The bridges were subjected to different load conditions. Different meshes were used in order to investigated the accuracy of the results. The comparison of the results were made between the combined method (BEM-FEM) and the finite strip method (FSM).

6.2 Slab on girder bridges

6.2.1 Twin girder bridges

In the following examples we will refer to the bridge without overhangs as bridge-type 1 and that with overhangs as bridge-type 2.

6.2.1.1 Bridge-type 1 under uniform load (Example 1)

In the first example a simply supported concrete slab with two girders was subjected to a uniform load of 10 kN/m^2. The geometry and material properties of the bridge are shown in Figure 6.1. The bridge was divided into two regions ; the first region represented the slab which was discretized using two different boundary elements (linear and quadratic elements). The second region consisted of the girders which were modeled using 4 and 8 nodal rectangular elements. Two different meshes were considered in this example. In the first mesh the slab was modeled using 16 linear elements and 20 nodes while the girder was discretized by a 8×1 mesh of 4-nodal linear elements (see Figures 5.9-a and 5.9-b). In the second mesh, the girder was discretized by 6×2 linear elements (i.e. two layers) while the deck idealization remained the same as the first mesh (see Fig. 5.9-c). In the third mesh, the bridge deck was modeled using 16 quadratic elements and 36 nodes and the girder was modeled by 6×1 quadratic elements (8-node element) as shown in Figure 6.2.

The deflections along the center of the span using the BEM-FEM and the FSM solutions are shown in Figure 6.15, which shows a close agreement between the two methods when 8×2 or 6×1 meshes are used.

In BEM-FEM, both linear and quadratic elements gave good results in this example. Bending moments, M_{xx}, along the center of the span computed using both methods are plotted in Figure 6.16. A significant difference can be seen when linear elements with one layer (8×1) are used. The M_{xx} converges quickly when two layers of linear elements or quadratic elements are used for the girders.

Figures 6.17 and 6.18 show the variation of the vertical deflection along the girder and the transverse moments at the center of the span. The results of the BEM-FEM using quadratic elements agree well with the FSM solution.

6.2.1.2 Bridge-type 1 under one truck (Example 2)

Example 2 involved a slab on two girders with the same geometry and material properties used for example 1. The loading consisted of wheel loads using a HS15-44 truck [34]. The wheel loads were distributed uniformly on small patches. The bridge dimensions and the loading position are given in Figure 6.3. Two meshes were used in the boundary element and finite element idealization.

In the BEM-FEM analysis, 20 linear boundary elements with 24 nodes, and

a 8×2 mesh with 27 nodes were used to simulate the behavior of the bridge as shown in Figures 5.9-a and 5.9-c. A second mesh was used to model the bridge using quadratic elements. The slab was discretized into 16 elements while each girder was modeled by a 6×1 mesh (see Figure 6.2).

The deflection along the center of the span is plotted with that obtained from finite strip method in Figure 6.19. The deflections obtained from both meshes using BEM-FEM and FSM compare favorably. In Figures 6.20 and 6.21 the resulting bending moment M_{yy} is plotted at x = 6.0 m (i.e. at the mid span) and at x = 7.0 m along the bridge width using quadratic elements. The results obtained from BEM-FEM agree closely with those obtained from the finite strip method except at the boundary of the bridge width. In Table 6.1 the bending moments, M_{xx}, along the center of the span are compared with the finite element solution using the two meshes in

6.2.1.3 Bridge-type 2 under two truck (Example 3)

In this example, the geometry and material properties are shown in Figure 6.4. The loading consisted of two H20-44 trucks [34] located at center of the bridge. The wheel loads were distributed uniformly on small patches as shown in Figure 6.4.

The bridge was first analyzed by the finite strip method. The slab was divided into 30 strips and each girder was divided into 4 strips. seventy symmetrical series terms were considered in the analysis. Then, the bridge was analyzed

by BEM-FEM using three different meshes.

The top slab was divided into two regions consisting of the entire slab and the overhangs. The two regions were modeled by linear and quadratic boundary elements as shown in Figure 6.5, while the girders were discretized using the same meshe described in Figure 5.8-b.

The results of the deflection along the center of the span and along the girder are presented in Tables 6.2 and 6.3. The deflection results obtained from BEM-FEM using quadratic elements agree closely when compared with the FSM solution. The maximum difference in the central deflection using linear elements is under estimated by 10% when it is compared with FSM. Further, the results of the longitudinal moment along the span are compared with FSM in Table 6.4. The difference in the results of the bending moment for both solutions was approximately 4% when quadratic elements were used and 6% with linear elements.

6.2.2 Multi girder bridge (Example 4)

A concrete slab with four steel girders subjected to a uniformly distributed load of 20 kN/m^2 was considered in this example. The bridge was 6.0 m long and 1.25 m deep. The slab and girders were 0.25 m and 0.02 m thick respectively with 2.50 m spacing between the girders. The material properties for the bridge deck and the steel girders are shown in Figure 6.6.

Due to symmetry, one half of the bridge was modeled. Quadratic elements were used in the boundary element and finite element idealizations. The entire slab was modeled by 16 quadratic boundary elements while the overhang was modeled by 14 quadratic boundary elements as shown in Figures 6.5-a and 6.5-b. Each girder was modeled by a 6×1 mesh of 33 nodal finite elements (see Fig. 6.2-b).

The resulting deflections along the center of the span and along the interior girders are plotted against the results of FSM in Figures 6.22 and 6.23. The results of the bending moments along the center of the span are also compared with those obtained from finite element solution in Figure 6.24. The results from the two solutions are in good agreement.

6.3 Box girder bridges

6.3.1 Single-cell box girder bridge

6.3.1.1 Bridge-type 1 under uniform load (Example 5)

A concrete single-cell box girder bridge 9.0 m long, 3.0 m wide and 1.5 m deep was analyzed in this example. The top and bottom slabs of the box were 0.25 m thick while the webs were 0.35 m thick. The bridge was loaded with a uniformly distributed load over the top slab. The dimensions of the bridge and the material properties are given in Figure 6.7. The box girder bridge

was divided into two regions. The first region consisted of the top slab which was modeled using boundary elements. The second region, which included the bottom slab and the girders, was modeled by finite elements.

Two different meshes were used to simulate the behavior of the bridge. In the first mesh, the top slab was discretized using 24 linear boundary elements while a 8×2 mesh was used to model the webs and the bottom slab (see Figures 6.8-a and 6.8-b). In the second mesh, the top slab was divided into 36 quadratic elements while the bottom slab and each web were discretized by a 6×1 mesh (see Figures 6.9-a and 6.9-b).

The center deflections along the top slab for the two meshes were compared for the two methods (i.e. BEM-FEM and FSM) as shown in Figure 6.25. A very good agreement is observed between the two solutions when both meshes are used.

The longitudinal moment along the center of the bridge and the transverse moment along the width of the bridge are plotted in Figures 6.26 and 6.27. The results obtained from the combined method for both meshes were in good agreement with the finite strip results. The combined method using linear elements gave higher values for the transverse moment near the boundary due to singularity (see Figure 6.27).

6.3.1.2 Continuous bridge-type 1 under eccentric load (Example 6)

Example 6 involved a continuous, two span concrete box girder with an eccentric point load in one of the span. The dimensions, loading and material properties are given in Figure 6.10. The top slab was modeled by 14 quadratic boundary elements with 32 nodes, while the webs and the bottom slab were modeled by finite elements using a 6×1 mesh. The webs and the bottom slab idealizations are shown in Figure 6.9-b.

The resulting deflection along girder no. 1 was compared with that obtained by [35] using a harmonic folded plate analysis. In Table 6.5, in spite of using a coarse mesh in this example, the maximum difference in the deflection between the two solutions was approximately 10%.

6.3.1.3 Bridge-type 2 under uniform load (Example 7)

A single-box girder bridge with overhangs subjected to uniform load of 10 kN/m^2 was considered in this example. The dimensions and material properties are shown in Figure 6.11.

In idealizing the bridge, the same modelling technique used in examples 5 and 6 was employed. The top slab including the overhangs was modeled by boundary elements and the bottom slab and the girders were modeled by finite elements. Two different meshes were used to demonstrate the accuracy of the results. The boundary element and finite element idealizations are shown in

Figures 6.8 and 6.9.

Figures 6.28 and 6.30 show the variation of deflection and longitudinal moment along the top span. The results show a good agreement with the finite strip solution when both linear (2 layers) or quadratic elements are used. The variation of deflection along the girders is improved when quadratic elements are used (see Figure 6.29). The results of the transverse moment at the mid span compare favorably for the FSM and the BEM-FEM when both meshes are used. Linear elements gave higher values for the moment near the boundary due to singularity (see Fig. 6.31).

6.3.1.4 Bridge-type 2 under concentrated loads (Example 8)

The bridge in example 7 with the same material properties was considered here. The loading consisted of four concentrated loads located at the center of the span as shown in Figure 6.12. Linear and quadratic elements were used in the boundary and finite element idealizations. The same meshes described in Figures 5.9 and 6.2 were used to model the bridge.

The deflection along the girders is plotted against the finite strip results in Figure 6.32. The results obtained from the two solutions are in good agreement when both linear and quadratic elements are used. The variation of the normal moment along the girder using quadratic elements was compared with FSM in Figure 6.33 and the results agree well.

6.3.2 Multi-cell box girder bridge

6.3.2.1 Two-cell box girder bridge under uniform load (Example 9)

A two-cell box girder bridge 6.0 m long and 1.45 m deep was chosen in this example. The thickness of the top and the bottom slabs were 0.25 m and 0.30 m respectively and the webs were 0.35 m thick. The top slab was subjected to a uniformly distributed load of 15 kN/m^2. The material properties are shown in Figure 6.13. Due to symmetry, only half of the bridge was analyzed. The entire slab and the overhang were discretized using 36 and 30 quadratic elements receptively while the bottom slab and the webs were modeled by a 6×1 mesh using 8-node element (see Figures 6.5-a, 6.5-b and 6.9-b). The bridge was analyzed using the combined method and the finite strip method. The vertical deflection and the longitudinal bending moments along the center of the top slab are plotted in Figures 6.34 and 6.35. The results of the bending moment and the deflection agree closely between the two methods.

6.3.2.2 Two-cell box girder bridge under four trucks (Example 10)

A 20.0 m long bridge with the same geometry and material properties as in example 9 was considered. The loading consisted of four HS15-44 trucks [34]. Details of the bridge are given in Figure 6.14. For the BEM-FEM analysis, the entire slab and the overhangs were only discretized by 44 and 38 quadratic elements respectively while a 8×1 mesh using 8-node element was used to

model the girders and the bottom slab. Details of the boundary element and finite element idealizations are given in Figure 5.11.

The deflection along the center of the top slab and the longitudinal moment along the center line of the first wheel loads obtained from BEM-FEM and FSM solutions are presented in Tables 6.6 and 6.7. The maximum difference in the deflection and the moment between the two solutions are 2% and 4% respectively.

In idealizing the bridge deck, the FSM mesh had to be adjusted in the transverse direction in order to fit the size of the wheel loads. To simulate the behavior of the bridge in this example, 64 longitudinal sections and 80 terms were used. In practical applications, usually coarse meshes are used to model real bridges under truck loads due to their complex geometry. However, in the FEM, more refined meshes are required in the vicinity of the truck loads in order to simulate the behavior of the bridge. Therefore a large number of equations and a significant storage capacity are required to obtain an accurate solution which becomes drawback in practical applications. In addition to that if the truck loads do not coincide with the finite element nodes, then the solution of the FEM will involve static distribution of loads. Therefore, the FEM would not give the desired level of accuracy due to these approximations. In the FEM and FSM the interior solution involves approximations and the mesh requires refinement in order to simulate the local stresses of the wheel loads.

The BEM-FEM provides a better alternative to FEM and FSM. As seen from example 10, the BEM-FEM is suitable to analyze bridges under wheel loads.

The interior solution involves no approximation and it gives an accurate results without using refined meshes. The number and the position of the trucks in example 10 do not affect the size of the boundary element mesh.

Table 6.1: Longitudinal moment along the span for Example 2

Span	FSM	BEM-FEM (kN.m/m)	
(m)	kN.m/m	Linear II	Quadratic
1.0	1.578	1.650	1.621
2.0	2.435	2.686	2.566
3.0	3.438	3.717	3.561
4.0	4.679	4.952	4.834
5.0	6.765	7.082	6.960
6.0	6.934	7.311	7.188
7.0	7.318	7.647	7.534
8.0	6.186	6.530	6.384
9.0	6.433	6.832	6.614
10.0	5.544	5.963	5.788
11.0	4.218	4.301	4.316

Table 6.2: Deflection along the span for Example 3

Span (m)	FSM (mm)	BEM-FEM (mm)	
		Linear II	Quadratic
1.0	0.179	0.163	0.181
2.0	0.329	0.298	0.331
3.0	0.404	0.362	0.406
4.0	0.459	0.413	0.461
5.0	0.524	0.478	0.526
6.0	0.544	0.507	0.545
7.0	0.315	0.297	0.315

Table 6.3: Deflection along the girder for Example 3

Span (m)	FSM (mm)	BEM-FEM (mm)
		Linear II
1.0	0.158	0.136
2.0	0.296	0.261
3.0	0.392	0.353
4.0	0.443	0.408
5.0	0.441	0.414
6.0	0.371	0.356
7.0	0.209	0.208

Table 6.4: Longitudinal moment along the span for Example 3

Span	FSM	BEM-FEM (kN.m/m)	
(m)	(kN.m/m)	Linear II	Quadratic
1.0	1.277	1.326	1.226
2.0	1.467	1.518	1.510
3.0	1.260	1.182	1.224
4.0	1.617	1.515	1.555
5.0	4.998	4.868	4.902
6.0	6.727	6.920	6.838
7.0	5.599	5.664	5.537

Table 6.5: Vertical girder displacements for Example 6

Span	Deflection (mm)	
(m)	BEM-FEM	Ref. [35]
15.0	2.97	2.68
30.0	4.05	3.88
45.0	2.44	2.41
60.0	0.	0.
75.0	1.41	1.58
90.0	1.68	1.88
105.0	1.09	1.18

Table 6.6: Deflection along the center of the span for Example 10

Span (m)	FSM (mm)	BEM-FEM (mm)
		8×1 mesh
2.0	6.93	6.84
4.0	12.73	12.48
5.8	16.97	16.64
8.0	20.44	20.23
10.0	22.36	21.97
13.0	19.13	18.92
16.0	12.74	12.54
17.2	9.62	9.43
18.0	6.93	6.83

Table 6.7: Longitudinal moment along the center of wheel loads for Example 10

Span (m)	FSM (kN.m/m)	BEM-FEM (kN.m/m)
		8 × 1 mesh
2.0	1.749	1.783
4.0	0.875	0.849
5.8	1.452	1.396
8.0	0.626	0.613
10.0	10.360	9.962
13.0	1.442	1.389
16.0	0.874	0.857
17.2	5.172	4.974
18.0	1.749	1.778

Loading = 10. kN/m^2

E = 2.5×10^4 Mpa

$\nu = 0.15$

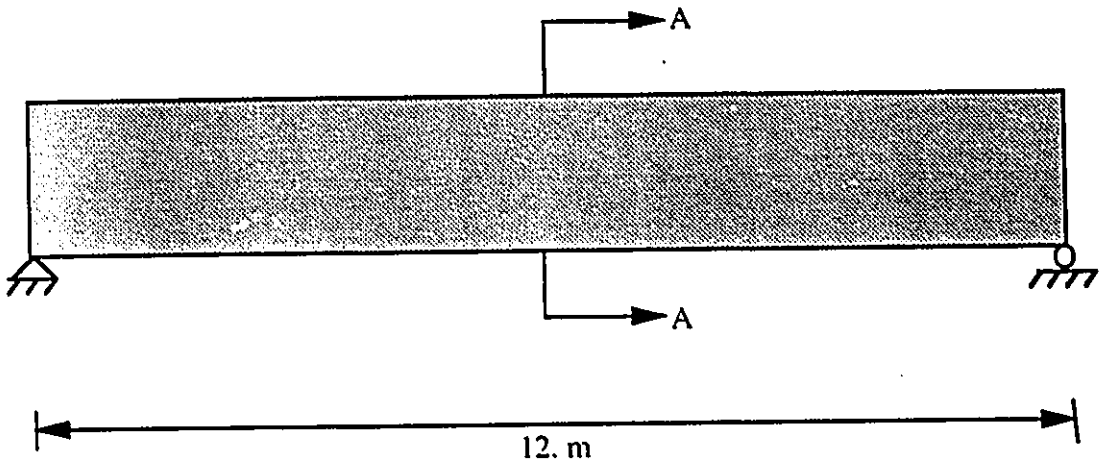

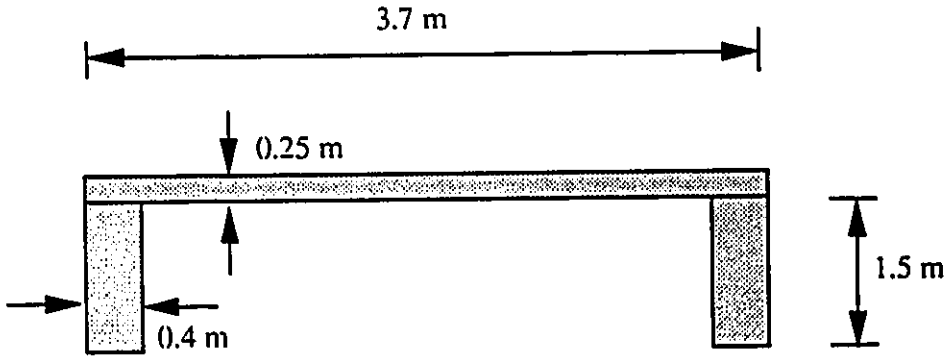

Cross section A-A

Figure 6.1 Geometrical and material properties of the bridge for example 1.

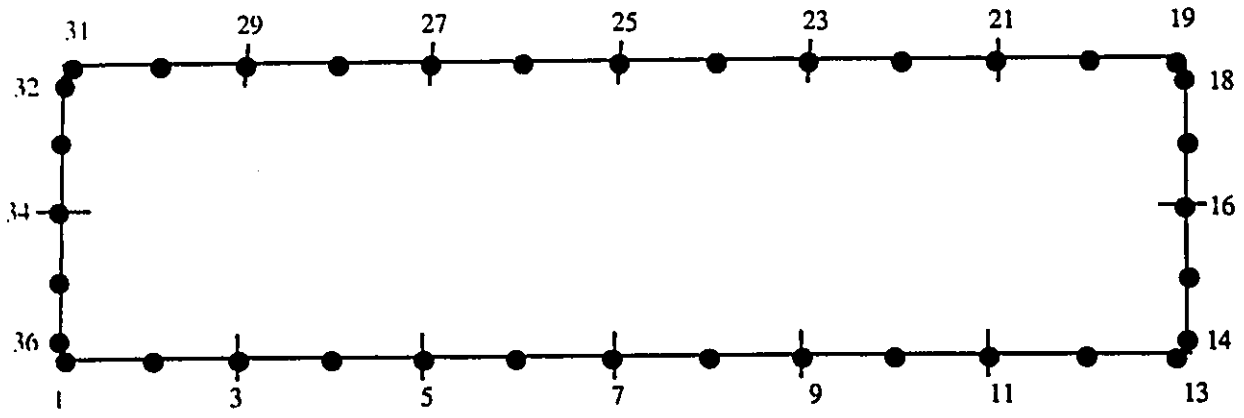

a) BE idealization for the slab using quadratic elements.

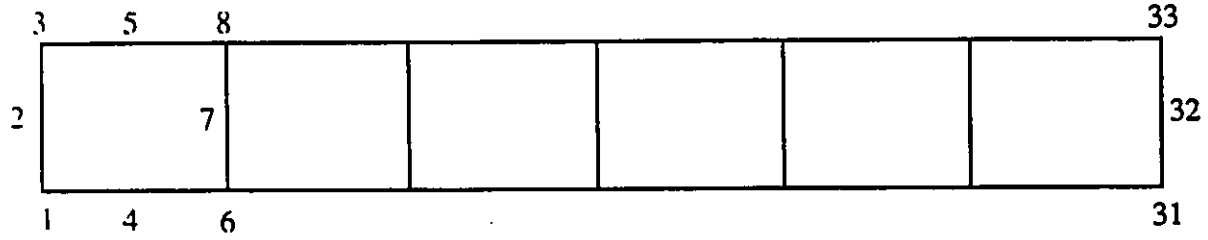

b) FE idealization for the girder (6x1 mesh).

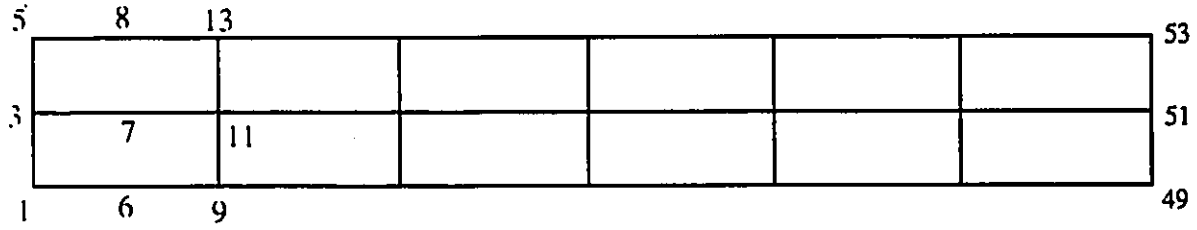

c) FE idealization for the girder (6x2 mesh).

Figure 6.2 BE and FE idealizations using quadratic elements.

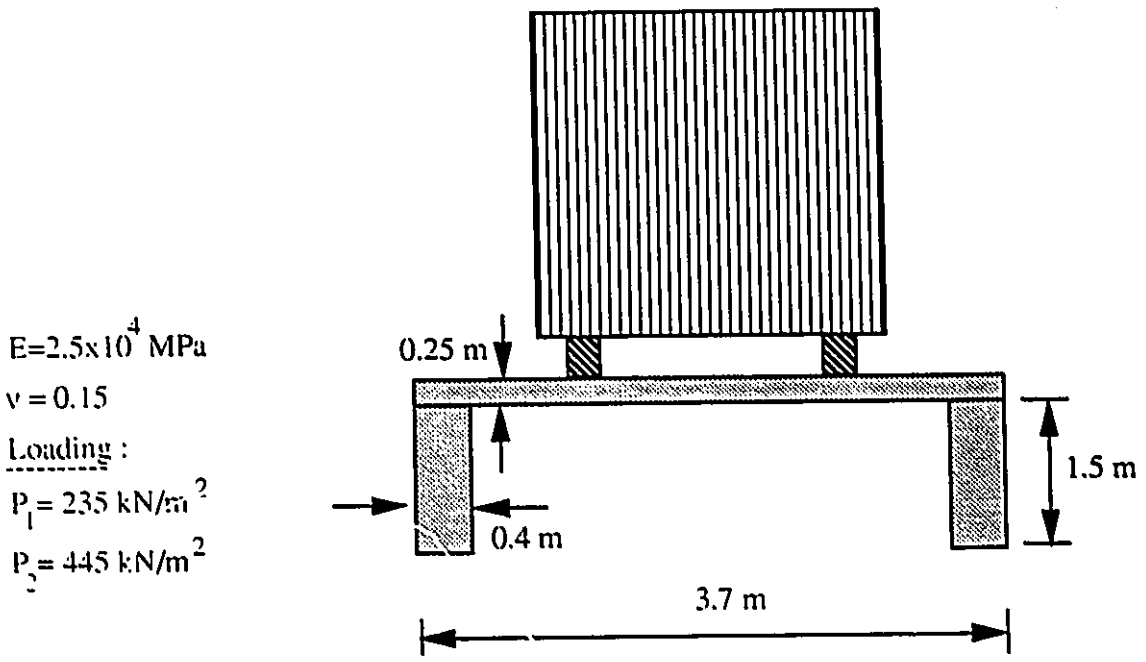

a) Cross section of the bridge.

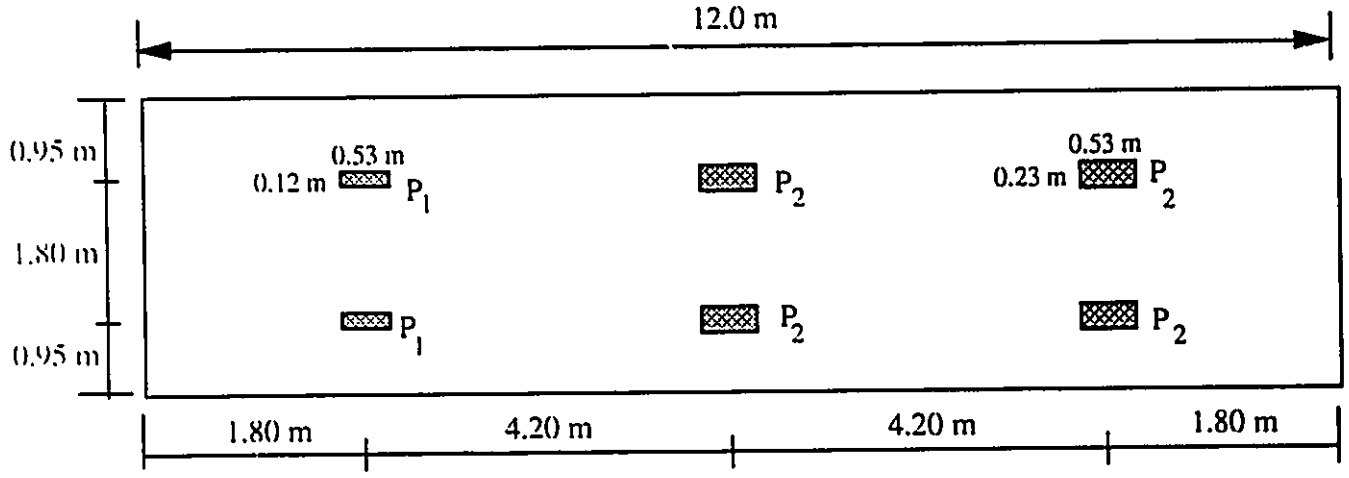

b) Loading position.

Figure 6.3 The bridge dimensions, material properties and loading for example 2.

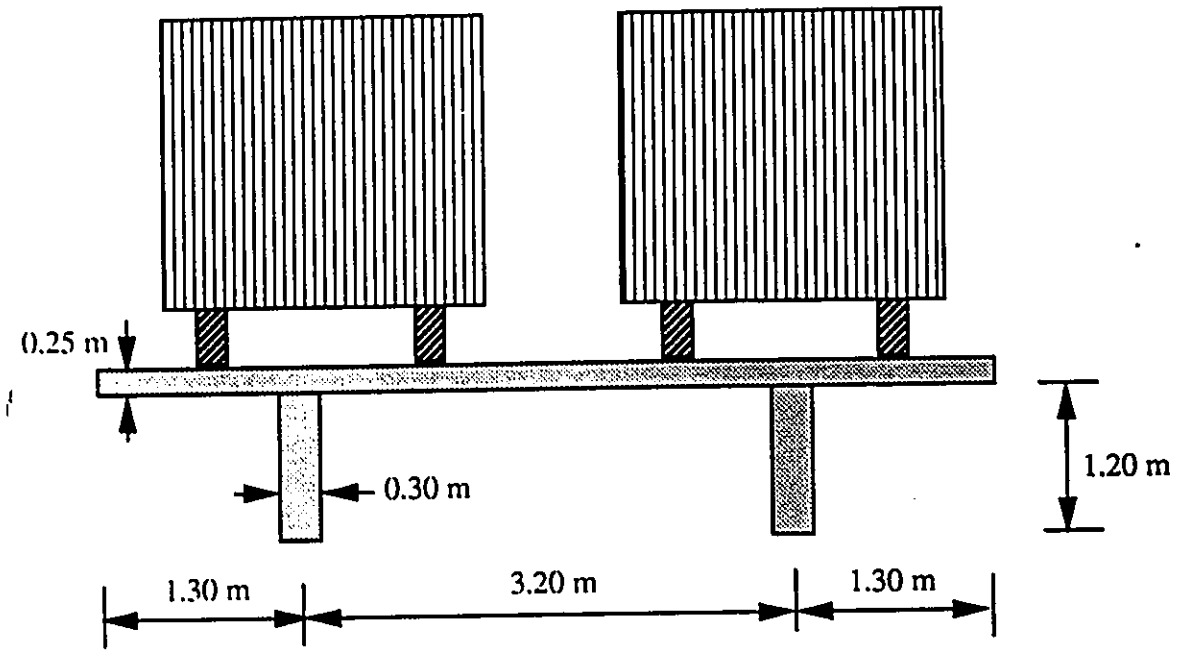

$E=2.5\times10^{4}$ MPa

$\nu = 0.15$

$P_1 = 285$ kN/m^2

$P_2 = 590$ kN/m^2

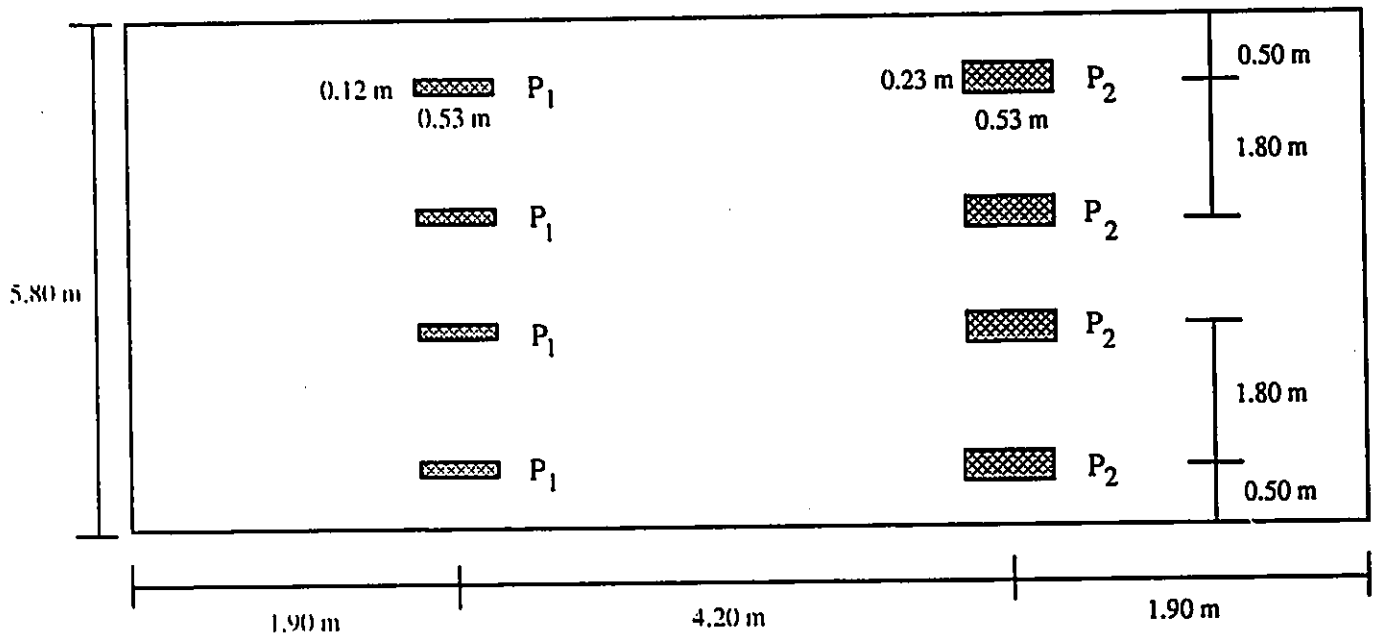

Figure 6.4 Details and loading of the bridge for example 3.

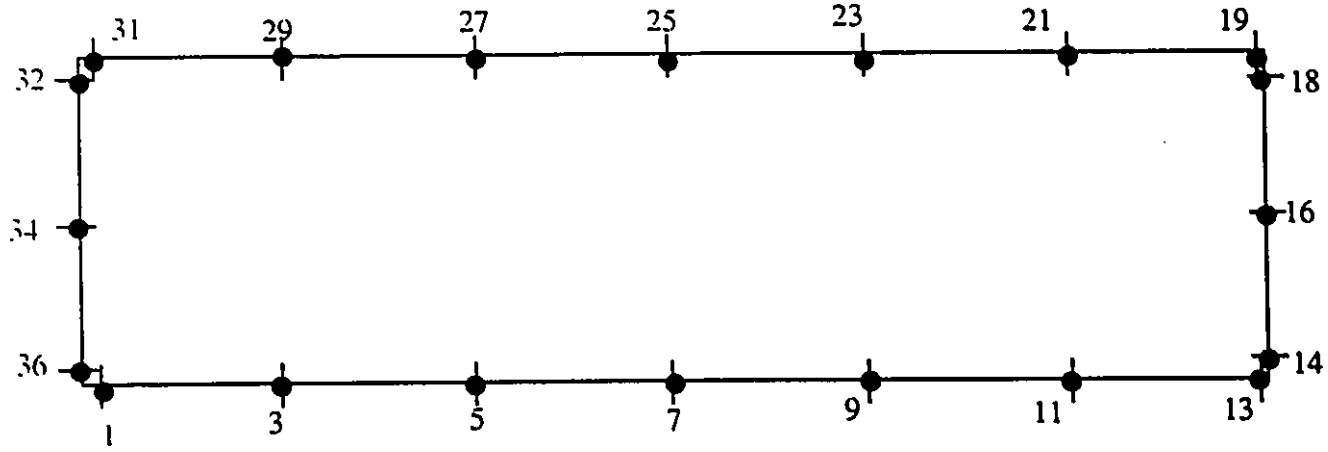

a) BE idealization for entire slab using quadratic elements.

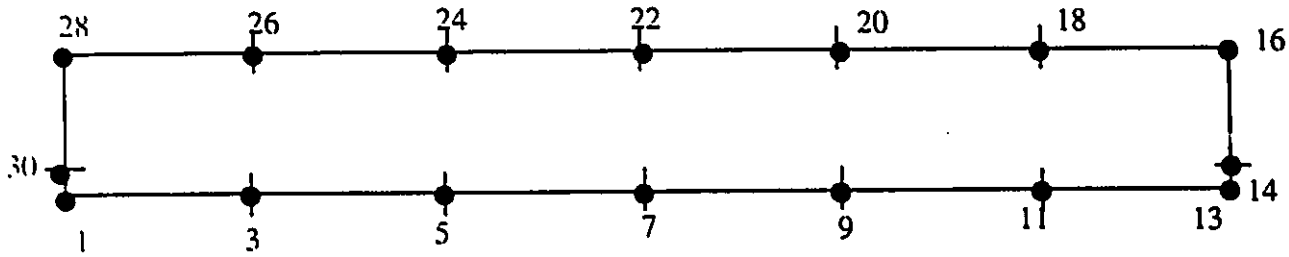

b) BE idealization for overhangs using quadratic elements.

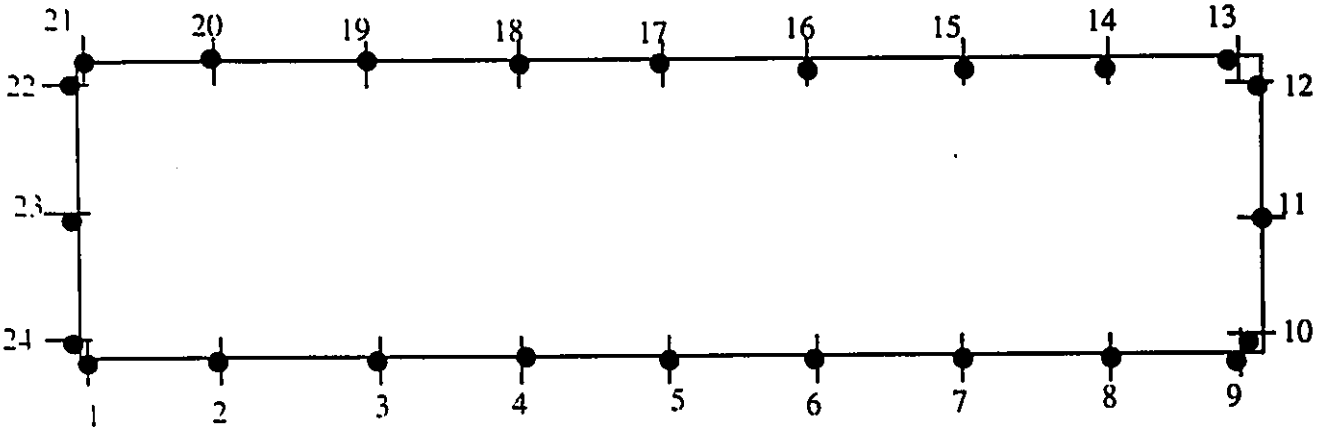

c)BE idealization for entir slab using linear elements

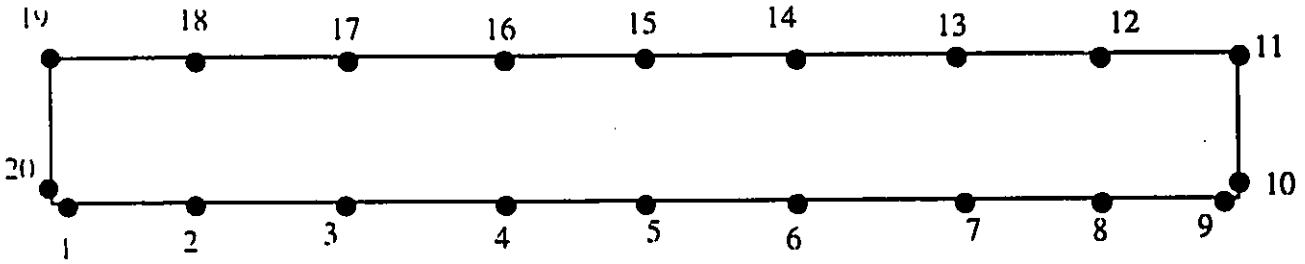

d)BE idealization for overhangs using linear elements.

Figure 6.5 BE ideaalization for the top slab.

Slab : $E = 2.5 \times 10^4$ MPa, $\nu = 0.15$

Girder: $E = 3.0 \times 10^5$ MPa, $\nu = 0.3$

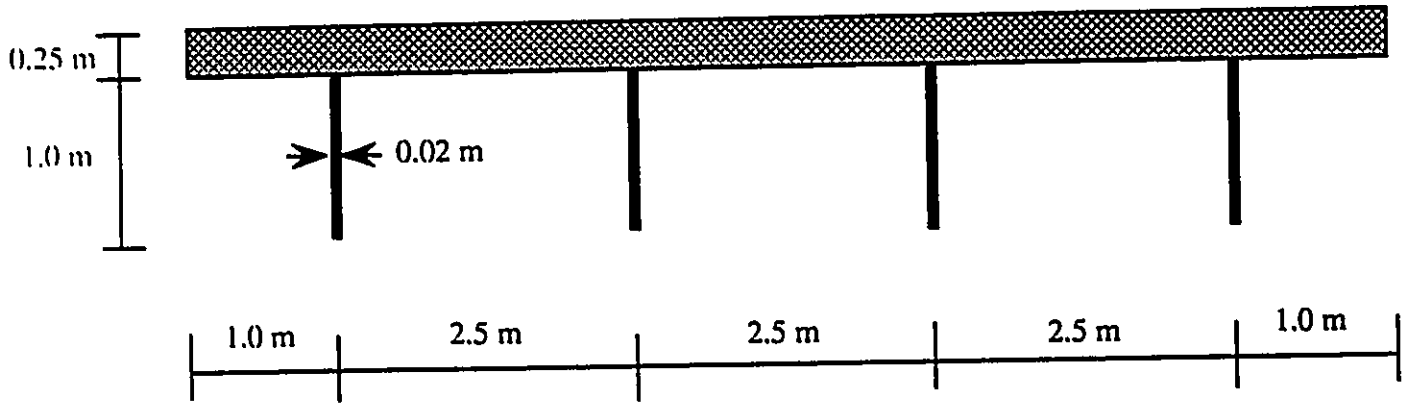

Figure 6.6 A slab on steel girders bridge.

Loading = 15. kN/m^2

E= 2.5 x10^4 MPa

$\nu = 0.15$

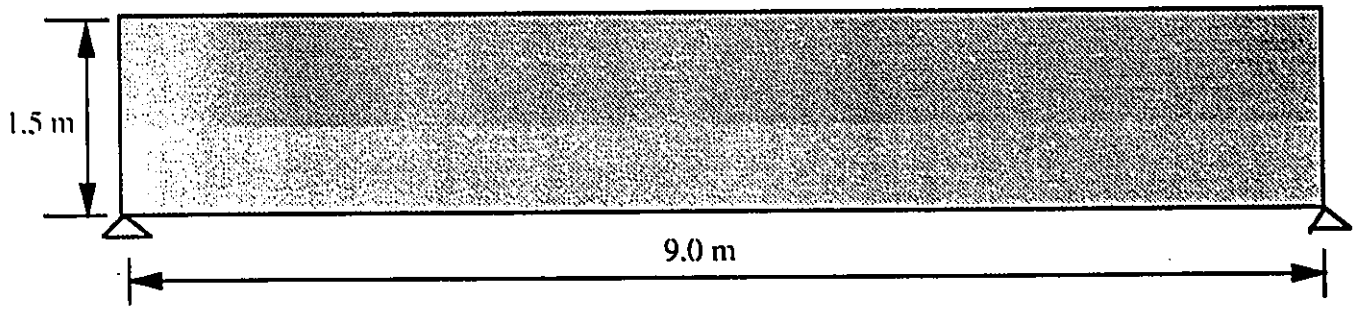

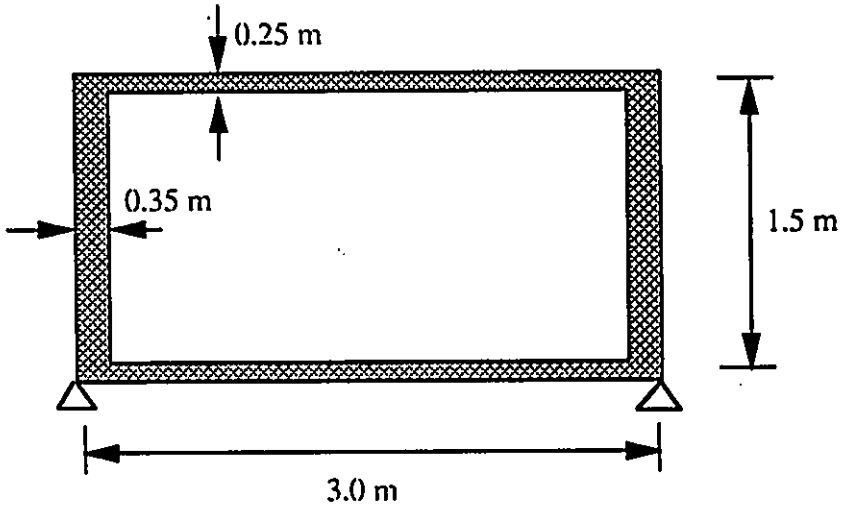

Figure 6.7 Details and loading of the birdge for example 5.

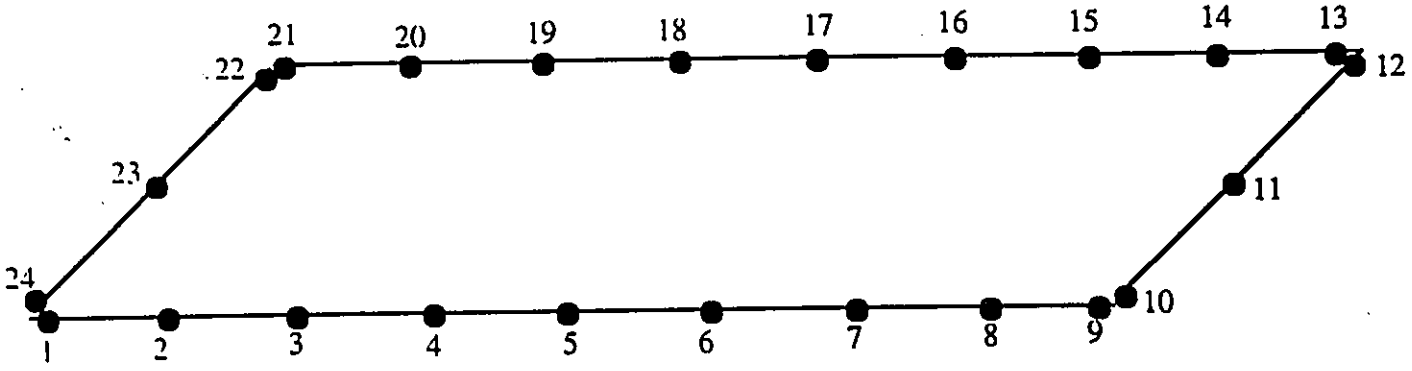

a) BE idealization for the slab using linear elements.

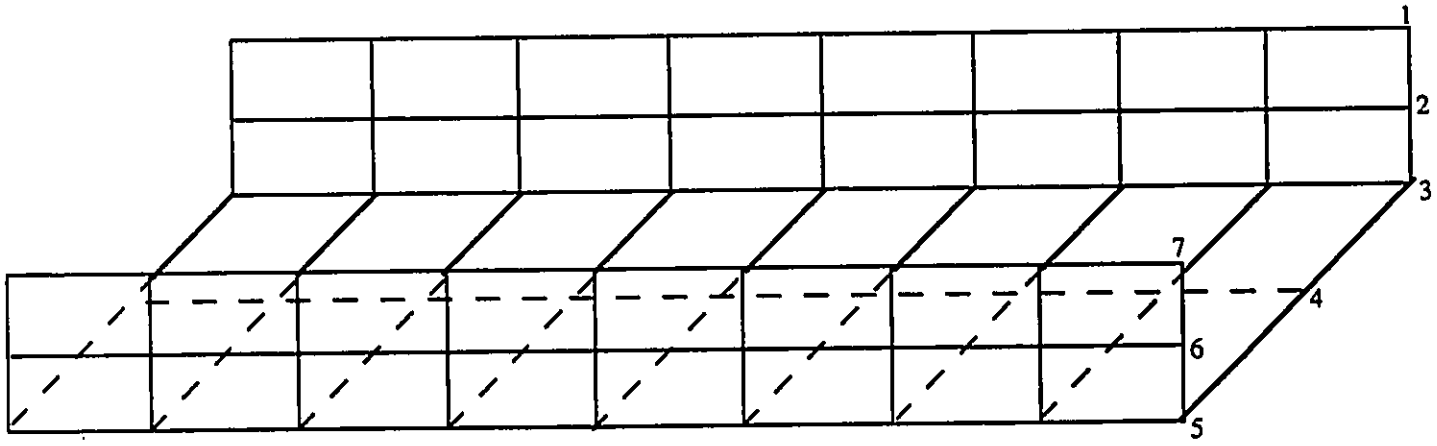

b) FE idealization for girders and bottom slab (8x2 mesh).

Figure 6.8 BE and FE idealizations for a single-cell bridge using linear elements.

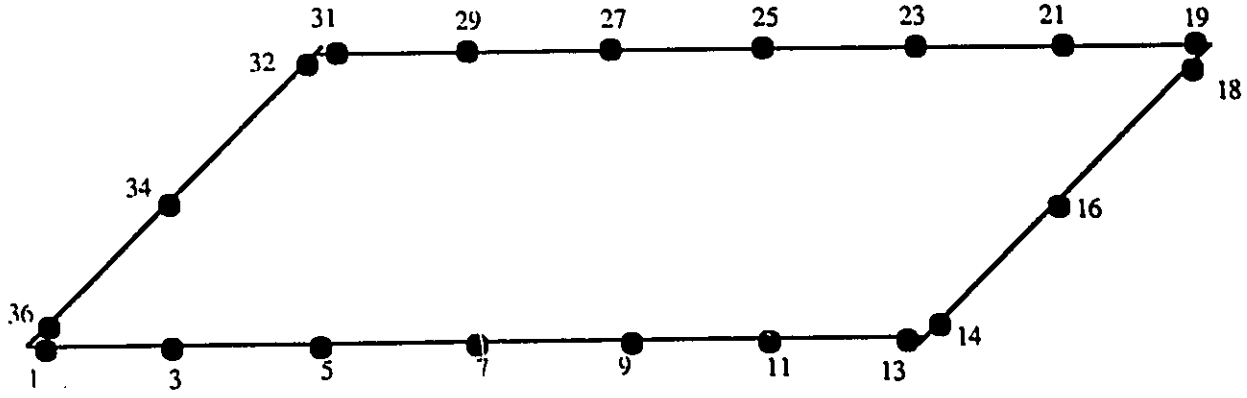

a) BE idealization for the slab using quadratic elements.

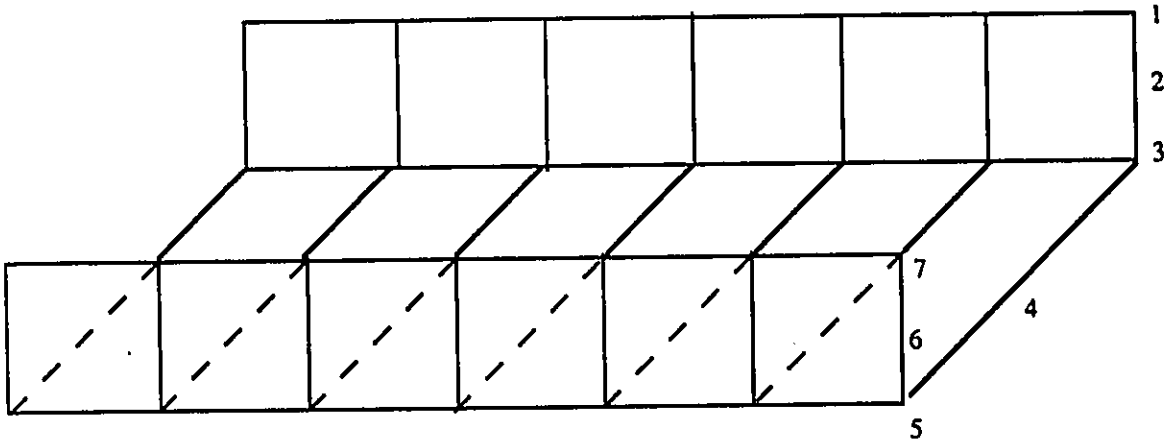

b) FE idealization for webs and bottom slab (6x1 mesh).

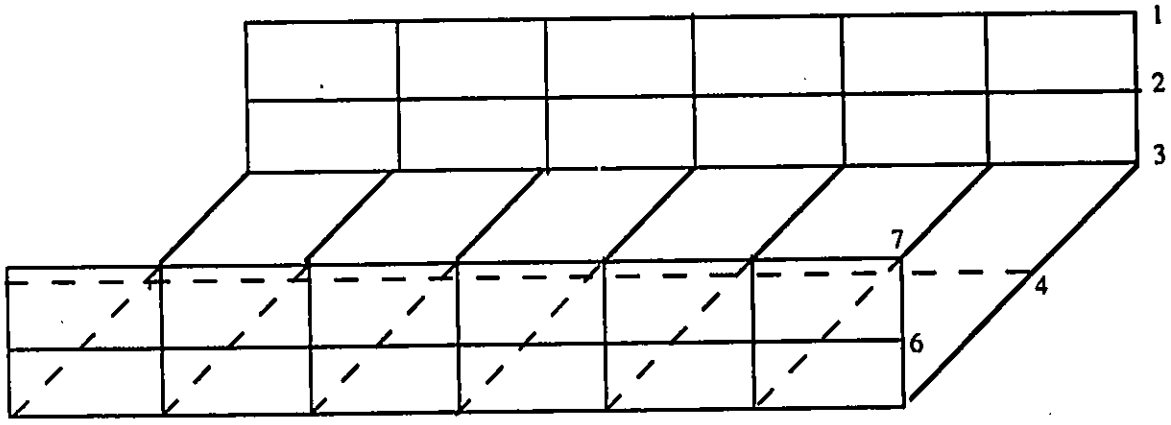

c) FE idealization for webs and bottom slab (6x2 mesh).

Figure 6.9 BE and FE idealization for a single-cell bridge using quadratic elements

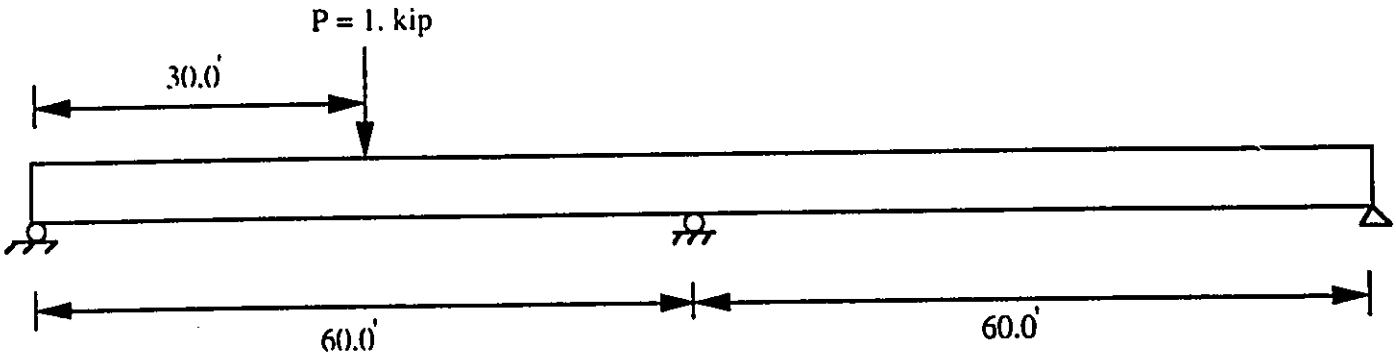

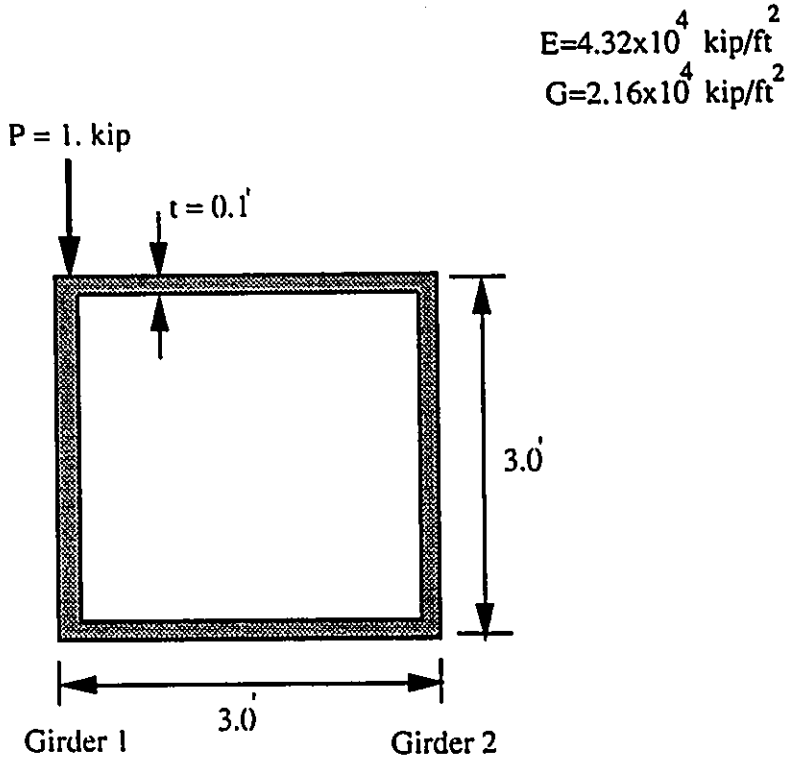

Figure 6.10 Details and loading of the birdge for example 6.

$E=3.2x10^3$ MPa
$\nu=0.15$
Load = 10 kN/m^2

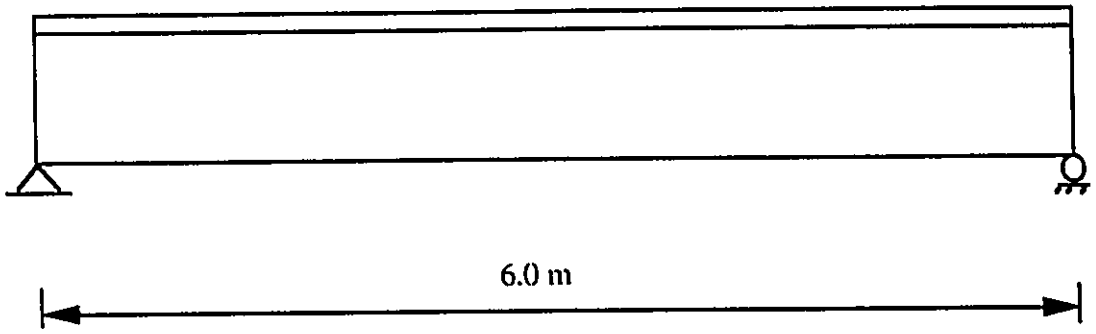

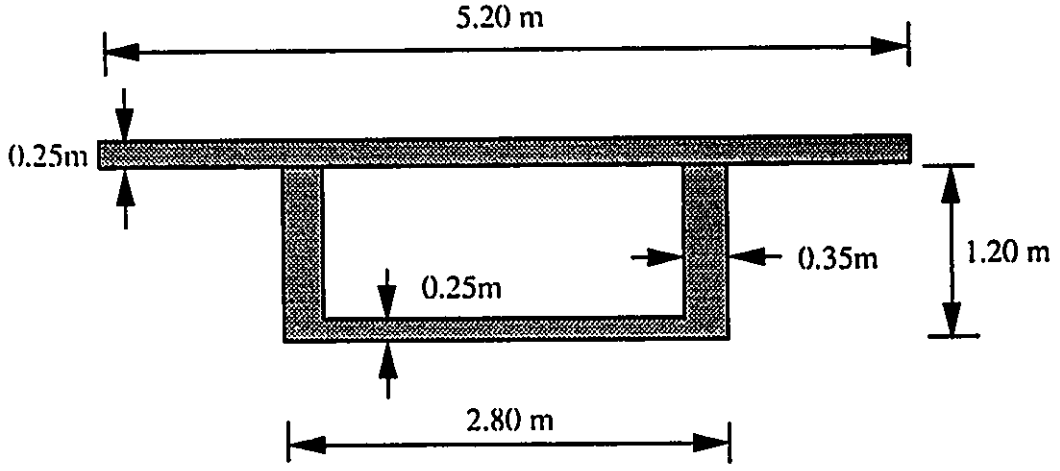

Figure 6.11 Geometrical and material properties of the bridge for example 7.

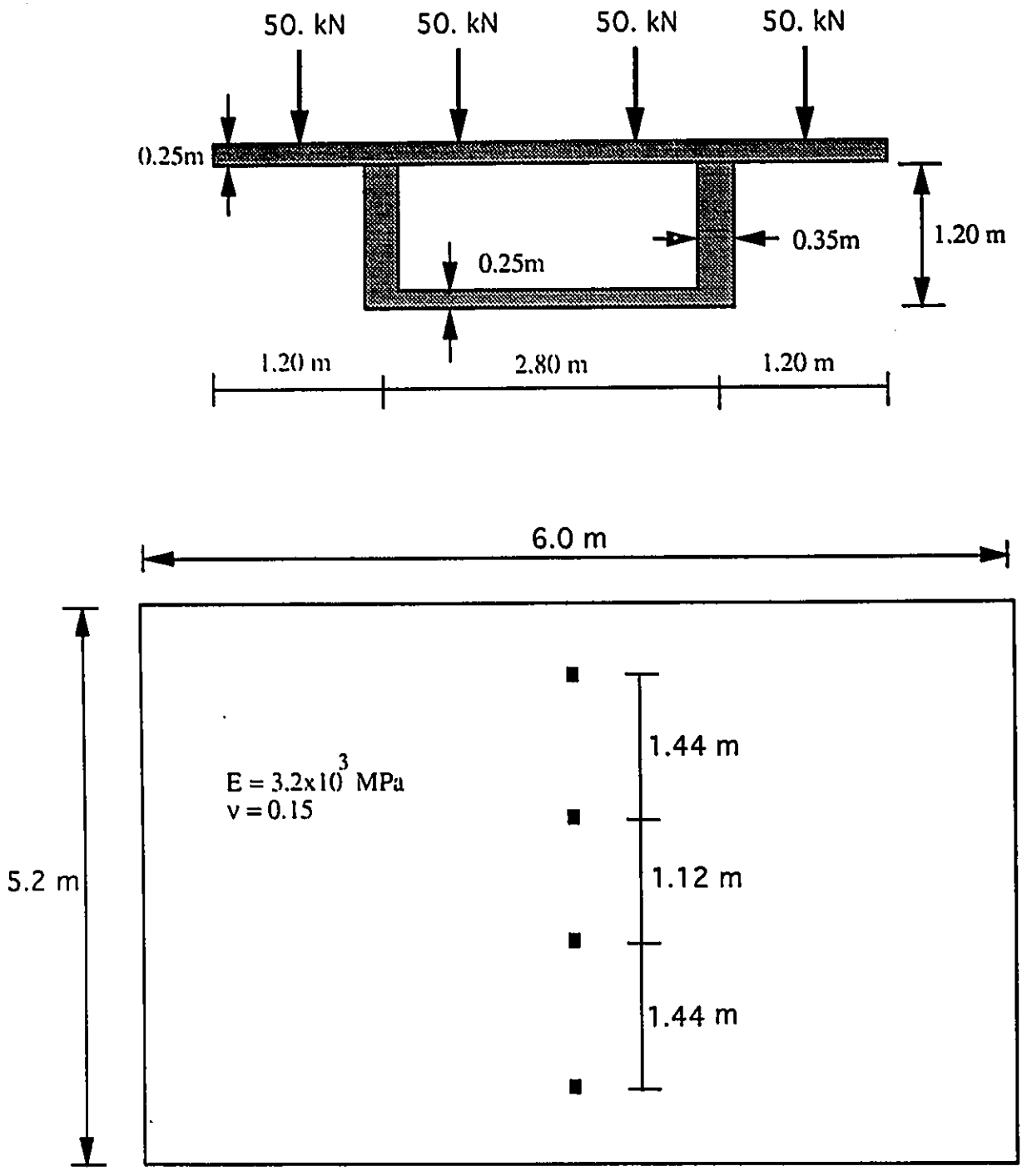

Figure 6.12 Dimensions and loading of bridge for example 8 .

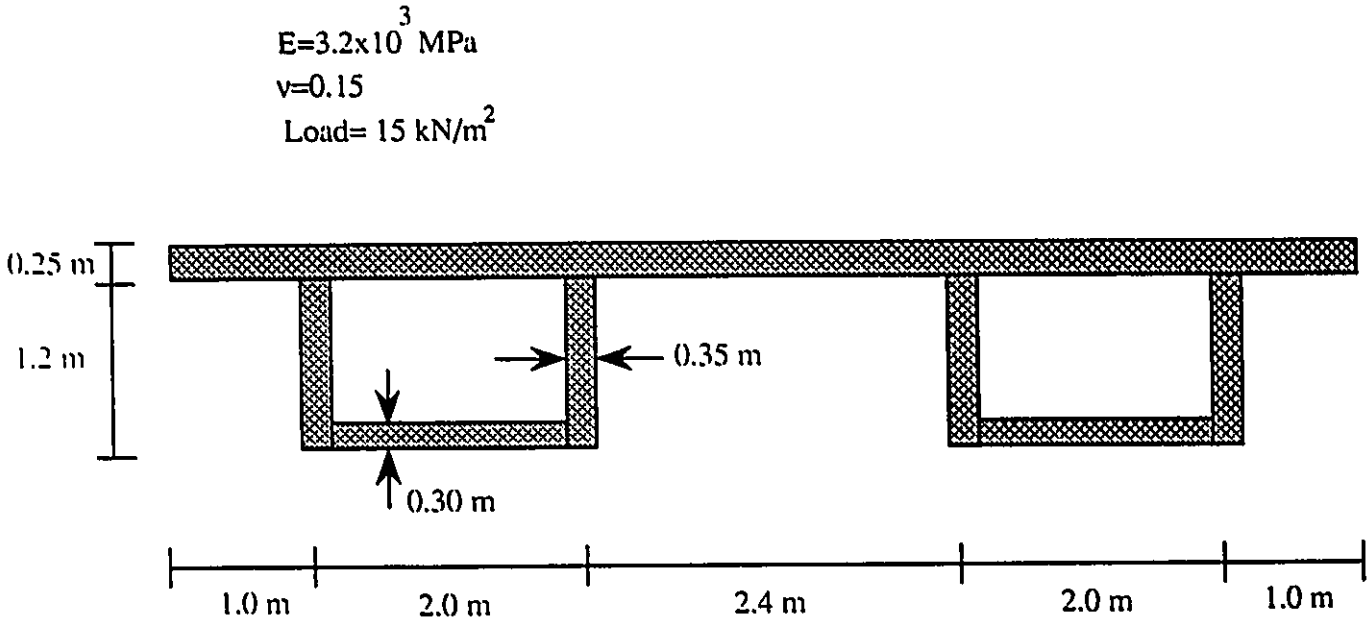

Figure 6.13 Two-cell box girder bridge.

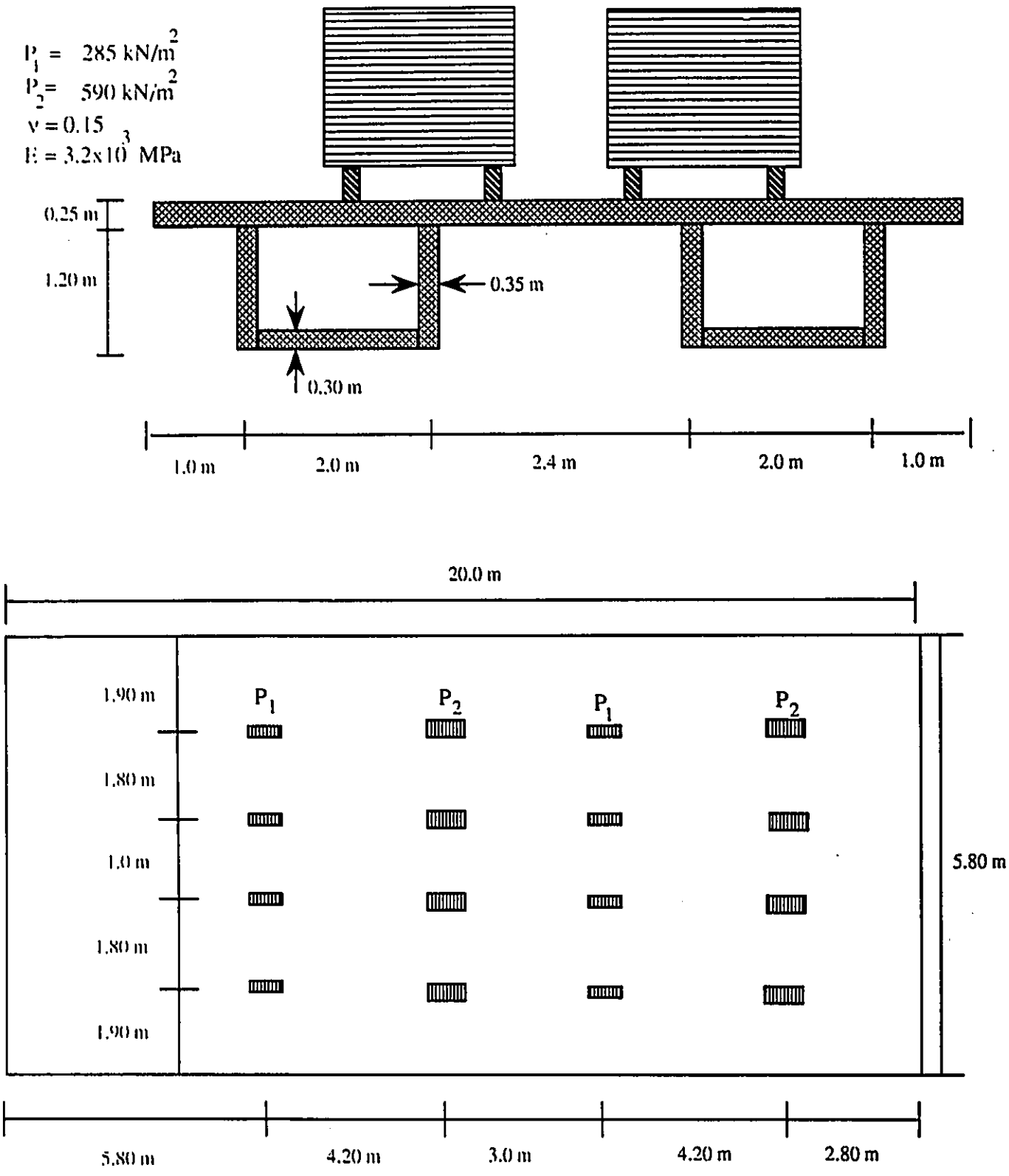

Figure 6.14 Two-cell box girder bridge under four trucks.

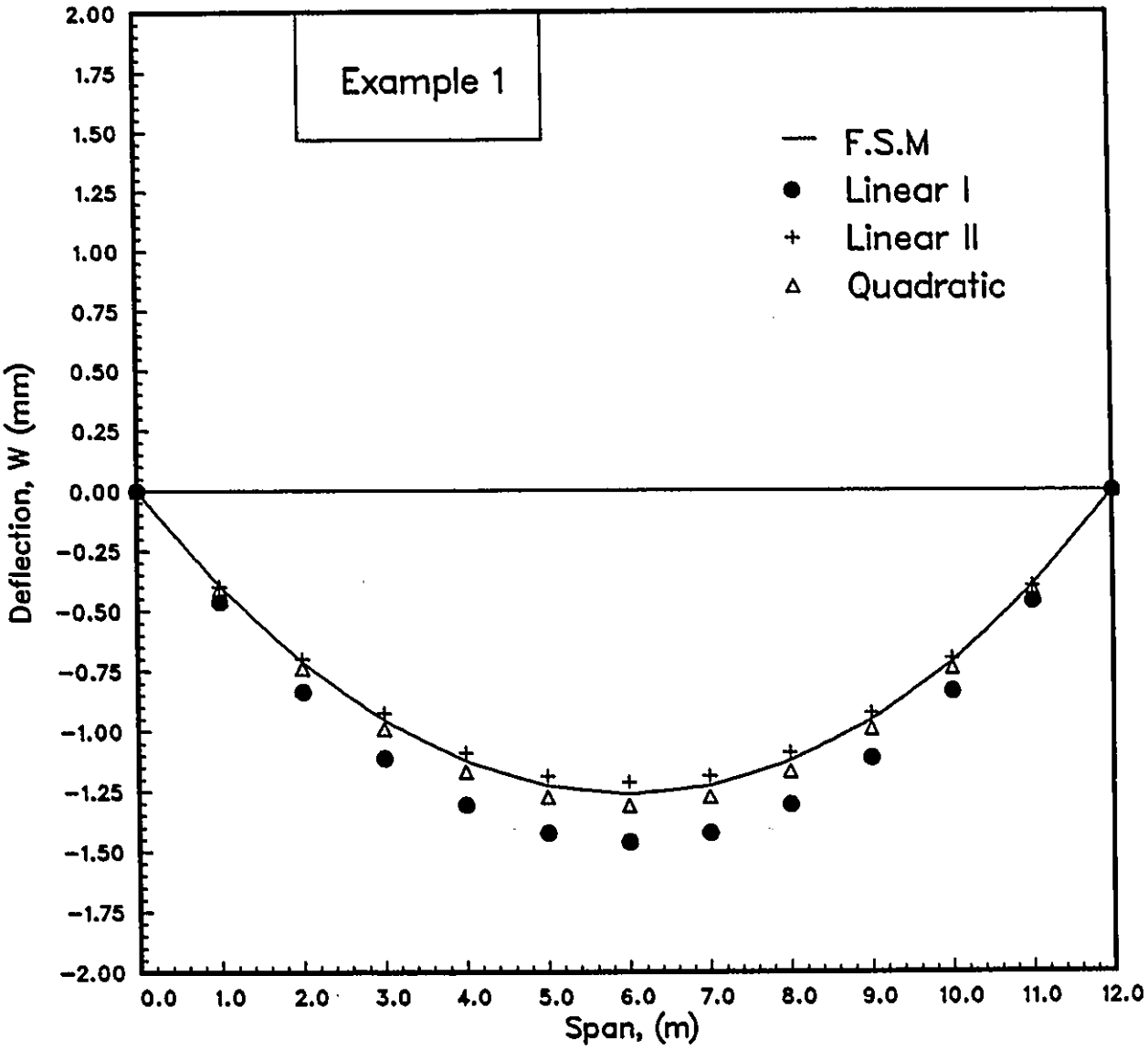

Figure 6.15: Vertical deflection along center of the span.

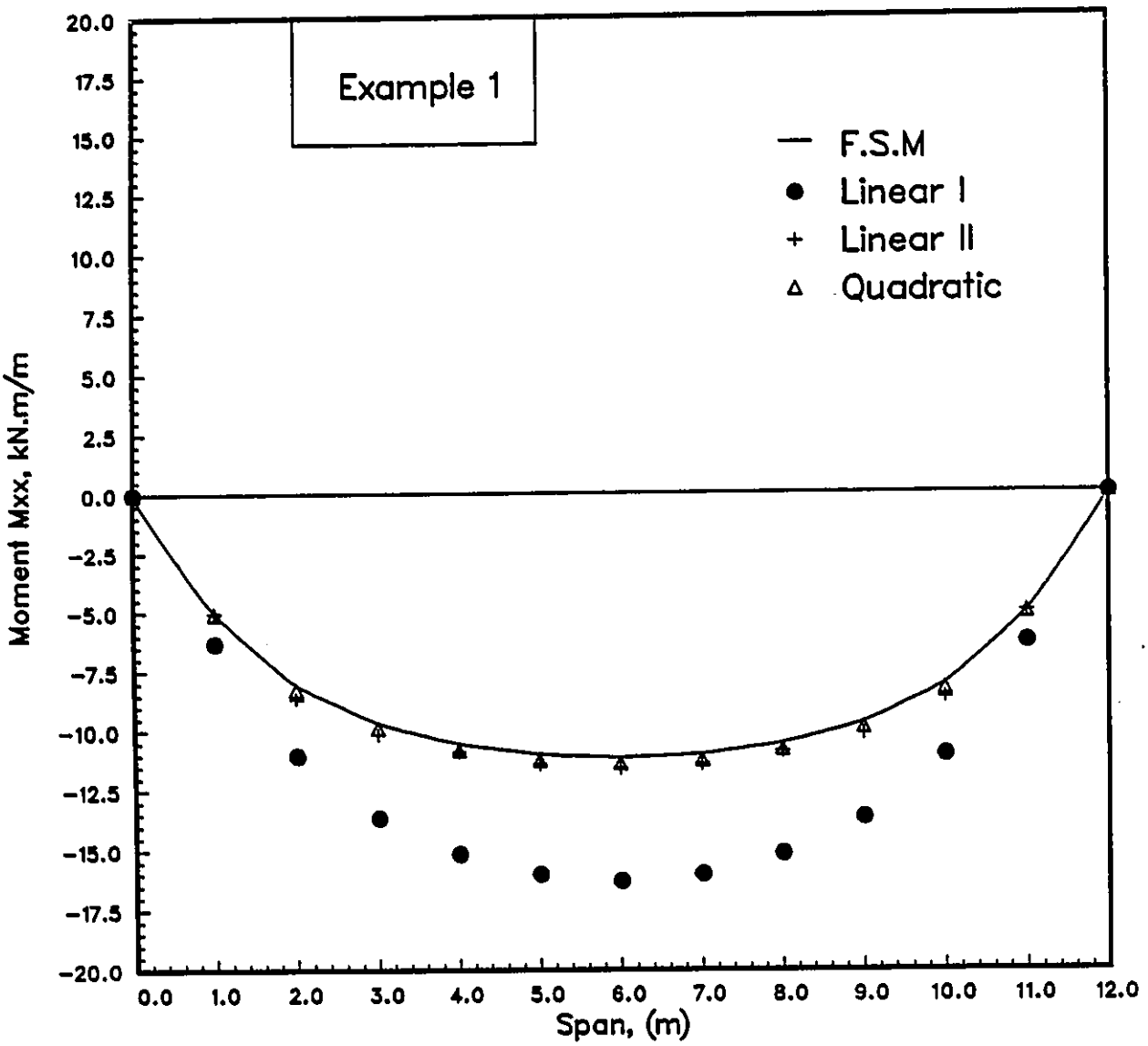

Figure 6.16: Variation of longitudinal moment along the span.

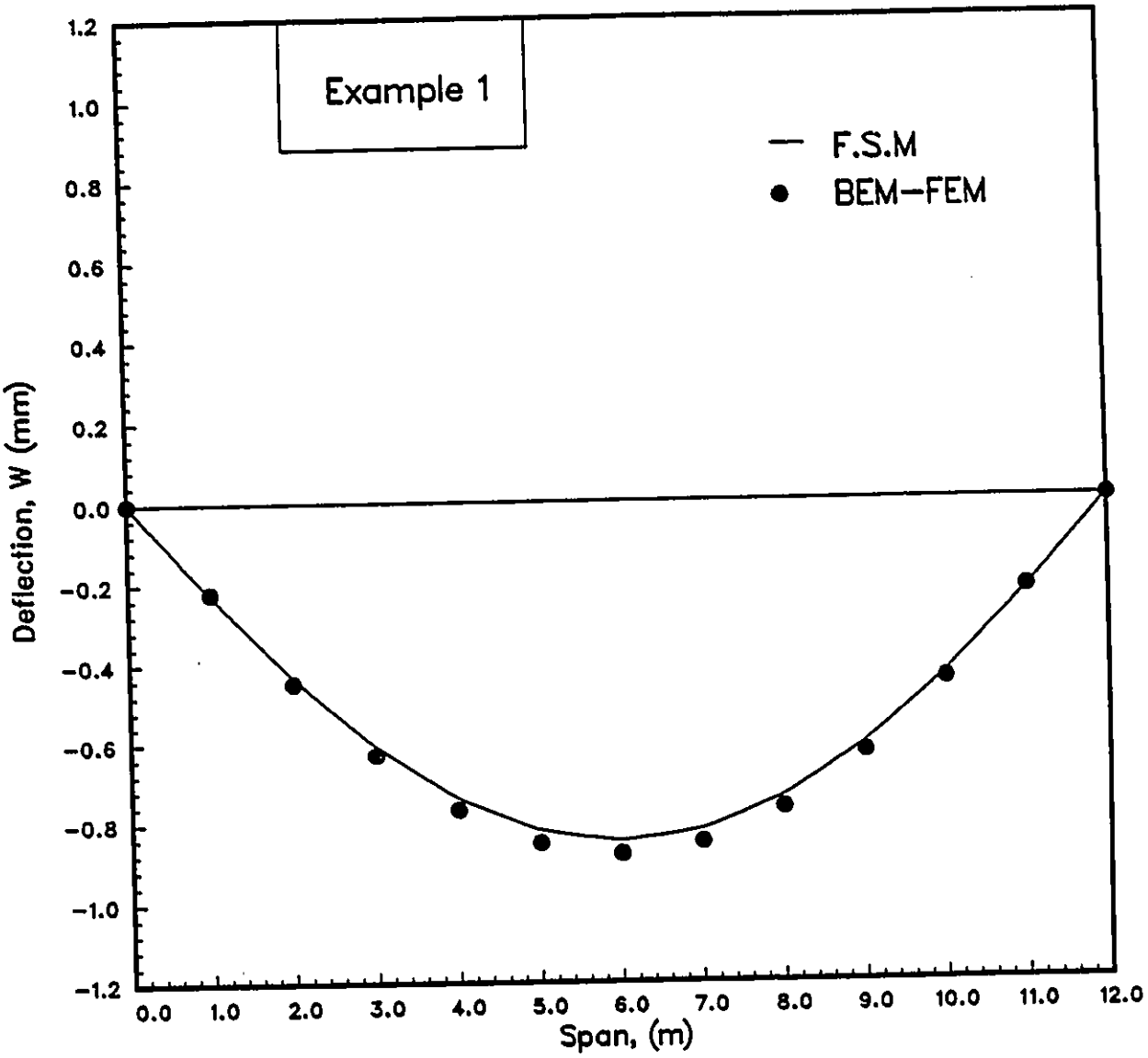

Figure 6.17: Vertical deflection along the girder.

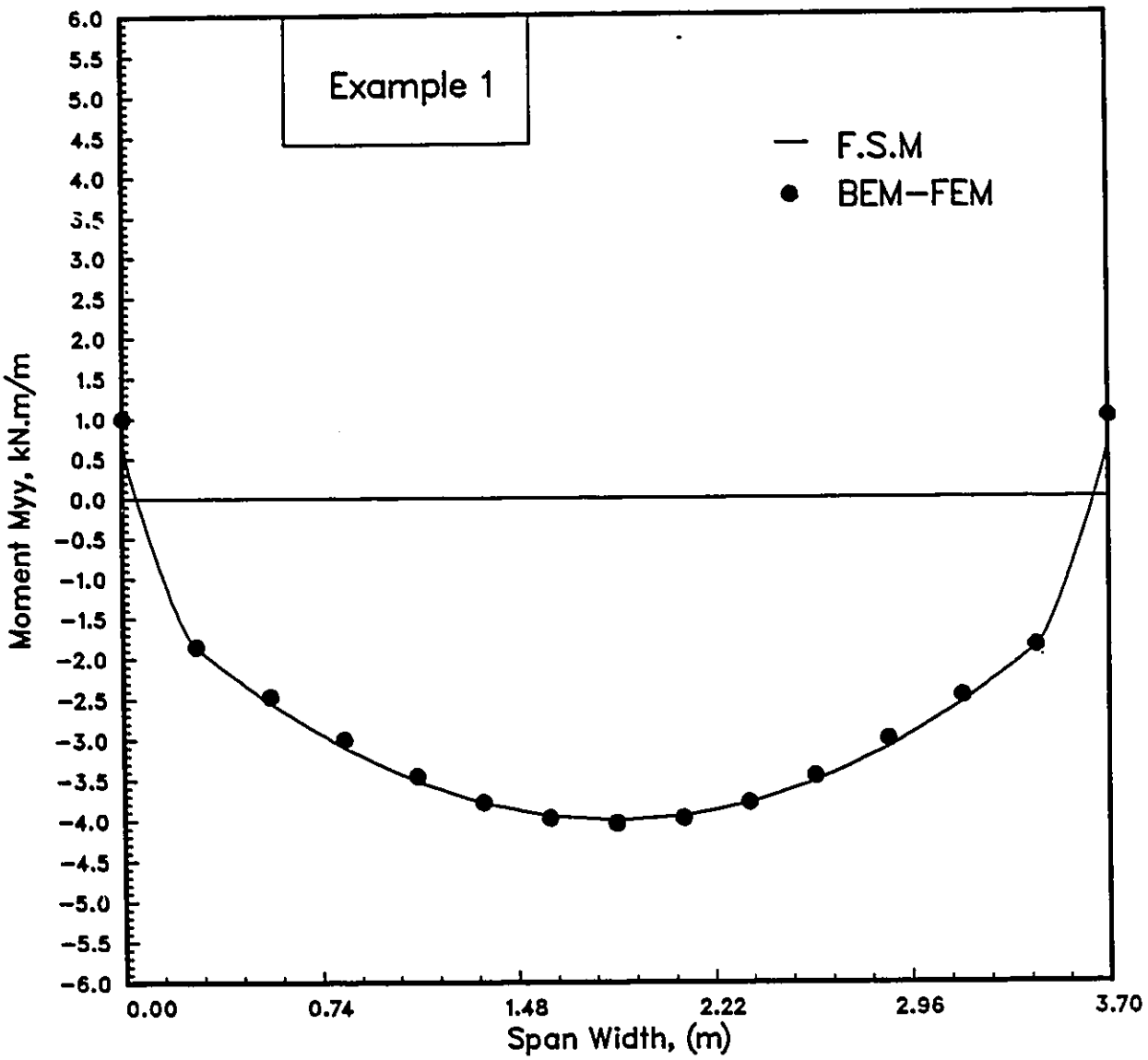

Figure 6.18: Variation of transverse moment at the mid span.

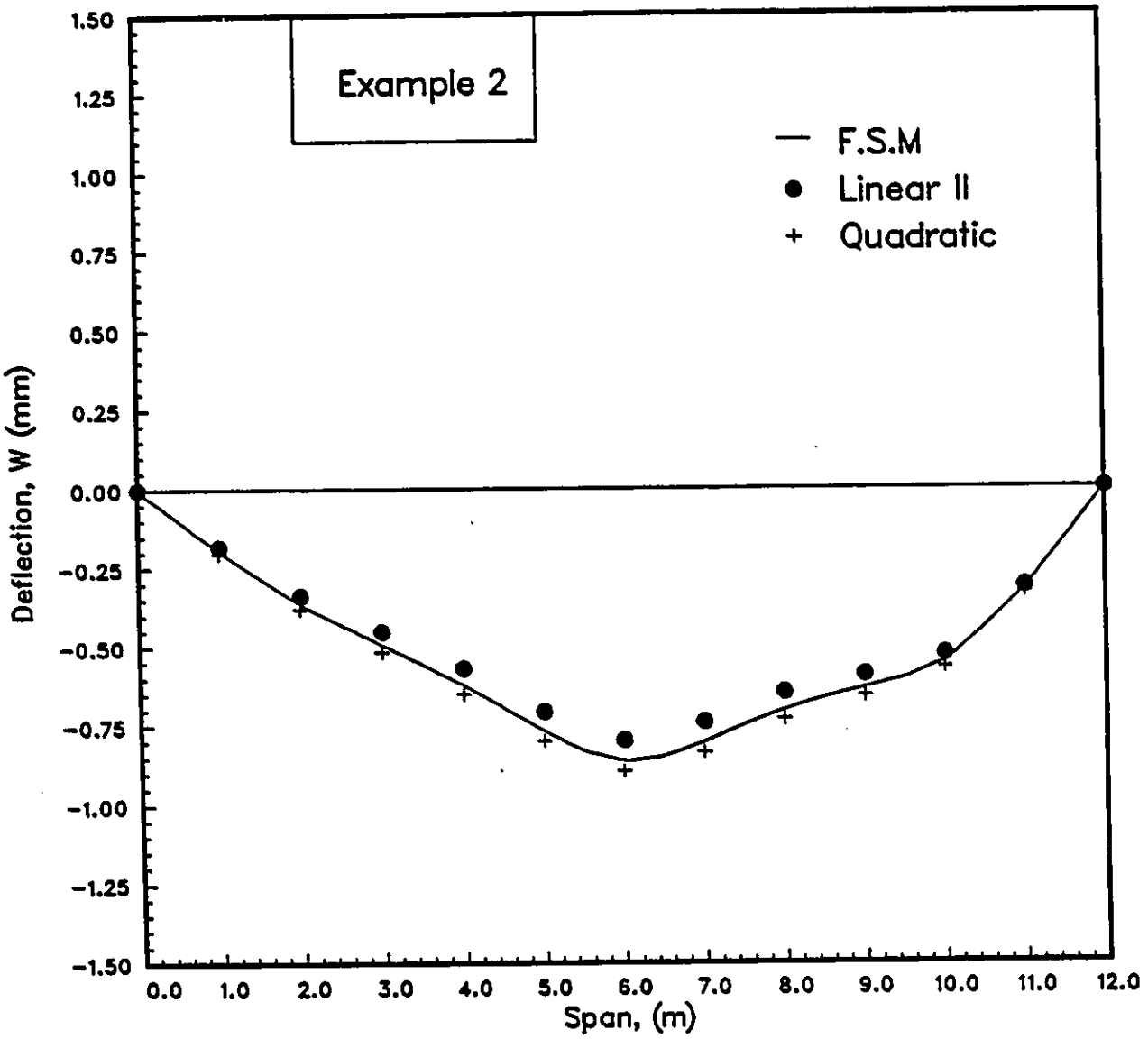

Figure 6.19: Vertical deflection along the center of span.

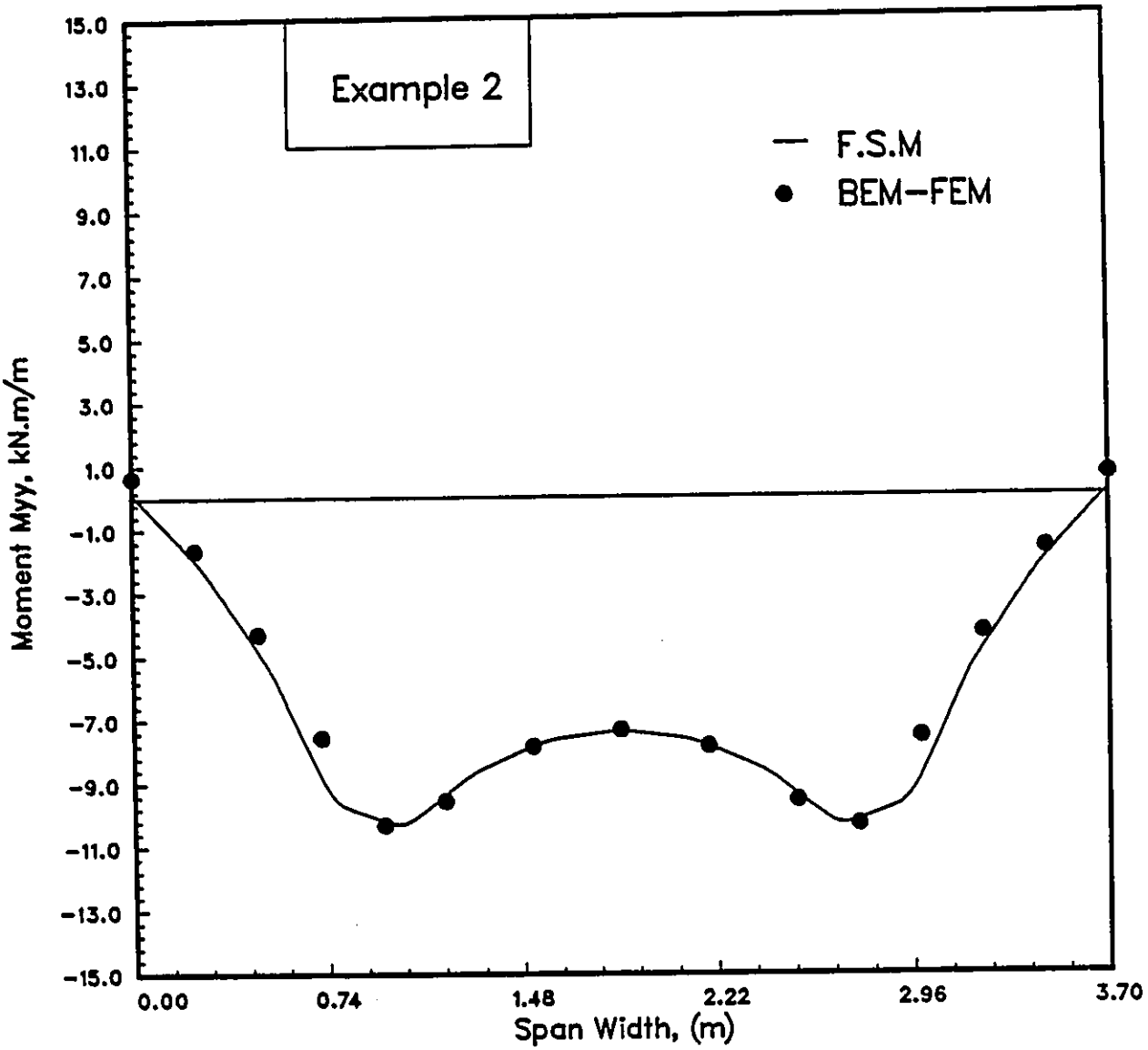

Figure 6.20: Variation of transverse moment at the mid span.

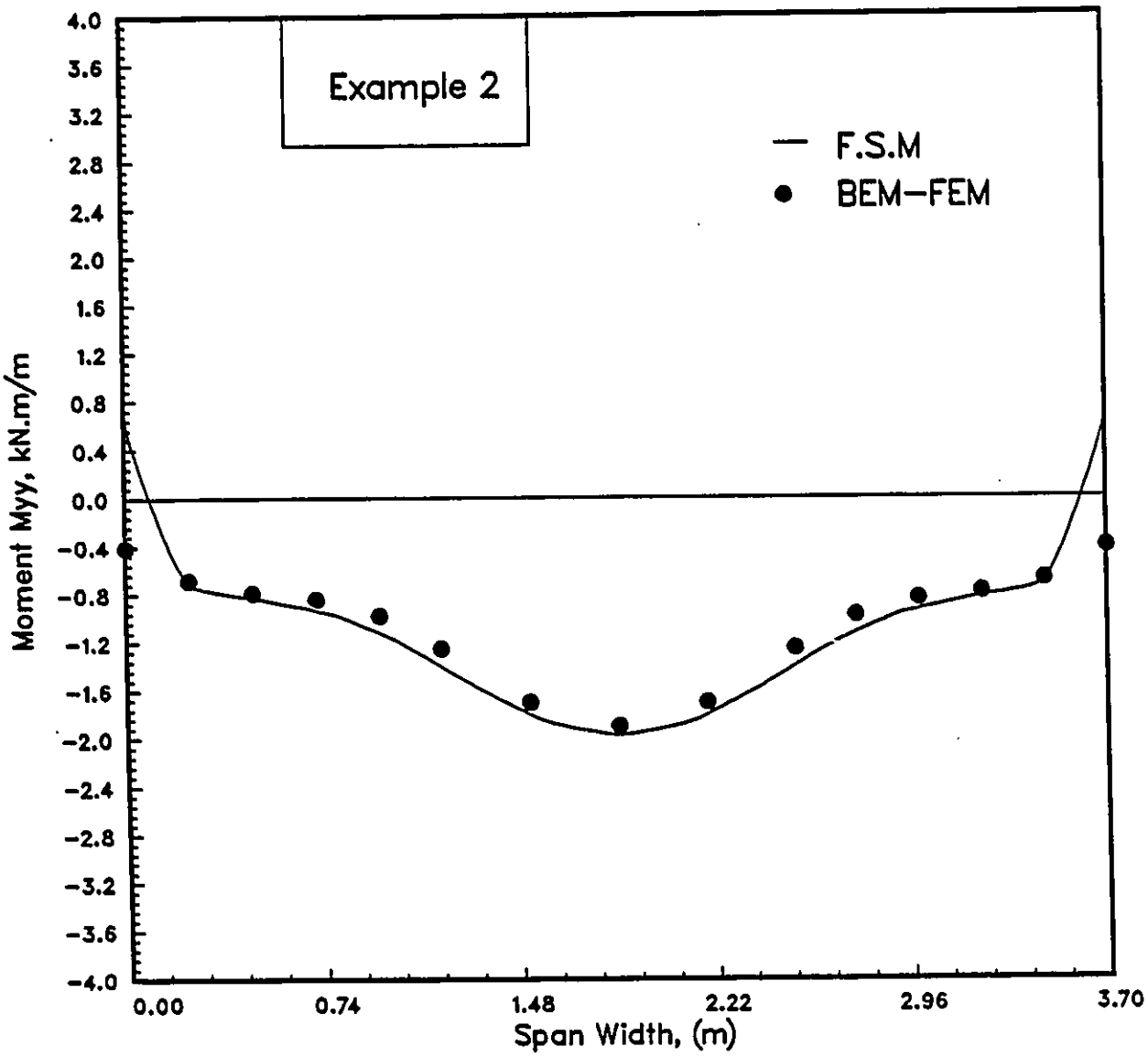

Figure 6.21: Variation of transverse moment at x = 7.0 m.

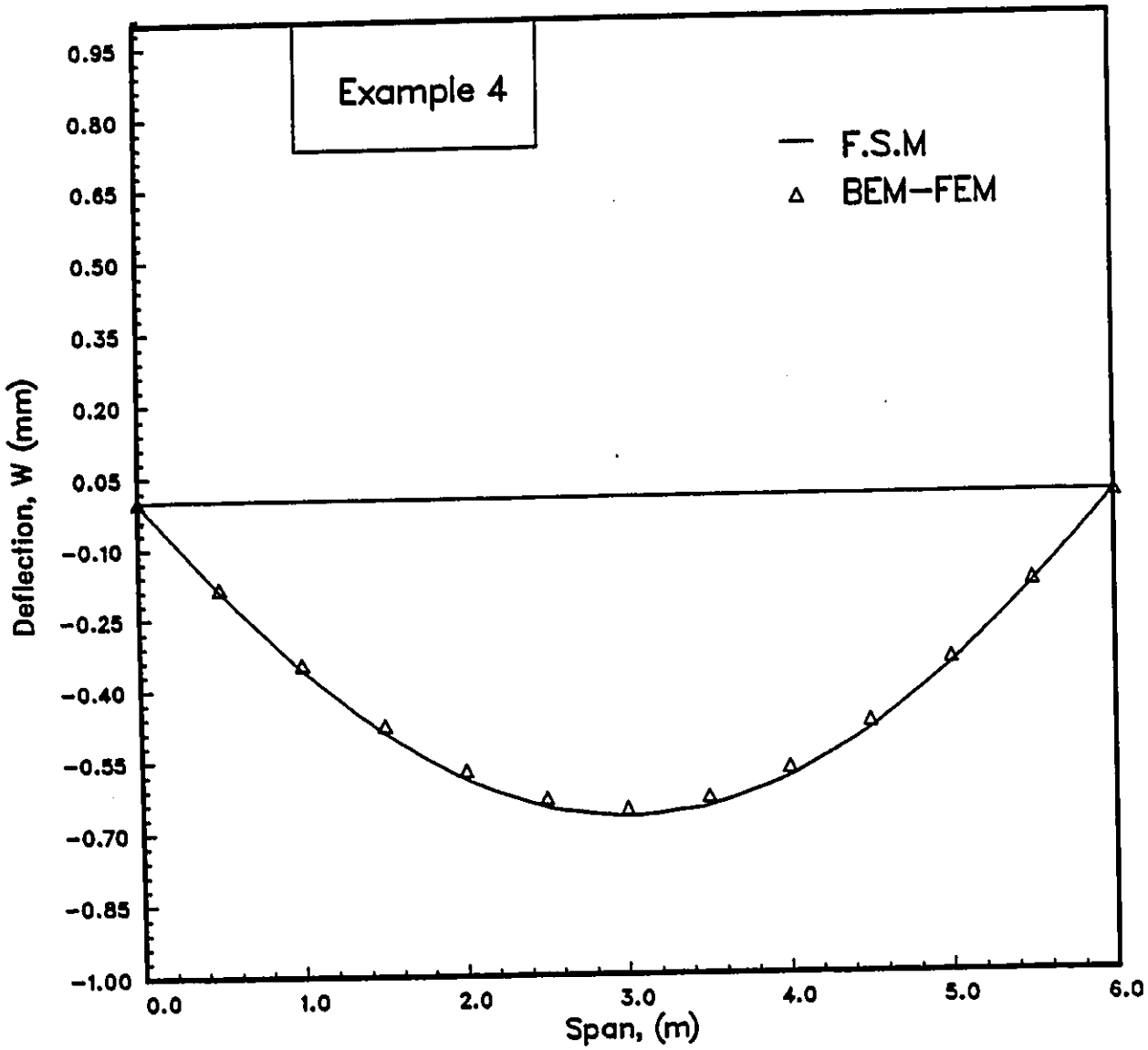

Figure 6.22: Vertical deflection along the center of span.

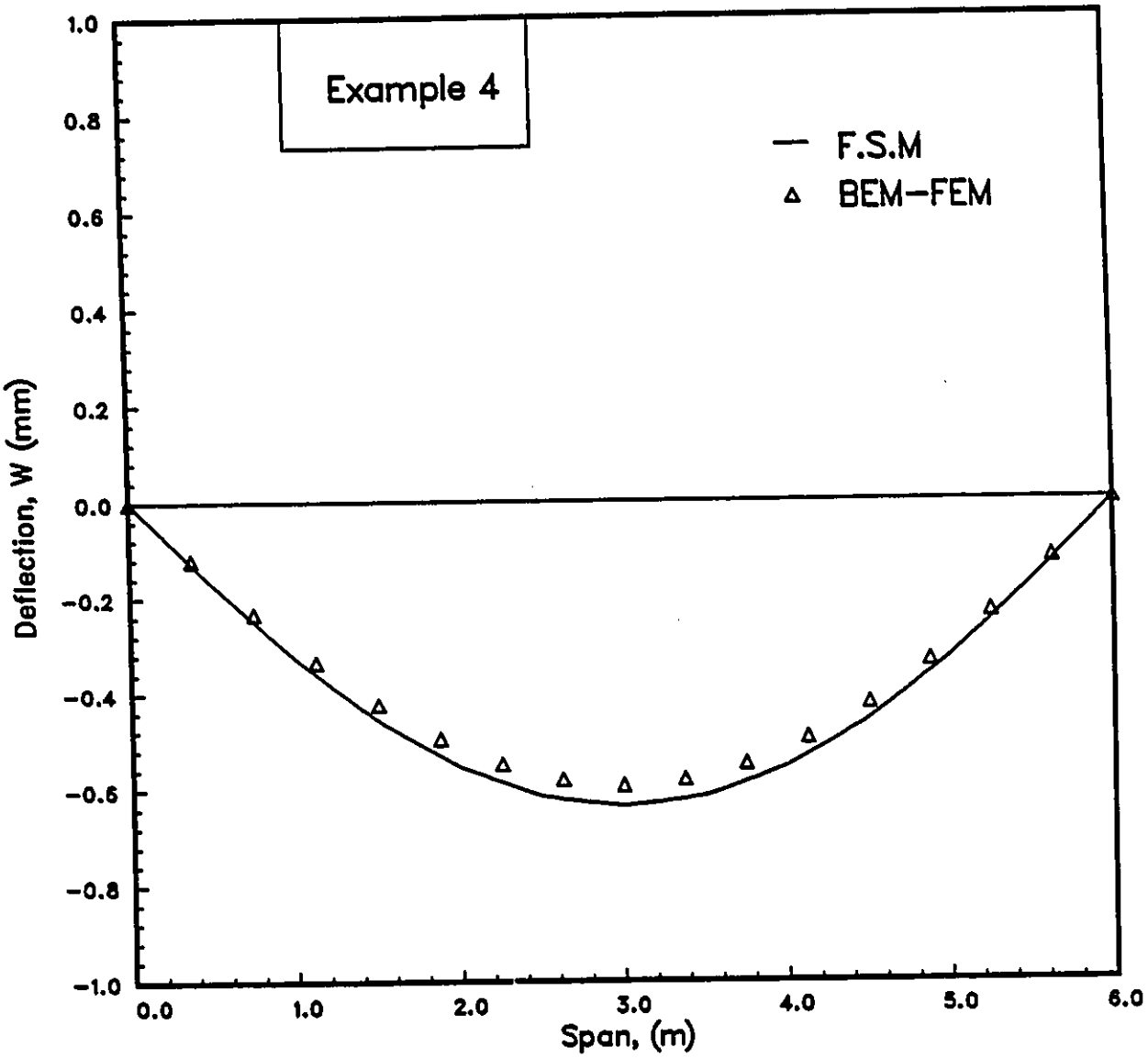

Figure 6.23: Vertical deflection along the interior girder.

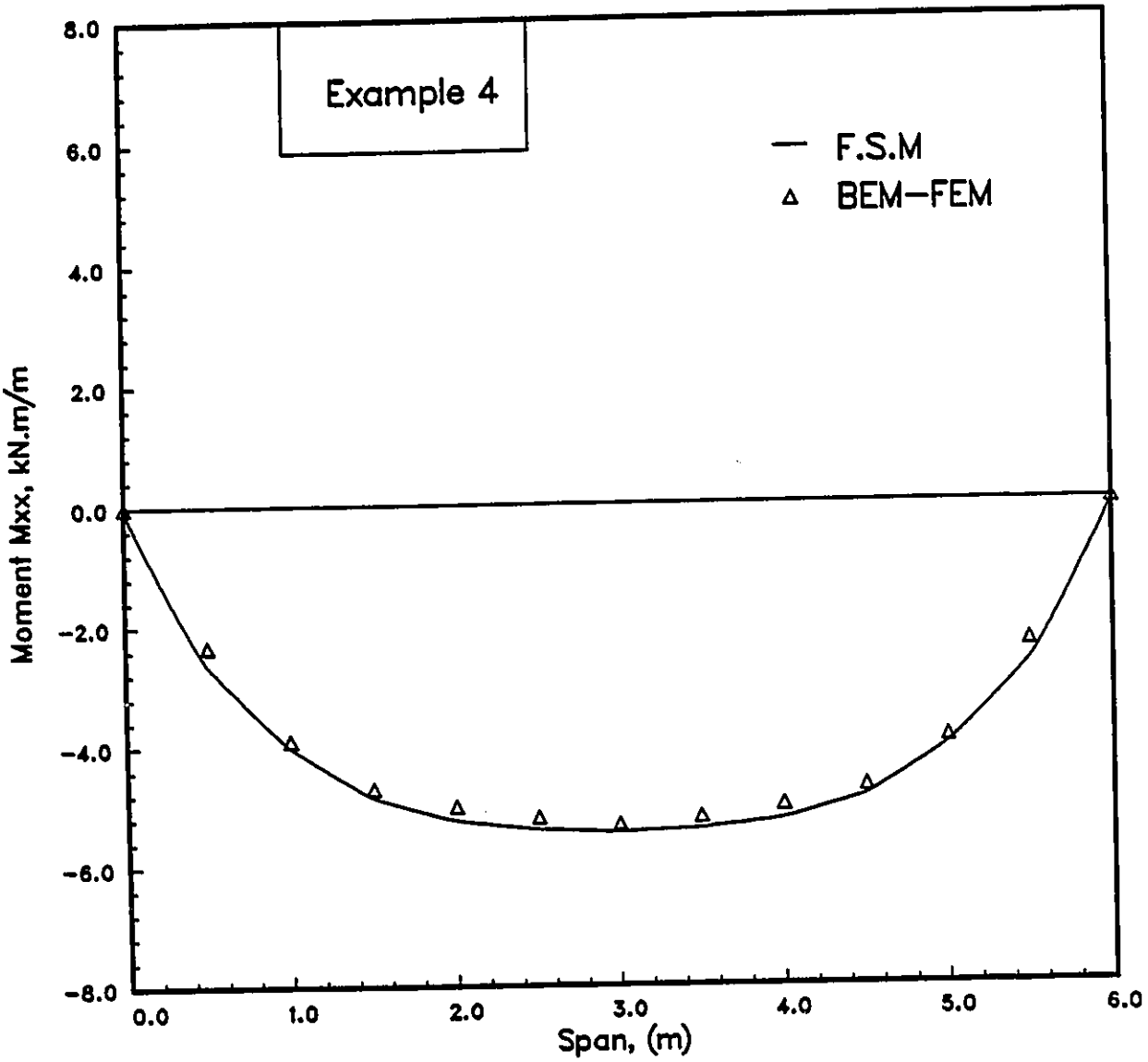

Figure 6.24: Variation of the longitudinal moment along the span.

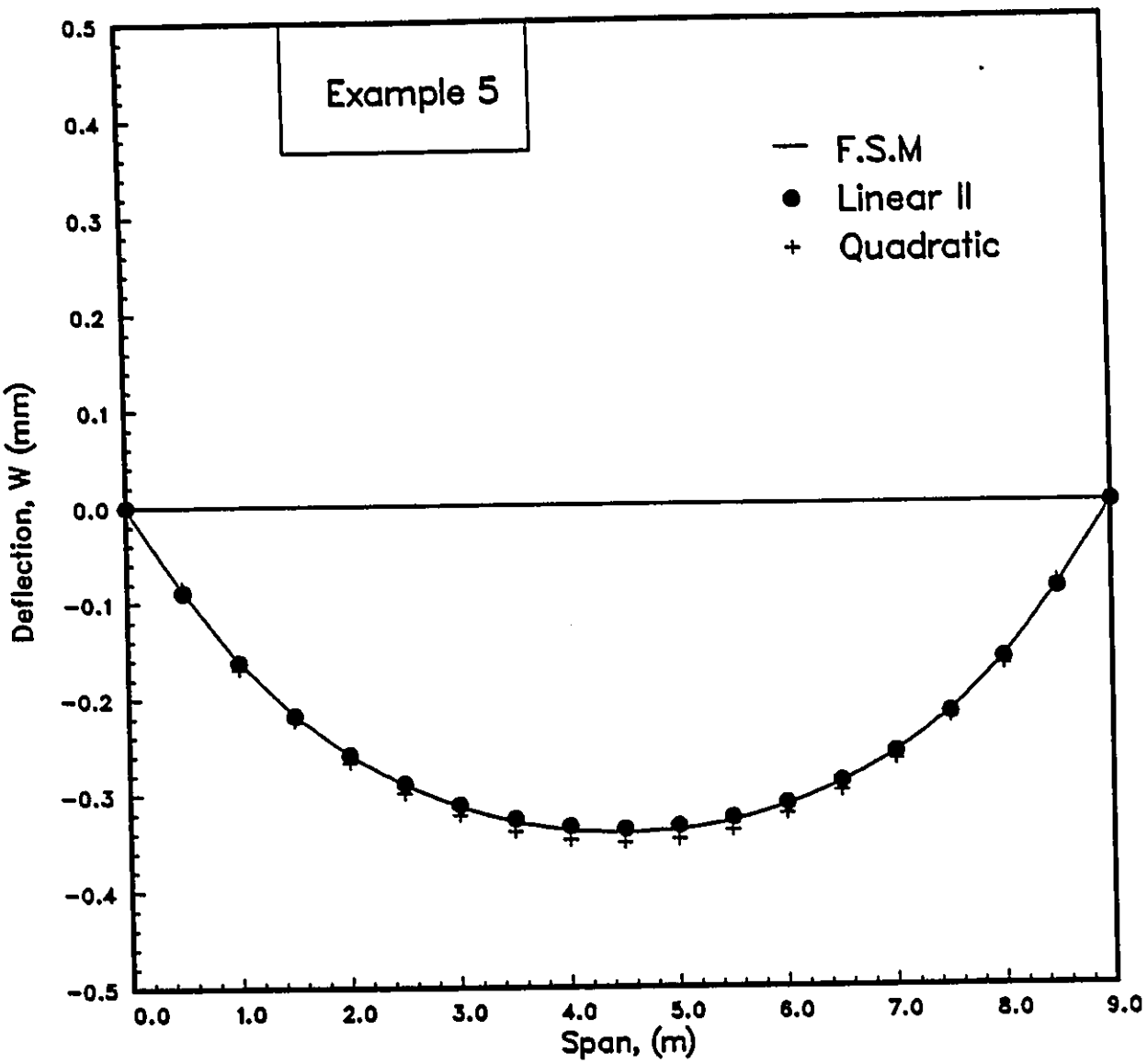

Figure 6.25: Vertical deflection along the center of span.

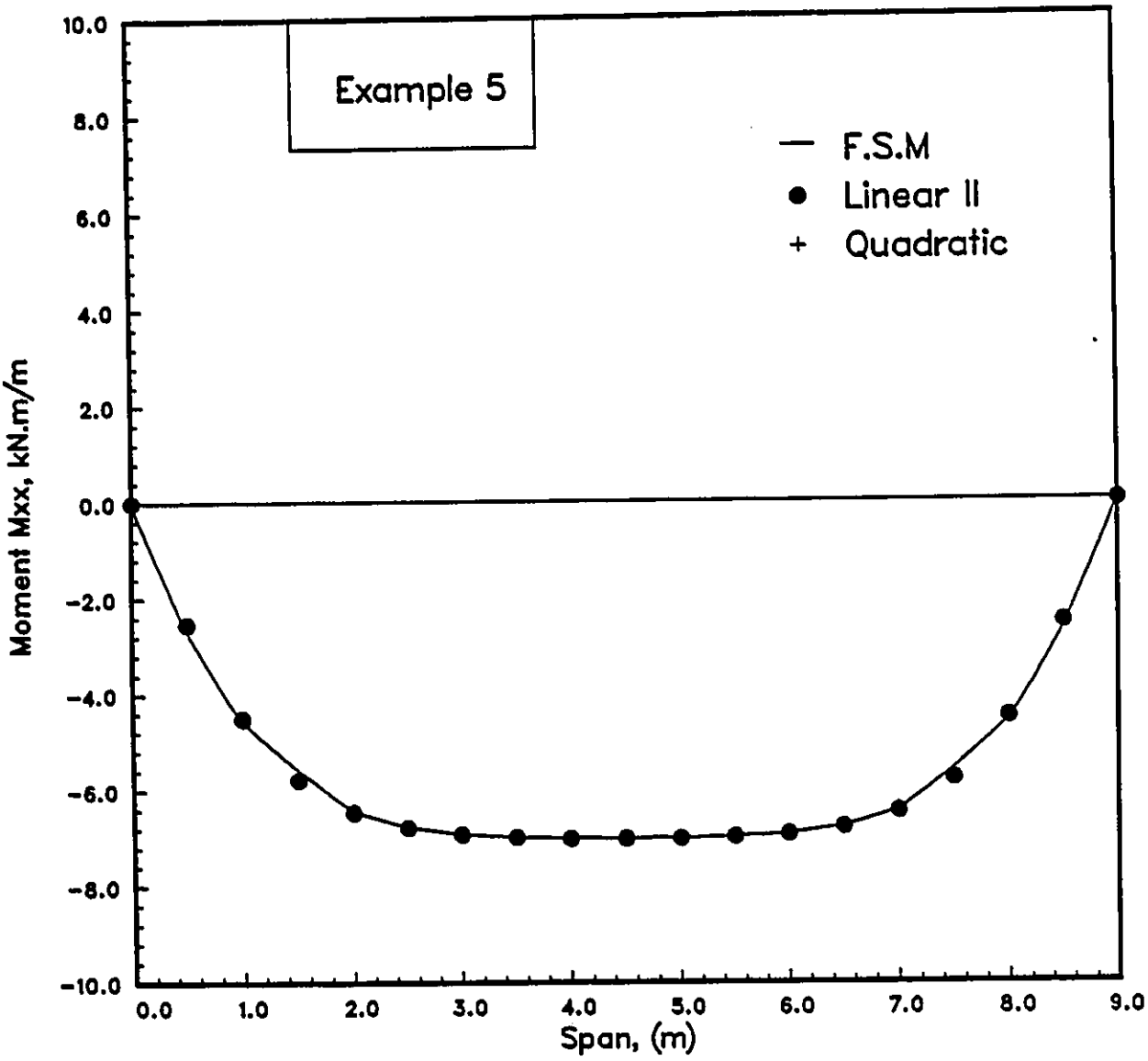

Figure 6.26: Variation of the longitudinal moment along the span.

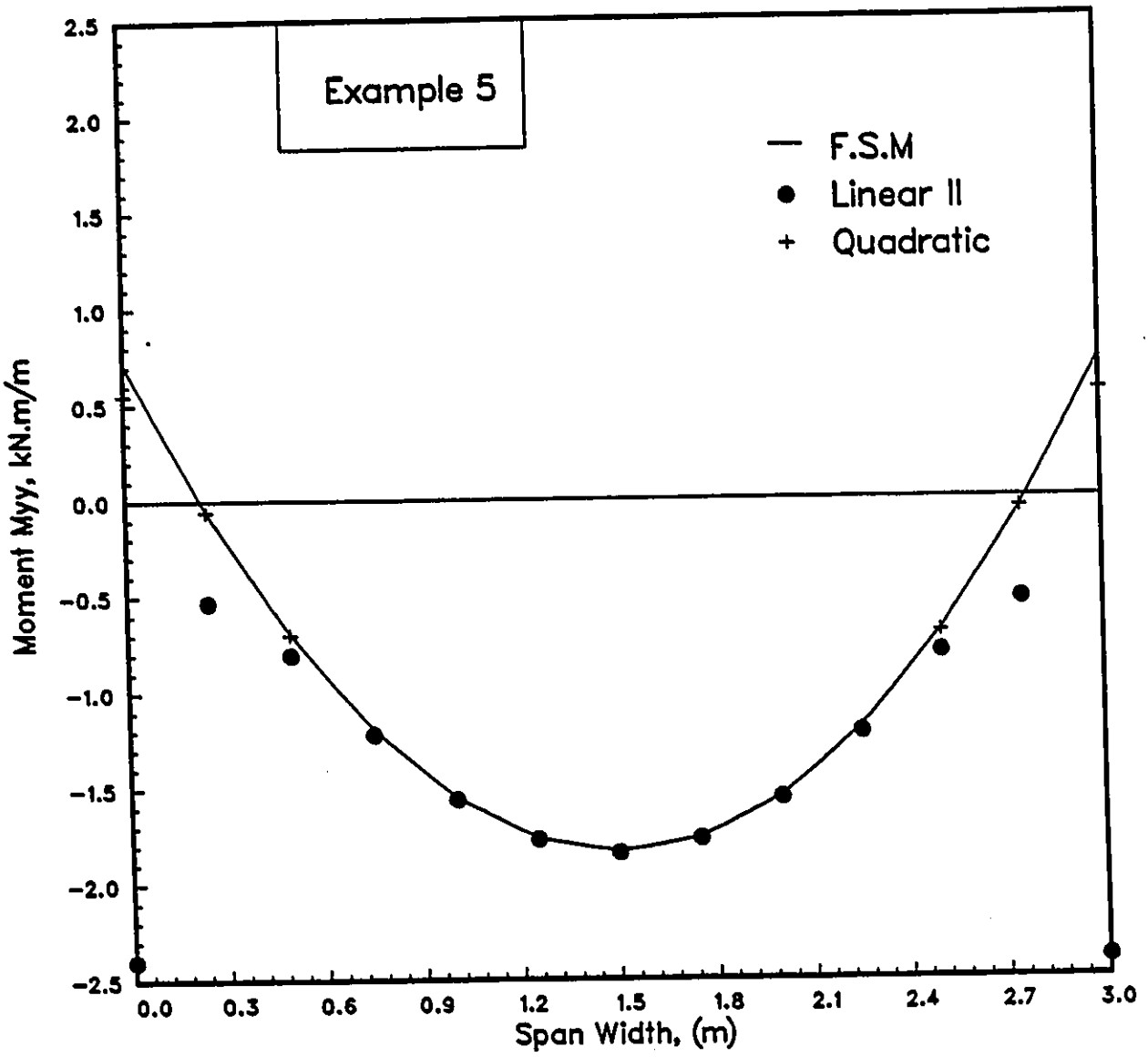

Figure 6.27: Variation of transverse moment at the mid span.

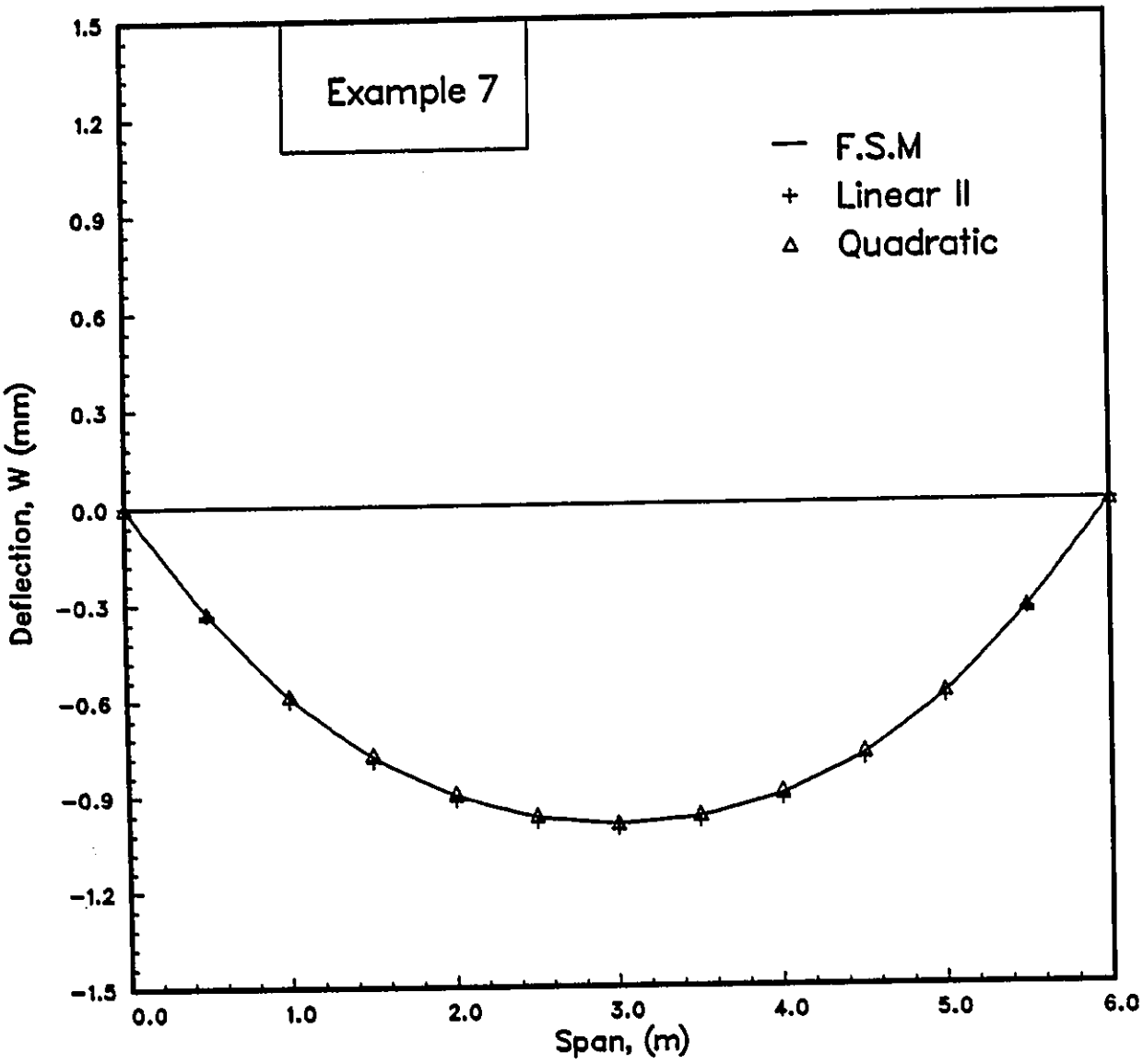

Figure 6.28: Vertical deflection along the center of span.

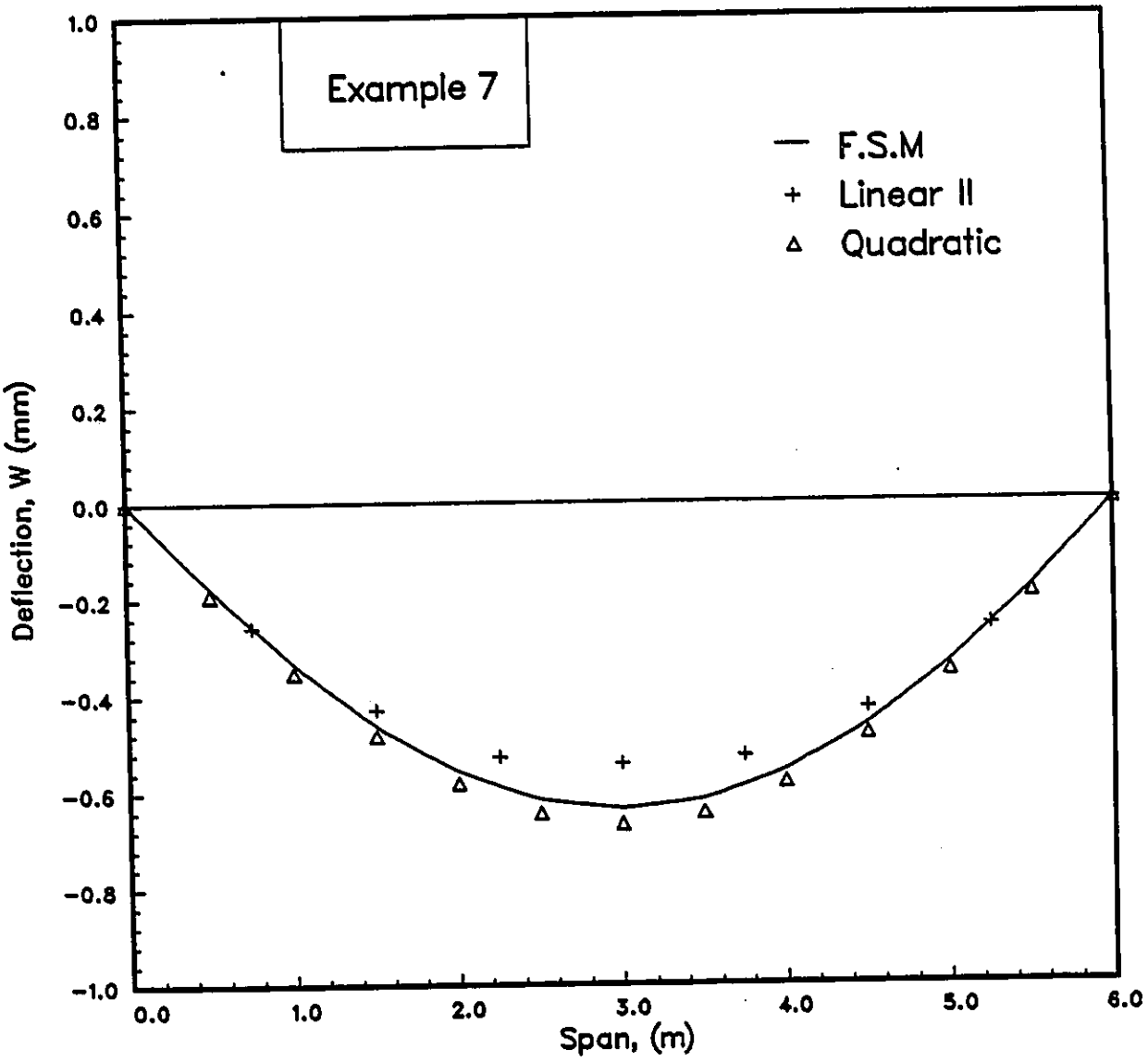

Figure 6.29: Vertical deflection along the girder.

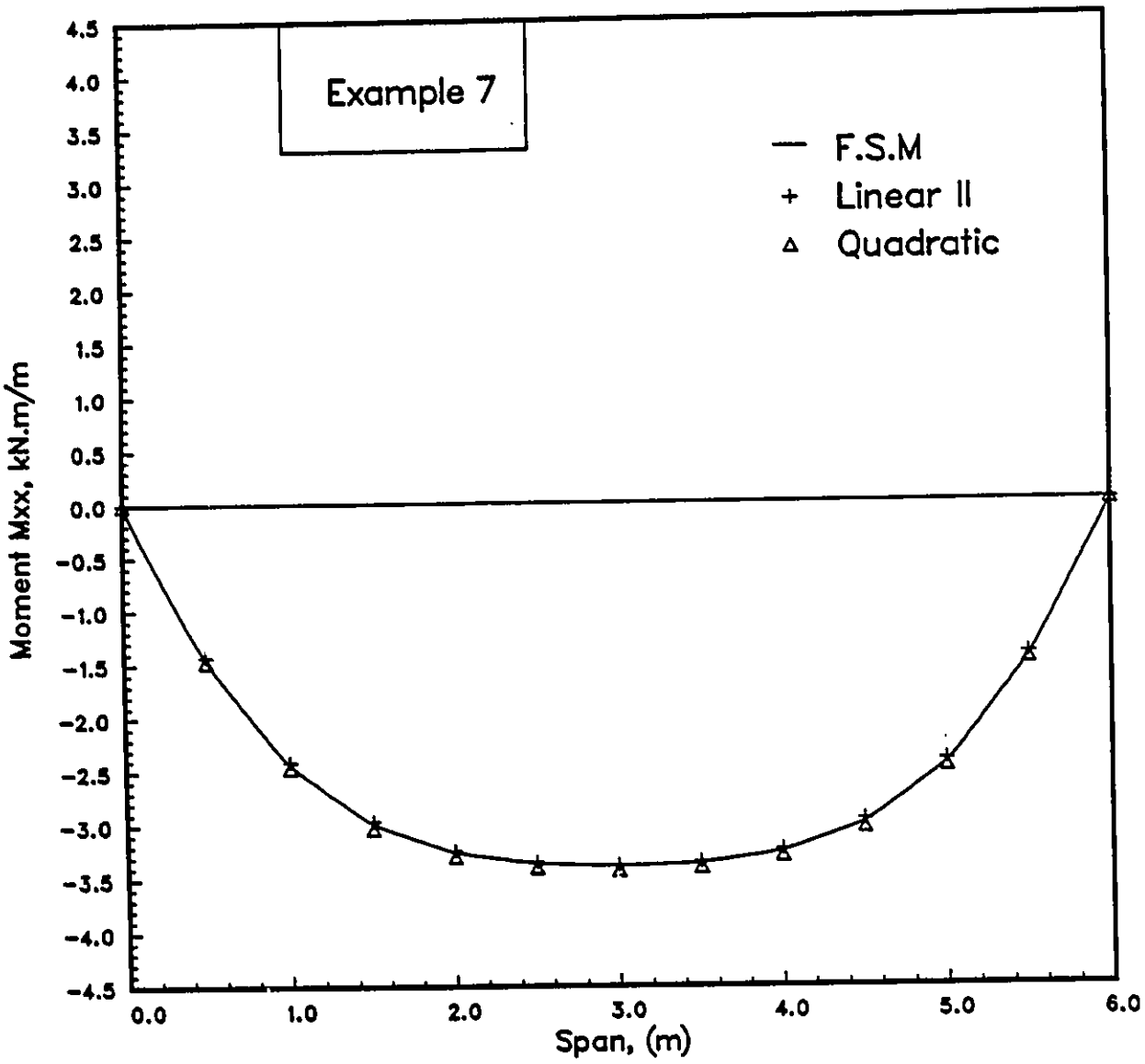

Figure 6.30: Variation of the longitudinal moment along the span.

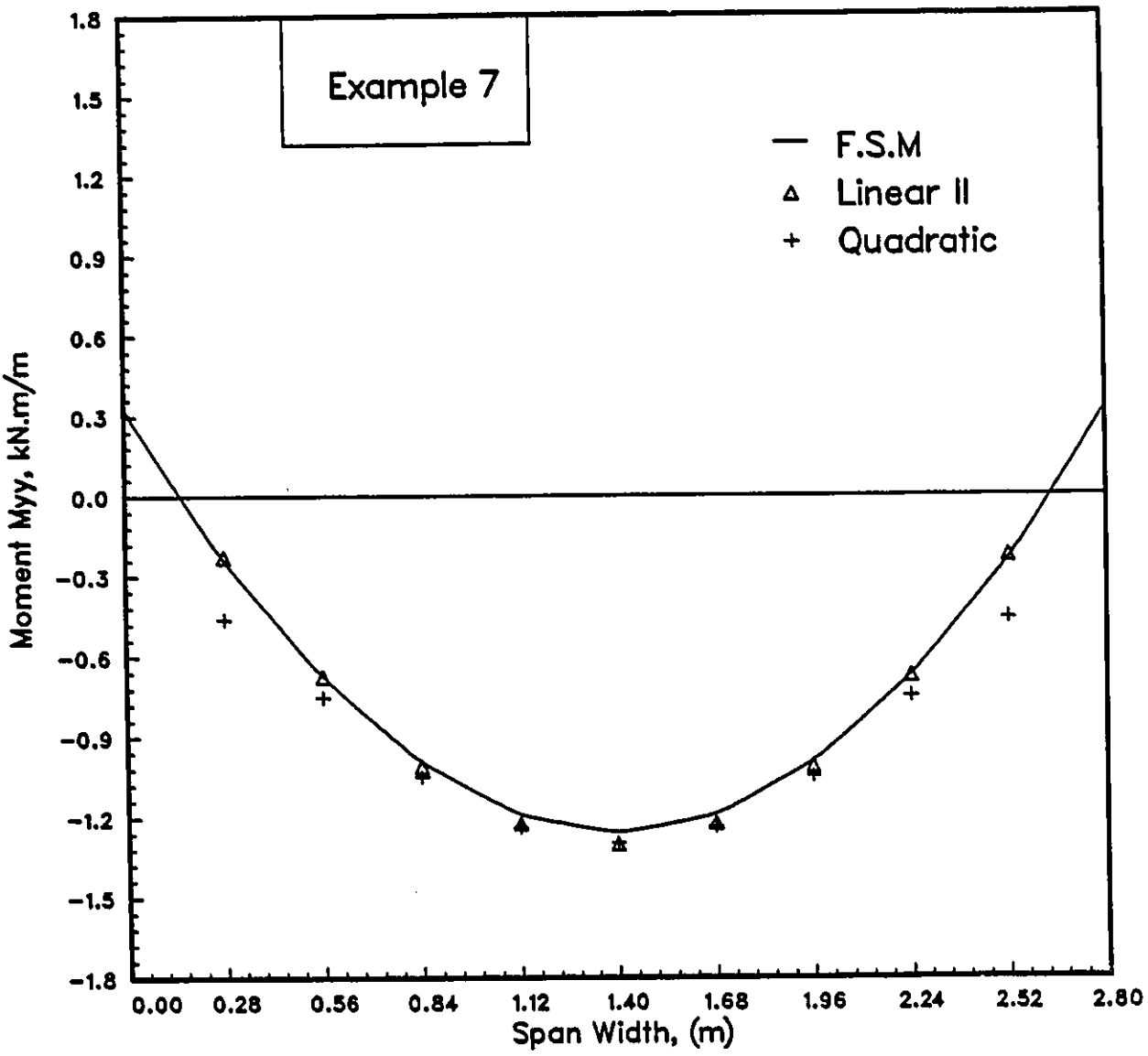

Figure 6.31: Variation of transverse moment at the mid span.

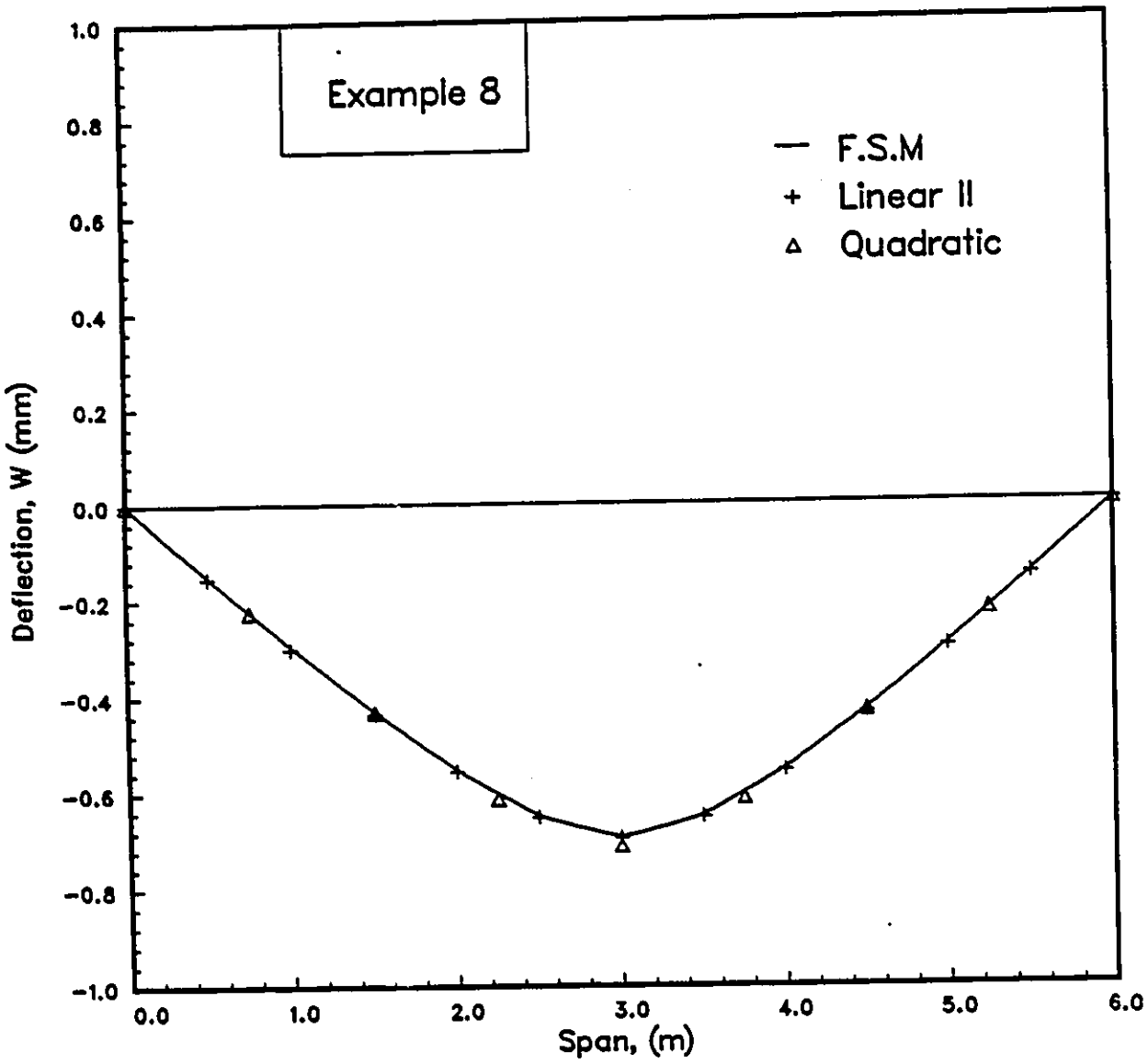

Figure 6.32: Vertical deflection along the girder.

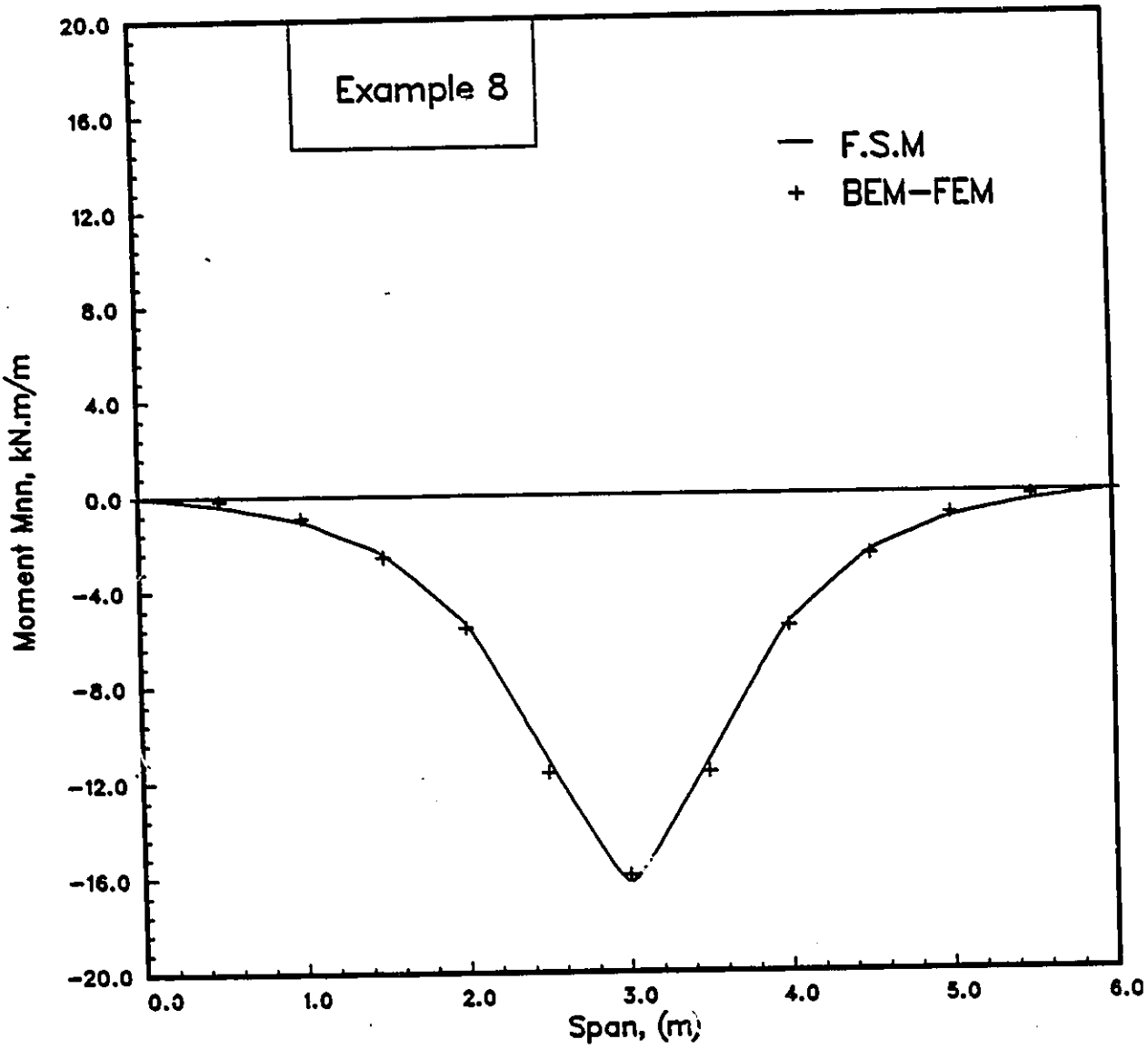

Figure 6.33: Variation of the normal moment along the girder.

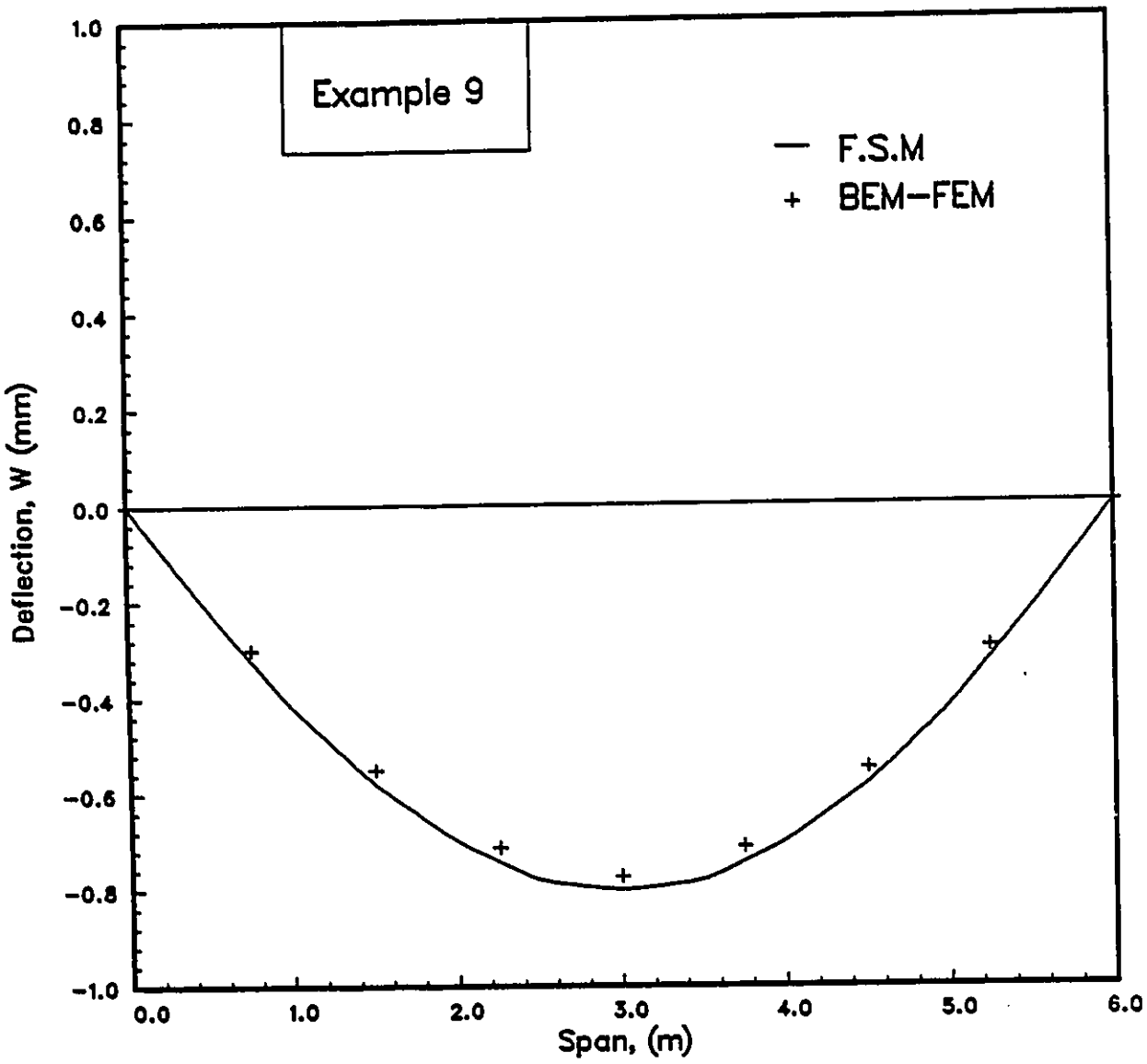

Figure 6.34: Vertical deflection along the center of span.

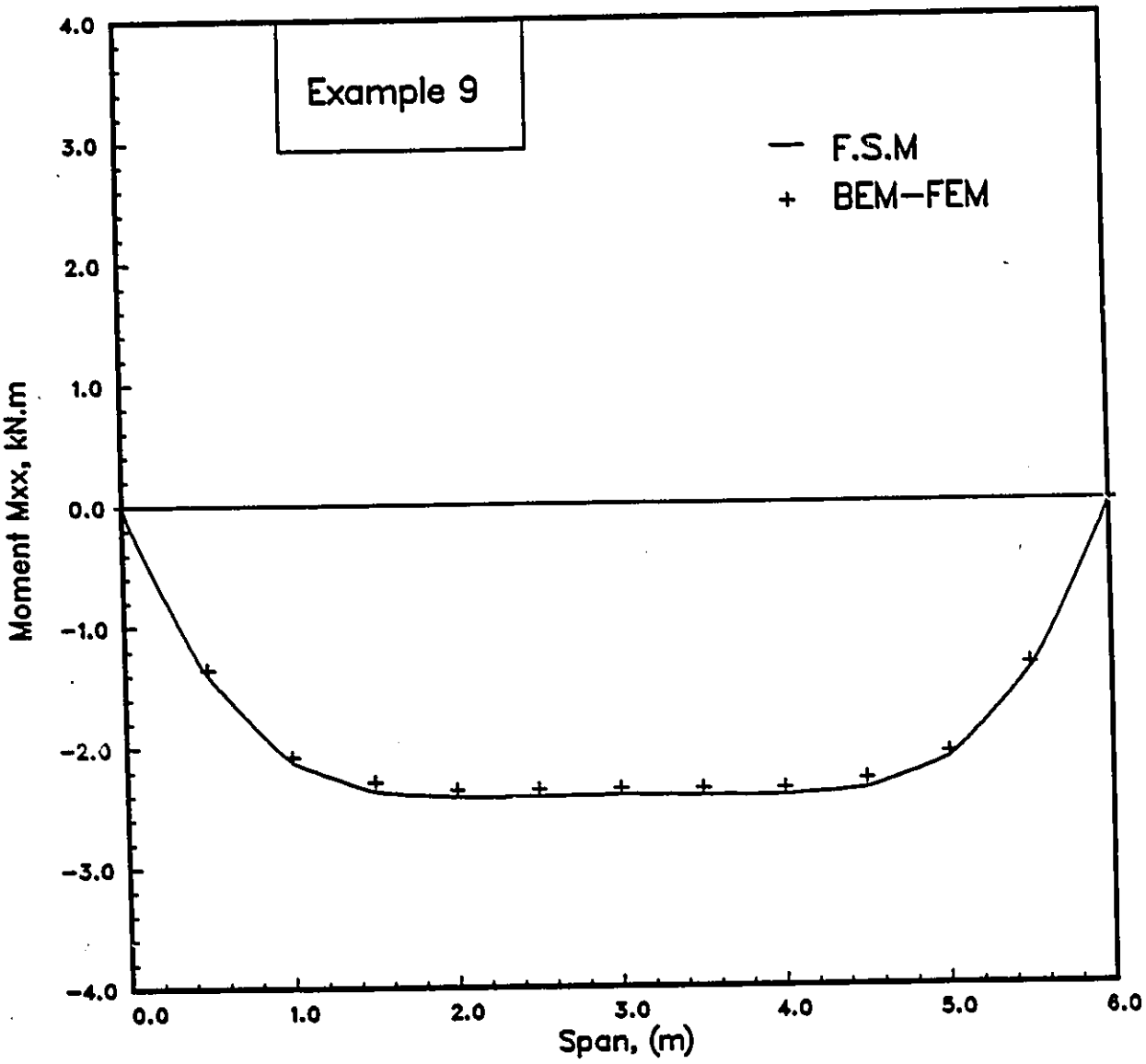

Figure 6.35: Variation of the longitudinal moment along the span.

Chapter 7

Conclusions And Recommendations

7.1 Summary and Conclusions

In this study, a mathematical procedure which combines the boundary element method with the finite element method was developed. Generally the two methods cannot be directly combined as they are normally formulated, since they do not relate the same sets of variables. The boundary element method relates displacements and tractions, whereas the finite element method relates nodal displacements and forces. Hence for coupling to be achieved one of the methods must be altered to make it compatible with the other method. The coupling technique was enhanced to analyze different types of bridges and the

compatibility requirements between the two methods for three-dimensional structures were satisfied.

A computer program combining the two methods (BEM-FEM) was developed and different types of bridges were successfully analyzed.

As a result of the present research, the following conclusions are drawn :

1. For analyzing bridges under truck loads, the combined method is a better alternative to FEM or FSM in terms of the simplicity, reduction of the input data and the computer time.

2. The performance of the coupling technique is significantly enhanced and extended to 3-dimensional structures and the compatibility requirements along the interface boundaries are fully satisfied.

3. Various types of bridges, such as single span bridge or continuous span bridge and straight or skewed bridges for both slab on girders and box girder bridges are successfully modeled by the combined method.

4. The numerical examples show, in general, the validity of the combined method (BEM-FEM) to analyze various types of bridges. The important design quantities such as longitudinal bending moments, vertical deflection and transverse bending moment are found to be in good agreement, when compared with the finite strip solution. For example, the maximum difference in the results of the deflection and the moment using quadratic elements was about 6%.

5. To obtain a sufficiently accurate solution, the FE idealization for the girders and the bottom slab would require at least two layers of 4-node element or a single layer of 8-node element.

6. The combined analysis is effective in simulating the local wheel loads effect.

7. The developed computer model uses linear, quadratic, as well as higher order elements. Using high order elements in the boundary element idealization is not necessary in order to obtain accurate results. However, high order elements reduce the required input data files.

8. In order to obtain a better solution for the boundary unknowns the source points should be located at a distance of 0.2 L, where L is the distance between two consecutive nodes.

7.2 Recommendations for Future Research

The following recommendations are made for future research :

1. The combined BEM and FEM, presented here, are applied only to slab on girder and box girder bridges. This work can be extended to include more complicated types of bridges and curved bridges.

2. The computer program developed in this study was based on flat shell element. Increasing the degree of freedom make the program more efficient

to handle more complicated types of bridges.

3. The combined analysis can be extended to include dynamic and non-linear analysis.

Bibliography

[1] Abdel-Akher A. (1988), On the application of the boundary element method to plate bending analysis", *Ph.D. Thesis, Carleton University.*

[2] Abdel-Akher, A. and Hartley, G. (1989), Evaluation of boundary integrals for plate bending, *International Journal for Numerical Methods in Engineering*, Vol 28, 75-93.

[3] Abdel-Akher, A. and Hartley, G. (1989), Boundary integration and interpolation for procedures plate bending, *International Journal for Numerical Methods in Engineering*, Vol 28., 1389-1408.

[4] Altiero, N. J. and Sikarskie, D. L. (1978), A boundary integral method applied to plates of arbitrary plan form, *Computers and Structures 9, 163-168.*

[5] Benarjee, P. K. and Watson, J. O. (1985), Developments in boundary element methods - 4, *Applied Science Publishers.*

[6] Benarjee, P. K. and Butterfield, R. (1979), *Developments in boundary element methods - 1*, Applied Science Publishers (Ltd.), London.

[7] Beer, G. and Meek, J. T. (1981), The coupling of boundary and finite element methods for infinite domain problems in elasto-plasticity, *Proc. 3rd Int. Seminar on Recent Advances in Boundary Element Methods* (Berbbia, Ed), Irvine, 575-591.

[8] Bezine, G. (1978), Boundary integral formulation for plate flexure with arbitrary boundary conditions, *Mech. Res. Comm. Vol. 5, 197-206.*

[9] Bezine, G. and Gamby, D.A. (1978), A new integral equation formulation for plate bending problems, *Recent advances in boundary element methods (C.A. Brebbia, Ed.)* Pentech press, London.

[10] Brady, B. H. and Bray, J. W. (1978), The boundary element method for determining stresses and displacements around long opening in a triaxail stress field, *Int. J. Rock Mech. Min. Sci. and Geomch.* Abtract, Vol. 15, 21-28.

[11] Brady, B. H. and Wassyng A. (1981), A coupled finite element-boundary element methods of stress analysis, *Int. J. Rock Mech. Min. Sci and Geomech. Abstarct*, Vol.18, 475-485.

[12] Brebbia, C.A. and Doninyuez, J. (1989), *Boundary Elements An Introductory Course*, McGraw Hill.

[13] Brebbia, C.A., Venturini, W.S. (1987), *Boundary Elements Techniques - Application Stress Analysis and Heat Transfer*, Computational Mechanics Publications.

[14] Brebbia C. A., Telles J. C. and Wrobel L. C. (1984), *Boundary Element Techniques; Theory and Application in Engineering*, Springer-Verlag. New York.

[15] Brebbia, C.A. and Georgiou, P. (1979), Combination of boundary and finite elements in elastostatics. *Appl. Math. Modelling*, Vol. 3, 212-220.

[16] Cheung M S., Li W. "Combined finite strip and finite element solutions for analysis of plates.", *Computers and Structures*, in review.

[17] Cheung M. S., (1971), *Finite Strip Analysis of Structures*, Ph.D Thesis, Dep. of Civil Eng., The University of Calgary.

[18] Cook R.D., (1981), *Concepts and Applications of Finite Element Analysis*, 2nd Edition.

[19] Costa, J.A. and Brebbia, C.A., (1984), Plate bending using B.E.M., *Proc. of the 6th Int. Conf. on Boundary Element Method in Eng.*, Southampton University, 343-363.

[20] Cruse, T. A. (1969), Numerical solutions in three-dimensional elastostatics, *Int. J. Solids Struct. 5*, 1259-1274.

[21] Estoff, O. and Autes, H. (1991), On FEM-BEM coupling for fluid-structure interaction analysis in the time domain, *Int. J. Num. Math. Eng.* Vol. 31, 1151-1168.

[22] Hasen, E. B. (1976), Numerical solution of integral differential and singular integral equations for bending problems, *J. Elasticity 6*.

[23] Hung, C. and Dawkins, W. P. (1988), Stress analysis of a U-frame structure by the coupling of boundary and finite element methods. *Engineering analysis*, Vol.5 No.2, 58-63.

[24] Jaswon, M. A. and Ponter, A. R. (1963), Integral equation method in potential theory, 1" *Proc. Roy. Soc. A 273.*

[25] Jaswon, M. A. and Maitte, M. (1968), An integral formulation of plate bending problems" *J. Eng. Math. 11, 83-93.*

[26] Kelly D. W., Mustoe G. G. and Zeinkiewicz O. c. (1979), Coupling boundary element methods with other numerical methods, *Developments in boundary element methods-1*, 251-285, Applied Science Publishers.

[27] Komatsu S., Nagai, M. (1982), Analytical combination of boundary element method and thin walled segment method and its application to box girder bridges; *Boundary Element Methods in Engineering, Proceeding of 4th international seminar*, Southampton, England, (Brebbia C. A., Ed.), Springer-Verlag.

[28] Issa, M. E. S. (1980), Application of boundary element method to certain elasticity problems", *M.Eng., Carleton University.*

[29] Matti, M. and Chakrabarty, S. K. (1974), Integral solution for simply supported polygonal plates", *Int. J. Eng. Sci. Vol. 12, 793-806.*

[30] Ministry of Transportation and Communications (1983), *Ontario Highway Bridge Design Code (OHBDC)*, 2nd edition, Ontario.

[31] NG, S. F., Cheung, M. S. and Xu, T. (1990), Application of the combined boundary element and finite element methods to slab and slab-on-girder bridges, *Boundary element XII, Vol. 1, 457-466*, Computational mechanics publications, Springer-Verlag.

[32] Ohstu, M. (1987), BEM-FEM coupling analysis in two-dimensional elasto-dynamics and elasto-statics, *Proc. of the 1st Japan-China symposium on boundary element methods.*, 37-45.

[33] Rizzo, F. J. (1967), An integral equation approach to boundary value problems of classical elastostatics, *J. Appl. Math. 25, 83-95.*

[34] Rowe, R.E (1962), *Concrete Bridge Design*, 1st Edition, John Wiley.

[35] Seible, F. (1982), Nonlinear Analysis and Ultimate Strength of multi-cell Reinforced Concrete Box Girder Bridges, *Dept. of Civil Eng., University of California, Report no. UCB/SESM-82/02.*

[36] Stern, M. (1979), A general boundary integral formulation for the numerical solution of plate bending problems, *Int. J. Solids Structures*, Vol. 15, 769-782.

[37] Stern, M. (1983), Boundary integral equation for bending of thin plates, *Progress in boundary element methods*, Vol.2 (C.A Brebbia, Ed.), Pentech Press, London.

[38] Stern, M. (1984), *Plate bending problems*, Boundary Element Technique in Computer Aided Engineering (C.A. Brebbia, Ed.), Series E: Applied Sciences-No. 84, 315-325.

[39] Stroud, A. J. and Secrest, D. (1966), *Gaussian Quadrature Formulas*, Prectice-Hall.

[40] Tan, C. L., (1982), The boundary element Method "A short Course", *Dept. of Mechanical and Aeronautical Eng., Carleton University, Ottawa.*

[41] Tells, J. C. and Brebbia, C. A. (1979), On the application of the boundary element method to plasticity, *Appl. Math. Modelling, Vol. 3 No. 6.*

[42] Timoshenko, S. and Woinosky-Krieger, S. (1959), *Theory of Plates and Shells, 2nd ed., McGraw Hill.*

[43] Totenham, H. (1979), The boundary element method for plates and shells, *Developments in boundary element methods-1, Applied Science Publishers Ltd., 173-205.*

[44] Wu, B. C. and Altiero, N. J. (1979), A boundary integral method applied to plates and arbitrary plan form and arbitrary boundary conditions", *Computers and Structures vol. 10, 703-707.*

[45] Zienkiewicz, O. C. (1979), *The Finite Element Method*, 3rd edition, McGraw Hill Book Company.

[46] Zienkiewicz, O. C., Kelly, D. W. and Bettess, P. (1977), The coupling of finite element and boundary solution procedures, *Int. J. Num. Math. Eng., Vol 11, 355-376.*

APPENDIX A

Description of the Computer Model

Major subroutines

INPUT1

This subroutine is called to input all the data required for B.E region.

BMAT and GHMAT

To compute the G and H system matrices and rearrange them according to the boundary conditions. Subroutines INTS, INT2, and EXTIN are sequentially called.

INTS and EXTIN

The boundary integration scheme is performed here for both bending and plane actions. The subroutines first loop over all elements and then over all nodes.

INT2

To compute the vector B due to applied loads by transforming the area integrations to boundary integrations.

MMAT

To form the distribution matrix M using Lagrangian interpolation.

SOLVE

To solve the global matrix for all the unknowns including g displacements and stresses, using Gauss elimination method.

FINST and INTER

Subroutines to compute the displacements and stresses at the internal points.

INPUT2

To read the input data for F.E region.

BENDING and INPLAN

To form the matrix K and vector F required for the F.E region. The subroutine MESH, SHAPE, STIFF, TRANS, ASSEM and COND are sequentially called.

MESH

To generate the rectangular element meshes. It generates the connectivity matrix and the global coordinates of the nodes.

SHAPE

Contains the expression of the interpolation functions for various order elements and their derivatives with respect to the local coordinates.

STIFF

To calculate the element stiffness matrix in the local coordinates.

TRANS

To transform the stiffness matrix to the global system.

ASSEM

Assembles the global stiffness matrices and applies the boundary conditions.

COND

To condense the non-interface degrees of freedom using Gauss elimination.

OUTPUT

This subroutine first prints the results of the displacements and stresses at the boundary nodes, then at the internal points for both bending and in plane actions.

There are also several small subroutines (not described in this section) which perform specialized tasks such as numerical integration, Lagrange interpolation,....etc.

Description of the input data

BEM input data

1. Title of the problem
2. Type of the bridge (CODE)
   - CODE = slab, for slab bridges.
   - CODE = girder, for slab on girder bridges.
   - CODE = box, for box girder bridges.
3. Material data (MTDAT)
   - E = young's modulus
   - PR = poisson's ratio
   - TH = thickness
4. Boundary generating (BGDATA)
   - NBN = number of boundary nodes
   - ND = number of specified boundary nodes
5. One line for each node contains : I, S(1), S(2)
   - I = node number
   - S(1) = x-coordinate
   - S(2) = y-coordinate

- Number of boundary elements (NBE)

- one line for each element contains : I, NP(I), JBE(I,1), JBE1, ICOND
  - I = element number.
  - NP(I) = degree of the element.
  - JBE(I,1)= first node number of the element.
  - JBE1 = last node number of the element JBE1.
  - ICOND = boundary conditions of the element.
    * ICOND = 1, for fixed boundary
    * ICOND = 2, for hinged boundary
    * ICOND = 3, for free boundary
    * ICOND = 4, for interface boundary

6. Loading (CLDATA or DLDATA)

- CLDATA = for concentrated loads
- One line for each node contains : XCF, YCF, FCF
  - XCF, YCF = coordinates of concentrated forces.
  - FCF = value of the concentrated force.
- DLDATA = for distributed loads
- One line for each node contains : NLN, XLN, YLN
  - NLN = number of loaded nodes.
  - XLN, YLN = coordinates (x and Y) of loaded nodes.
- One line for each loaded element: I, JLE(I,J), W(I), J=1,4

- I = loaded elements
- JLE(I,J) = node number in each element
- W(I) = value of the loads

7. Internal points (IPDATA)

   - number of internal points (NIP)
   - One line for each internal point : I, XIN(I), YIN(I)
     - I = internal points number
     - XIN, YIN = coordinates (x and Y) of internal points

8. End of BEM data (ENDATA)

FEM input data

1. Element type IET
   - IET = 1, for linear quadrilateral
   - IET = 2, for quadratic quadrilateral
2. Node per element NPE
   - NPE = 4, if IET = 1
   - NPE = 8 or 9, if IET = 2

   - number of subdivision in the x-direction (NX)
   - number of subdivision in the y-direction (NY)
     - distance between nodes along x-direction (DX(I))

- distance between nodes along y-direction (DY(I))

3. Material properties and thickness

   - E1 = young's modulus in x-direction
   - E2 = young's modulus in y-direction
   - NUE = poisson's ratio
   - G12 = shear modulus in x-y direction
   - h = thickness

4. number of specified degrees of freedom (NSDF)

   - One line for each degree of freedom : IBDF(I), VBDF(I)
     - IBDF = number of specified degree of freedom .
     - VBDF = value of specified degree of freedom

5. Intensity of the uniform load (PO)

6. number of specified forces (NBSF)

   - One line for each force contains : JBSF(I), VBSF(I)
     - JBSF(I) = node number of each specified force
     - VBSF(I) = value of the force

APPENDIX B

INPUT DATA

Slab on girders bridge

MTDATA

25000000.,0.15,.247

BGDATA

24,8

1,3.7,0.652,24

9,3.7,8.652,10

10,3.7,8.652,9

12,0.,8.652,13

13,0.,8.652,12

21,0.,0.,22

22,0.,0.,21

24,3.7,0.,1

4

1,8,1,9,4

2,8,10,12,2

3,8,13,21,5

4,8,21,22,2

LDDATA

4

1,2.117,4.212

2,2.117,4.440

3,1.583,4.440

4,1.583,4.212

1

1,1,2,3,4,-900.

IPDATA

2

1,1.85,1.

2,1.85,2.

JNDATA

9,1,21

ENDATA

2,8,1

4,1

1.,1.,1.,1.,0.

0.75,0.

25000000.,25000000.,10869565.,10869565.,0.15,.4

2

14,20